LBL-24017 c.2

Lawrence Berkeley Laboratory
UNIVERSITY OF CALIFORNIA

CHEMICAL BIODYNAMICS DIVISION

RECEIVED
LAWRENCE
BERKELEY LABORATORY

JAN 8 1988

LIBRARY AND
DOCUMENTS SECTION

Spectroscopic Studies of Energy Transfer in Photosynthetic Reaction Centers of Higher Plants

S. Tabbutt
(Ph.D. Thesis)

September 1987

TWO-WEEK LOAN COPY

This is a Library Circulating Copy which may be borrowed for two weeks.

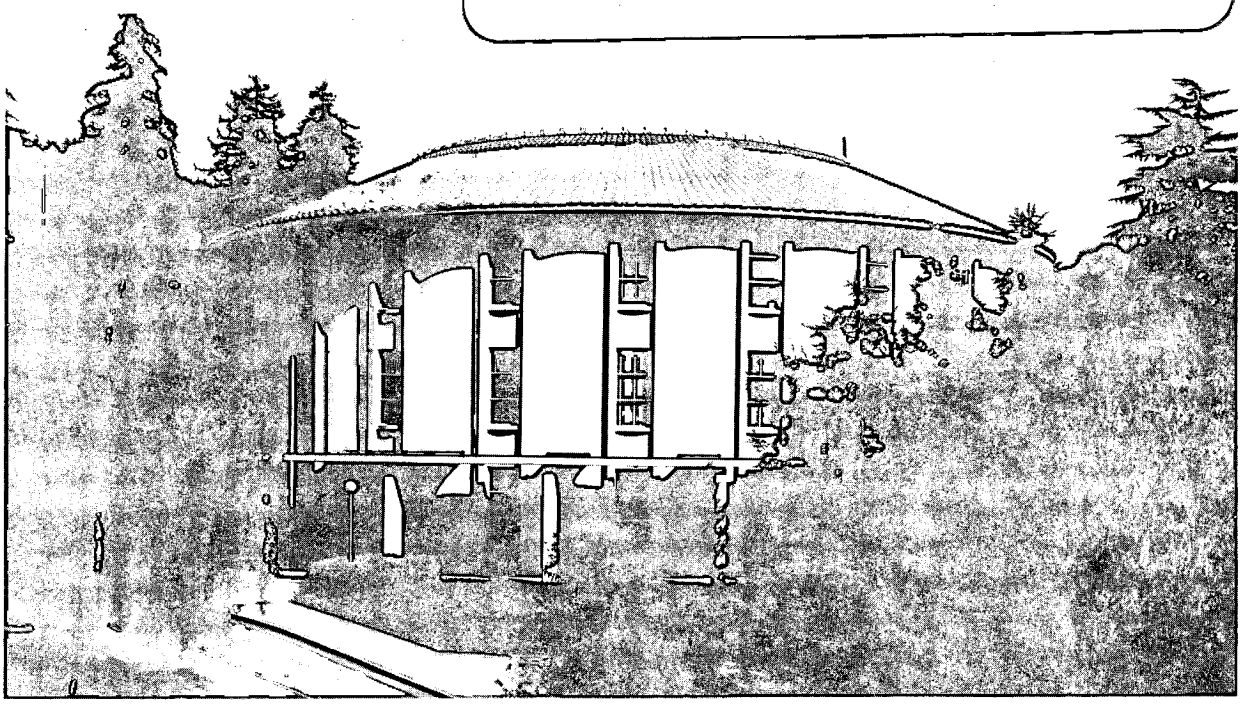

LBL-24017 c.2

Prepared for the U.S. Department of Energy under Contract DE-AC03-76SF00098

DISCLAIMER

This document was prepared as an account of work sponsored by the United States Government. While this document is believed to contain correct information, neither the United States Government nor any agency thereof, nor the Regents of the University of California, nor any of their employees, makes any warranty, express or implied, or assumes any legal responsibility for the accuracy, completeness, or usefulness of any information, apparatus, product, or process disclosed, or represents that its use would not infringe privately owned rights. Reference herein to any specific commercial product, process, or service by its trade name, trademark, manufacturer, or otherwise, does not necessarily constitute or imply its endorsement, recommendation, or favoring by the United States Government or any agency thereof, or the Regents of the University of California. The views and opinions of authors expressed herein do not necessarily state or reflect those of the United States Government or any agency thereof or the Regents of the University of California.

Spectroscopic Studies of Energy Transfer in Photosynthetic Reaction Centers of Higher Plants

Sarah Tabbutt

Ph.D. Thesis

Lawrence Berkeley Laboratory
University of California
Berkeley, California 94720

September 1987

The United States Department of Energy has the right to use this thesis for any purpose whatsoever including the right to reproduce all or any part thereof.

Spectroscopic Studies of Energy Transfer in Photosynthetic Reaction Centers of Higher Plants

Copyright c 1987

Sarah Tabbutt

Spectroscopic Studies of Energy Transfer in Photosynthetic Reaction Centers of Higher Plants

Sarah Tabbutt

Abstract

The focus of this thesis is excitation transfer and primary photochemistry in spinach chloroplasts and sub-chloroplast particles. The predominant instrumental approach is fluorescence, both steady state yield and picosecond kinetics. The fluorescence kinetics are measured with a synchronously pumped, mode-locked dye laser excitation source and a reverse single photon-counting timing detection system.

Very little has been reported on the fluorescence properties of photosystem I (PS I) due to its relatively weak emission compared to photosystem II (PS II) and the light harvesting complexes. Using a PS I complex isolated from spinach, without PS II and peripheral light harvesting complexes, I am able to report many fluorescence properties of the PS I reaction center. PS I centers have two emission bands, 690nm and 722nm. The 690nm fluorescence kinetics has an instrument limited (25ps) rise and is best fit to three exponential decay components: slow, 2.2-2.5ns; middle, 250-300ps; and fast, 40-100ps. Both the yield and kinetics are temperature independent (77-295K). The 722nm emission is dramatically temperature dependent. At 295K the fluorescence lifetimes at 720nm are identical to those at 690nm. The following effects are observed upon lowering the temperature: the lifetimes of all three decay components increase; a measurable risetime (>25ps) grows in at temperatures below 265K; and the fluorescence intensity at 722nm increases about 20-fold from 295K to 77K. These studies provide excitation transfer rates and activation energies within the PS I centers. The PS I emission data can be explained by two Chl a species: an antenna pool emitting at 690nm and the reaction center (primary donor and/or primary acceptor) emitting at 722nm.

I monitored CP1 fluorescence intensity under various photochemical conditions. Under continuous actinic illumination the fluorescence intensity (690nm) decreases by about 20% and with the same kinetics as the optical bleaching at 699nm which reflects $P700^+$ formation. The kinetics and magnitudes of the fluorescence decrease and photobleaching have

similar dependence upon: excitation intensity, ascorbate concentration, ferri/ferrocyanide redox titration and phenazinemethosulfate (PMS) concentration. I find that the oxidation of P700 quenches PS I fluorescence. Thus, fluorescence can be used to monitor the kinetics of primary photochemistry in the PS I reaction center.

The effects of linolenic acid on PS II is also addressed by monitoring the steady state emission and picosecond fluorescence kinetics of chloroplasts and PS II sub-chloroplast particles. As the PS II reaction center becomes closed (unable to accept further excitation) the fluorescence intensity increases, reflecting an increase in the lifetime (1.0 to 2.0ns) and relative yield (20% to 90%) of the slow decay component. The different effects of the electron transfer inhibitors, DCMU and linolenic acid, upon PS II fluorescence is reported. DCMU is known to block electron transfer between the two bound quinone acceptors, Q_A and Q_B. Fluorescence measurements indicate that linolenic acid blocks electron transfer prior to the DCMU site, and electron paramagnetic resonance measurements show that charge separation still occurs in the presence of linolenic acid. Thus, linolenic acid appears to block electron transfer between the primary acceptor, Ph, and the first bound quinone, Q_A.

In conclusion, this work applies fluorescence measurements to address questions concerning the mechanisms and kinetics of energy transfer and primary photochemistry in PS I and PS II.

Acknowledgements

This research was supported by the Director, Office of Energy Research, Office of Basic Energy Sciences, Division of Biological Energy Conversion and Conservation of the Department of Energy, under contract DE-AC03-76SF00098, by a grant from the National Science Foundation (PCM82-10524). The University of California San Diego, School of Medicine provided the additional financial assistance necessary to complete this work.

The support of our research group at the Laboratory of Chemical Biodynamics has been tremendous. Several individuals have been especially helpful and supportive. Dr. Steve Worland showed me the basics of research; he is an exceptional teacher and an enthusiastic scientist. Dr. Kerry Karukstis, Dr. John McCracken, Dr. John Casey, Sara Hoover, Trish Maxson, Vickie DeRose and Ann McDermott have all been generous with their time and ideas. Dr. Ward Brown, Dr. Cindy Buhse, Gary Smith and Beth Klingel have been irreplaceable at critical times. Dr. Richard Malkin provided important and helpful criticism during the completion of this work. My director, Dr. Ken Sauer, helped me out of dead-ends, steered me back on course when necessary and provided an essential source of motivation. Most importantly, I want to thank my family and friends for their patience and support.

Table of Contents

Abstract 1

Acknowledgements i

Abbreviations v

Chapter One: An Introduction to the Photosynthetic Light Reactions.

1.1 Photosynthesis 1

1.2 Introduction 2

1.3 Photosystem II 3

1.4 Photosystem I 7

1.5 References 12

Chapter Two: Energy Transfer and Fluorescence.

2.1 Introduction 16

2.2 Excitation Migration 16

2.3 Fluorescence 17

2.4 Instrumentation 18

2.5 Deconvolution and Kinetic Analysis 21

2.6 References 27

Chapter Three: Fluorescence and EPR Characterization of Linolenic Acid Inhibition in PS II.

3.1 Acknowledgements 28

3.2 Introduction 28

3.3 Materials and Methods 30

3.4 Absorption and Emission Spectra 32

3.5 Results of EPR Measurements: P680 Spin Polarized Radical Pair Triplet 32

3.6 Results of Fluorescence Induction Curves 39

3.7 Results of the Fluorescence Decay Kinetics 44

3.8 Reversibility of Fluorescence Decay Characteristics 47

3.9 Discussion 50

3.10 References 57

Chapter Four: Preparation and Characterization of the PS I Reaction Center Complex, CP1

4.1 Introduction 59

4.2 Materials and Methods 59

4.3 Peptide Composition 62

4.4 Absorption and Emission Spectra of the CP1 Complex 62

4.5 EPR Spectroscopy of the CP1 Complex 69

4.6 Photobleaching of the CP1 Complex 74

4.7 Summary 78

4.8 References 79

Chapter Five: Variable Fluorescence in CP1

5.1 Introduction 81

5.2 Materials and Methods 82

5.3 Photobleaching and Variable Fluorescence 83

5.4 Excitation Intensity 88

5.5 Ascorbate and PMS 92

5.6 P700 Redox Titration 95

5.7 Discussion 95

5.8 References 104

Chapter Six: Temperature Dependence of CP1 Fluorescence

6.1 Introduction 105

6.2 Materials and Methods 106

6.3 Fluorescence Excitation Spectra 110

6.4 Temperature Dependence of CP1 Emission 110

6.5 Fluorescence Dependence on the Oxidation State of P700 115

6.6 Picosecond Fluorescence Kinetics at 295K 121

6.7 Picosecond Fluorescence Kinetics at 77K 126

6.8 Dependence of the Prompt Fluorescence Kinetics at 77K on the Oxidation State of P700 126

6.9 Temperature Dependence of Fluorescence Yields from Kinetic Measurements ... 135

6.10 Picosecond Fluorescence Kinetics at 680nm as a Function of Temperature 135

6.11 Picosecond Fluorescence Kinetics at 730nm as a Function of Temperature 142

6.12 Activation Energies at 730nm 150

6.13 Discussion 157

6.14 References 165

Chapter Seven: Future Experiments 166

Abbreviations

Abs	absorbance
ATP	adenosine triphosphate
BSA	bovine serum albumin
Chl	chlorophyll
CIDEP	chemically induced dynamic electron polarization
CP1	PS I reaction center-enriched chlorophyll-protein complex
DCMU	3-(3,4-dichlorophenyl)-1,1-dimethyl urea
DCPIP	2,6-dichlorophenolindophenol
DPC	diphenylcarbazide
ENDOR	electron nuclear double resonance
EPR	electron paramagnetic resonance
F_0	minimum level of fluorescence after dark adaptation
F_{max}	maximum level of fluorescence
FWHM	full width at half maximum
LHC	light harvesting complex
NADPH	nicotinamide adenine dinucleotide phosphate, reduced
Ph	pheophytin, primary PS II acceptor
PMS	phenazinemethosulfate
PMSF	phenylmethanesulfonyl fluoride
PMT	photomultiplier tube
PS I	photosystem one
PS II	photosystem two
P700	primary donor of PS I
P680	primary donor of PS II
Q_A	primary quinone acceptor
Q_B	secondary quinone acceptor
RPT	radical pair spin polarized triplet
SDS-PAGE	sodium dodecyl sulfate polyacrylamide gel electrophoresis
Tris	tris(hydroxymethyl)aminomethane

Chapter One: An Introduction to the Photosynthetic Light Reactions

1.1 Photosynthesis

Photosynthesis is the process by which biological organisms (plants, algae and some bacteria) convert light energy to chemical energy. The overall chemical equation for plant photosynthesis is

$$6CO_2 + 6H_2O \rightarrow^{h\nu} \rightarrow C_6H_{12}O_6 + 6O_2$$

where chemical energy is produced in the form of simple sugars. Higher plant photosynthesis is described by two processes. The dark reactions convert CO_2 to sugars. The light reactions absorb photons, split water into molecular oxygen and produce chemical energy.

The light reactions in green plants are comprised of three basic steps. (1) Photons are absorbed by pigments (primarily chlorophyll) whose excitation is transferred to and trapped by pigment-protein complexes denoted reaction centers. (2) Chemical energy is stabilized in the reaction center by ion-pair formation. (3) The charge separation is maintained by a series of electron donors and acceptors. The final electron donor is H_2O and the terminal electron acceptor is nicotinamide adenine dinucleotide phosphate, $NADP^+$. The electron transport chain is coupled to the phosphorylation of adenosine diphosphate (ADP). Thus, light energy is trapped, water is oxidized to molecular oxygen and chemical energy is produced in the form of ATP and NADPH during the light reactions in photosynthesis.

The light reactions occur in the chloroplast thylakoid membranes. The thylakoids are lipid-protein membranes structured as large flattened sacs. Thylakoids are divided into stacked regions called grana and unstacked regions called stroma.

The thylakoids contain four types of pigment protein complexes necessary for oxygen-evolving photosynthesis: cytochrome b_6/f complex, light harvesting complexes, photosystem I and photosystem II. The light harvesting complexes (LHC) are protein-bound chlorophyll a/b responsible for photon trapping and excitation transfer to the reaction centers. The various LHCs differ in their pigment and protein composition and are associated preferentially with one of the two photosystems [1,2]. The reaction center complexes (PS I and PS II) are where the charge separation and initial photochemistry occur. Each reaction center has a primary donor

comprised of specialized protein bound chlorophyll a molecules. The primary donors account for less than 1% of the total chlorophyll in the chloroplast [3]. PS II and PS I function in series to transfer electrons from the oxygen evolving complex to $NADP^+$.

1.2 Introduction

This work addresses photon absorption, excitation transfer and primary photochemistry in the PS I and PS II reaction centers of spinach. Most experiments are performed on isolated PS I or PS II subchloroplast or reaction center complexes. The prevailing spectroscopic techniques monitor fluorescence yields and lifetimes, although optical spectroscopy and electron paramagnetic resonance (EPR) spectroscopy are also employed. All questions address the initial energy transfer mechanisms and kinetics of the photosynthetic light reactions.

The wide range of subjects covered requires a comprehensive introduction. This chapter describes the electron transfer components of PS I and PS II, focusing on the chemical identity, spectroscopic properties and electron transfer kinetics. Chapter Two covers excitation migration of the photosynthetic antenna and reaction center chlorophylls: photon absorption by the antenna, exciton delocalization, energy transfer, excitation trapping, ion-pair formation and charge recombination. These events are described with respect to their effects on the fluorescence lifetimes, yields and emission wavelengths of PS I and PS II.

We measured the fluorescence yields and lifetimes to locate the site of electron transfer inhibition by linolenic acid on the acceptor side of PS II (Chapter Three). Our data are best explained by a linolenic acid block of electron transfer at the first bound quinone acceptor. The site of inhibition by linolenic acid is more immediate to the primary donor than is the site of electron transfer inhibition by the widely used inhibitor DCMU. Thus, as an inhibitor, linolenic acid opens the doors to a variety of experiments that should confirm the chemical identity and provide electron transfer kinetics of acceptors preceding the primary bound quinone in PS II.

Fluorescence emitted from the PS I reaction center is relatively weak. Chloroplast fluorescence is dominated by three emission bands (at 77K): 685nm from PS II centers [4], 680nm from PS II associated LHC [4] and 735nm from PS I associated LHC [2,5,6]. As a result, very little has been reported on emission specifically from the PS I reaction center. I isolated a PS I reaction center complex without these highly fluorescent components and have measured

many of its fluorescence properties. Under continuous illumination, I observe variable fluorescence from the PS I centers that is dependent on the oxidation state of P700 (Chapter Five). $P700^+$ appears to quench fluorescence; as the PS I reaction centers close, the fluorescence yield decreases. This is an intriguing contrast to PS II fluorescence, which increases as the centers close.

The kinetics and mechanisms of excitation transfer among the immediate PS I antenna and trapping by the primary donor are of particular interest. The dramatic temperature dependence of the fluorescence yield and lifetimes lend much insight into the energetics of the system (Chapter Six). Is the fluorescence emitted from the reaction center or the antenna? Is the 100ps fluorescence rise at 722nm related to the 100ps fluorescence decay at 690nm and evidence of energy transfer?

1.3 Photosystem II

The PS II reaction center complex is located primarily in the granal regions of the thylakoid membranes. The ultimate electron donor to PS II is the water-splitting, oxygen-evolving complex. Although oxygen evolution and electron donation to PS II is an exciting area in photosynthesis, this work will discuss only the excitation migration, primary photochemistry and initial electron transfer aspects of PS II.

PS II is closely associated with the LHC a/b chlorophyll protein which provides most of its excitation. The mechanisms of excitation transfer to the reaction center are described in Chapter Two. Excitation is trapped in the PS II reaction center by the primary donor P680 (680nm being the PS II long wavelength absorption maximum). The transient absorption spectrum of P680 is characteristic of a chlorophyll a species [7]. The narrow linewidth of the $P680^+$ EPR signal ($g = 2.002$, width = 7-8G [8,9]) is indicative of a chlorophyll a dimer. However, its redox potential ($> .9V$) is more consistent with a chlorophyll a monomer. The precise structure of P680 remains unclear.

The primary acceptor in PS II is a pheophytin a molecule (Ph) [10] with a reduction potential of -610mV [11]. Dithionite reduced PS II samples illuminated at 296K (for 30s) and immediately cooled to 77K, produce an EPR singlet (at 6K) characteristic of reduced Ph ($g = 2.0033$, width = 12.5G) [12]. The photoinduced optical changes associated with the reduction of Ph include

absorption decreases at 680nm, 545nm, 518nm and 422nm, and absorption increases at 448nm and 605nm [10]. The spectral characteristics of Ph are similar to those of the BPh acceptor (I) found in bacterial reaction centers [13].

The secondary acceptor in PS II is an iron-quinone complex designated Q_A. It has two single-electron redox potentials: -45mV and -245mV (with a 50mV/pH unit dependence) [14]. The EPR signal (at 5K) of Q_A^- is a broad peak at g = 1.82 characteristic of a Q^- - Fe^{+2} complex [15]. PS II samples illuminated at 220K (for 90s) and immediately frozen to 77K exhibit an EPR spectrum (at 6K) of an asymmetric doublet (g = 2.00, width = 52-55G) which has been assigned to an exchange interaction between Ph^- and Q_A^- [12]. The light-induced optical changes due to Q_A reduction include an absorption increases at 450nm and 330nm and a decrease in absorption at 275nm reflecting semiquinone anion formation [16]. In addition, absorption shifts occur at 545nm and 685nm which are probably due to pheophytin or carotenoid molecules closely associated with Q_A [17]. Q_A passes electrons to the plastoquinone pool via a plastoquinone, Q_B, which acts as a two electron carrier [18].

Room temperature variable fluorescence (at 680nm) from PS II is proposed to be a direct measure of the oxidation state of Q_A and the state of the PS II reaction center [19]. When Q_A is oxidized, the centers are "open" and the fluorescence level is at a minimum, F_0; when Q_A is reduced, the centers are "closed" and the fluorescence is at a high level, F_{max}. Electron transfer from Q_A to Q_B can be blocked by DCMU or low temperatures (below 220K). Subsequent illumination results in an accumulation of Q_A^-, and the fluorescence increases to its maximum level, F_{max}. A more detailed discussion of energy transfer and fluorescence is included in Chapter Two.

The identity of the immediate electron donor to $P680^+$ (Z) is not known and may be a different species depending on the sample conditions. The reduction kinetics of $P680^+$ have been measured. In dark-adapted, oxygen evolving chloroplasts 35-55% of the $P680^+$ is reduced on the first flash with a halftime of 20-50ns, 15-35% of the $P680^+$ is reduced in subsequent flashes with a halftime of 280-400ns and the remaining $P680^+$ is reduced in μs [20-23]. The kinetics of the ns phases are proposed to be dependent upon the S-states of the oxygen evolving complex [24]. The ns phases are absent in PS II centers where oxygen evolution is inhibited, and $P680^+$ reduction is slowed to 2-20μs [25].

Figure 1.1 Electron transfer components of PS II.

(A) Reduction potentials (in parentheses) and EPR signals of the oxidized donors and reduced acceptors. (B) Electron transfer halftimes.

Fig. 1.1A

	oxygen →→→ evolving complex	Z →	P680 → [8,9]	Ph → [10-12]	Q_A(Fe) → [14,15]	Q_B/PQ Pool [18]
E_m:	—	—	(>900mV)	(-610mV)	(-45mV, -245mV)	(+100mV)
EPR:	multiline signal	Signal II	g=2.002	g=2.0033	g=1.82	
			ΔH=7-8G	ΔH=12.5G	broad	

Fig. 1.1B

Z P680 Ph Q_A — 100-400ps (295K) [25] — Z P680$^+$ Ph Q_A^-

80-150μs (295K) [63,64]

Z P680 Ph Q_A^- — 1-2ns (295K) [65,66] — Z P680$^+$ Ph$^-$ Q_A^-

Z P680$^+$ Ph Q_A^- — 35-55%, 20-50ns; 15-35%, 280-400ns; 30%μs, (295K) [19-22] — Z$^+$ P680 Ph Q_A^-

The photochemical components of the PS II reaction center are: Z P680 Ph Q_A Q_B. The electron transfer rates and midpoint potentials are summarized in Fig. 1.1.

1.4 Photosystem I

The PS I reaction center is located primarily in the stromal regions of the thylakoids of higher plant chloroplasts. Primary photochemistry and electron transfer occur in a complex of several pigment-bound proteins.

There are at least two light harvesting complexes, LHCP1a and LHCP1b, associated specifically with PS I [26]. Both complexes have absorption maxima at 676nm and Chl a/b ratios of 3-4. LHCP1a is comprised of 22 and 23kD polypeptides (determined by SDS-PAGE) and has a fluorescence emission maximum (at 77K) of 680nm with a 730nm shoulder. LHCP1b has a 20kD polypeptide and an emission maximum (at 77K) of 730nm with a 680nm shoulder [26]. Energy transfer mechanisms from these light harvesting complexes to the PS I reaction centers are described in Chapter Two.

The PS I primary donor, P700 (long wavelength absorption maximum is 700nm), is a chlorophyll a species with reported midpoint potential values ranging from +400mV [27] to +500mV [28,29]. $P700^+$ has an EPR signal designated Signal I (g = 2.0025, width = 7.1G) [30]. The optical changes associated with P700 oxidation include absorption decreases at 698nm (the P700 extinction coefficient is $\Delta\epsilon_{698}$ = 64mM^{-1} cm^{-1} [31]), 685nm and 435nm [Fig. 4.6]. The narrow linewidth of Signal I [32], the ENDOR splittings of $P700^+$ [33] and the exciton interaction of the CD spectra [34] are characteristic of a Chl a dimer. However, studies of ^{13}C-enriched, deuterated algae suggested that $P700^+$ is a monomeric Chl a enol (ring V) [35]. In addition, the large zero-field splittings [Fig. 4.5] of the EPR spin-polarized radical pair triplet, thought to be located on P700, are the same as those observed for the Chl a monomer [36]. The exact structure of P700 remains unclear.

The primary acceptor, A_0, has been directly observed only by EPR. The reported steady state EPR measurements of A_0^- are both isotropic signals but differ in field position between

g = 2.0017, linewidth = 11.5G [37] and g = 2.0024 [38]. Time resolved EPR produced the chemically induced dynamic electron polarization (CIDEP) signal of an isotropic A_0 at g = 2.0031 [39]. The g values of 2.0024 and 2.0031 are consistent with reduced pheophytin a or chlorophyll a molecules. $P700^+ A_0^-$ can recombine to form a radical pair spin polarized triplet (RPT). The presence of a RPT, which can be detected at 10K by EPR, is a useful method for confirming the primary photochemical activity of the reaction center.

A_0 passes electrons to A_1. Only recently have the EPR signals of these two reduced acceptors been distinguished from a combined A_0^- A_1^- signal. A_1^- has an asymmetric EPR signal measured between g = 2.0051 and 2.0054, with a 8 - 10.5G linewidth [37-39]. This is consistent with a quinone species [40]. It is possible that the phylloquinone (vitamin K_1) recently found in PS1 [41] is related to A_1. Optical absorption changes initially assigned to A_1 reduction include decreases at 445nm and 700nm and increases at 480nm and 672nm, and were assigned to a Chl a dimer [42]. However, these changes may reflect a contribution from A_0 reduction. The redox potentials of A_0 and A_1 have not yet been determined.

An iron-sulfur protein X (A_2), with a mid-point potential of -730mV (pH 10) [43,44], accepts electrons from A_1. X^- has a characteristic EPR signal with $g_x = 2.08$, $g_y = 1.87$, $g_z = 1.76$ (Fig. 4.4) [45,46]. The reduction of X produces several optical changes: a blue shift near 450nm and absorbance increases at 670nm and 690nm. The longer wavelength changes have been attributed to the negative charge on X affecting the absorbance properties of neighboring Chl a molecules [47]. Charge separation and electron transfer to the state $P^+ A_0 A_1 X^-$ occurs in 200ps (at 295K) [48], while recombination takes 250μs (at 295K) [49], Fig. 1.2. A stable X^- is most often produced by reducing (dithionite, pH 10) the subsequent electron acceptors Fd_B and Fd_A and illuminating while cooling to 77K. Chemical analysis shows that each PS I reaction center has 10-14 non-heme iron atoms and 10-12 acid-labile sulfides thought to comprise X, Fd_A and Fd_B [50]. Optical [51] and Mössbauer [52] measurements predict X to be a 4Fe4S center. X-ray absorption spectral studies indicate that X may be a pair of 2Fe2S centers [53].

Iron-sulfur centers Fd_B (E_m = -580mV to -590mV) and Fd_A (E_m = -530mV to -550mV) [54,55] are the terminal bound acceptors of the PS I electron transfer chain. Reduction of centers Fd_A and Fd_B produces a broad optical bleaching centered at 430nm [56], thus the alternate label P430. Illumination at cryogenic temperatures reduces Fd_A, observable by EPR (g_x = 2.05, g_y = 1.94, g_z = 1.86); reduction with dithionite (pH 10) and cooling in the dark (to 77K) also reduces Fd_B (g_x = 2.07, g_y = 1.93, g_z = 1.88) [55,57]. The EPR spectrum of $Fd^{-}_{B,A}$, Fig. 4.4, is not the sum of Fd^{-}_{B} and Fd^{-}_{A}, indicating that there is a magnetic interaction between the two centers.

All PS I electron transfer components described are bound to membrane proteins whose molecular weights have been estimated by sodium dodecyl sulfate polyacrylamide gel electrophoresis (SDS-PAGE; 2% SDS). P700 and A_0 are bound to an apoprotein which runs at 63-65kD on SDS gels. In addition, X has recently been reported to be bound to the same apoprotein [58,59]. Fd_B and Fd_A are associated with a 19kD polypeptide [60].

The donor side of PS I is composed of the electron transfer components cytochrome f (cyt f) and plastocyanin (PC). Cyt f has a molecular weight of 31kD and a mid-point potential of 360mV (determined in *Chlamydomonas reinhardtii*). PC is a copper protein with a known crystal structure [61], a molecular weight of 10.5kD and a mid-point potential of 370mV. PC reduces $P700^+$ with half-times of 20μs and 200μs while cyt f reduces oxidized PC with half-times of 70-130μs and 440-860μs [62]. However, in most PS I subchloroplast isolation procedures, including those used in this work, these endogenous donors to $P700^+$ (cyt f and PC) are removed.

In summary, the identified electron transfer components of *in vivo* spinach PS I consist of:

$$cytf \rightarrow PC \rightarrow P700 \rightarrow A_0 \rightarrow A_1 \rightarrow X \rightarrow Fd_B \rightarrow Fd_A.$$

The mid-point potentials and EPR signals of the PS I acceptors are summarized in Fig. 1.2A. The electron transfer rates are summarized in Fig. 1.2B.

Figure 1.2 Electron transfer components of PS I.

A. Reduction potentials (in parentheses) and EPR signals of the reduced acceptors and oxidized donors.

B. Electron transfer half-times. A represents A_0 and A_1 since no room temperature data are yet available to distinguish them kinetically. The state P A X represents centers where Fd_B and Fd_A are absent.

Fig. 1.2A

	P700→ [28-30]	A_0→ [37-39]	A_1→ [37-39]	X→ [43-46]	Fd_B→ [54,55,57]	Fd_A
E_m:	(400-500mV)	—	—	(-730mV)	(-585mV)	(-540mV)
EPR:	g=2.0025	g=2.0024-2.0031	g=2.0051-2.0054	g_x=2.08	g_x=2.07	g_x=2.05
				g_y=1.87	g_y=1.93	g_y=1.94
				g_z=1.76	g_z=1.88	g_z=1.86
	ΔH=7.1G	—	ΔH=8-10.5G	—	—	—

Fig. 1.2B

P A X $Fd^{=}_{B,A}$ — 10-30ps (295K) [67-69] → P^+ A^- X $Fd^{=}_{B,A}$

P A X $Fd^{=}_{B,A}$ — 3μs and 10ns (295K) [48] → P^+ A X^- $Fd^{=}_{B,A}$

P A X^- $Fd^{=}_{B,A}$ — 200ps (295K) [48]; 250μs (295K) [49]; 130ms (5K) [47] → P^+ A^- X^- $Fd^{=}_{B,A}$

10-30ps (295K [69]; 3μs (295K) [49]; 1.3ms (5K) [49]

1.5 References

[1] Thornber, J.P. (1975) ***Ann. Rev. Plant Physiol.*** 26, 127-158.

[2] Lam, E., Ortiz, W. and Malkin, R. (1984) ***FEBS Lett*** 168, 10-14.

[3] Sauer, K. (1975) ***Bioenergetics of Photosynthesis***, ed. Govindjee, Academic Press, New York. pp. 115-181.

[4] Butler, W. (1978) ***Ann. Rev. Plant Physiol.*** 29, 345-378.

[5] Mullet, J.E., Burke, J.J. and Arntzen, C.J. (1980) ***Plant Physiol.*** 65, 823-827.

[6] Anderson, J.M., Brown, J.S., Lam, E. and Malkin, R. (1983) ***Photochem. Photobiol.*** 38, 205-210.

[7] Haveman, J. and Mathis, P. (1976) ***Biochim. Biophys. Acta*** 440, 346-355.

[8] Malkin, R. and Bearden, A.J. (1975) ***Biochim. Biophys. Acta*** 396, 250-259.

[9] Visser, J.W.M., Rijgersberg, C.P. and Gast, P. (1977) ***Biochim. Biophys. Acta*** 460, 36-46.

[10] Fujita, I., Davis, M.S. and Fajer, J. (1978) ***J. Amer. Chem. Soc.*** 100, 6280-6282.

[11] Rutherford, A.W., Mullet, J.E. and Crofts, A.R. (1981) ***FEBS Lett*** 123, 235-237.

[12] Klimov, V.V., Dolan, E. and Ke, B. (1980) ***FEBS Lett*** 112, 97-100.

[13] Okamura, M.Y., Feher, G. and Nelson, N. (1982) ***Photosynthesis: Energy Conversion by Plants and Bacteria, Vol. 1.*** ed. Govindjee, Academic Press, NY pp. 195-274.

[14] Horton, P. and Croze, E. (1979) ***Biochim. Biophys. Acta*** 545, 188-201.

[15] Nugent, J.A., Diner, B.A. and Evans M.C.W. (1981) ***FEBS Lett*** 124, 241-244.

[16] Bensasson, R. and Land E.J. (1973) ***Biochim. Biophys. Acta*** 325, 175-181.

[17] van Gorkom, H.J. (1974) ***Biochim. Biophys. Acta*** 347, 439-442.

[18] Bouges-Bocquet, B. (1973) ***Biochim. Biophys. Acta*** 314, 250-256.

[19] Klimov, V.V., Klevanik, A.V., Shuvalov, N.A. and Krasnovsky, A.A. (1977) ***FEBS Lett*** 82, 183-186.

[20] Van Best, J.A. and Mathis, P. (1978) ***Biochim. Biophys. Acta*** 505, 178-188.

[21] Schlodder, E., Brettel, K., Schatz, G.H. and Witt, H.T. (1984) ***Biochim. Biophys. Acta*** 765, 178-185.

[22] Eckert, H., Renger, G. and Witt, H.T. (1984) ***FEBS Lett*** 167, 316-320.

[23] Sonnevald, A., Rademaker, H. and Duysens, L.N.M. (1979) ***Biochim. Biophys. Acta*** 548, 536-551.

[24] Bouges-Bocquet, B. (1980) ***Biochim. Biophys. Acta*** 594, 85-103.

[25] van Gorkom, H.J. (1985) ***Photosyn. Res.*** 6, 97-112.

[26] Lam, E., Ortiz, W. and Malkin, R. (1984) ***FEBS Lett.*** 168, 10-14.

[27] Evans, M.C.W., Sihra, C.K. and Slabas, A.R. (1977) ***Biochem J.*** 150, 335-362.

[28] Knaff, D.B. and Malkin, R. (1973) ***Arch. Biochem. Biophys.*** 159, 555-562.

[29] Kok, B. (1961) ***Biochim. Biophys. Acta.*** 48, 527-533.

[30] Commoner, B., Heise, J.J. and Townsend, J. (1956) ***Proc. Nat. Acad. Sci.*** 42, 710-718.

[31] Hiyama, T. and Ke, B. (1972) ***Biochim. Biophys. Acta*** 267, 160-171.

[32] Norris, J.R., Uphaus, R.A., Crespi, H.L. and Katz, J.J. (1971) ***Proc. Nat. Acad. Sci.*** 68, 625-629.

[33] Norris, J.R., Scheer, H., Druyan, M.E. and Katz, J.J. (1974) ***Proc. Nat. Acad. Sci.*** 71, 4987-4900.

[34] Philipson, K.D., Sato, V.L. and Sauer, K. (1972) ***Biochemistry*** 11, 4591-4594.

[35] Wasielewski, M.R., Norris, J.R., Crespi, H.L. and Harper, J. (1981) ***J. Am. Chem. Soc.*** 103, 7664-7666.

[36] Uphaus, R.A., Norris, J.R. and Katz, J.J. (1974) ***Biochem. Biophys. Res. Comm.*** 61, 1057-1063.

[37] Gast, P., Swarthoff, T., Ebskamp, F.C.R. and Hoff, A.J. (1983) ***Biochim. Biophys. Acta*** 722, 163-175.

[38] Bonnerjea, J. and Evans, M.C.W. (1982) ***FEBS Lett*** 148, 313-316.

[39] McCracken, J. and Sauer, K. (1984) ***Advances in Photosynthesis Research, Vol. I*** ed. Sybesma, C., Junk Publishers, The Hague, The Netherlands, pp. 585-588.

[40] McCracken, J. (1983) ***Ph.D. Thesis***, University of California, Berkeley, p. 237.

[41] Schoeder, H.U. and Lockau, W. (1986) ***FEBS Lett.*** 199, 23-27.

[42] Shuvalov, V.A. and Asadov, A.A. (1979) ***Biochim. Biophys. Acta*** 545, 296-308.

[43] Heathcote, P., Williams-Smith, D.L., Sihra, C.K. and Evans, M.C.W. (1978) ***Biochim. Biophys. Acta*** 503, 333-342.

[44] Ke, B., Dolan, E., Sugahara, K., Hawkridge, F.M., Demeter, S. and Shaw, E.R. (1977) ***Plant Cell Physiol.*** 3, 187-199.

[45] Evans, M.C.W., Sihra, C.K. and Cammack, R. (1976) ***Biochem. J.*** 158, 71-77.

[46] McIntosh, A.R. and Bolton, J.R. (1976) ***Biochim. Biophys. Acta*** 430, 555-559.

[47] Shuvalov, V.A., Dolan, E. and Ke, B. (1979) ***Proc. Nat. Acad. Sci.*** 76, 770-775.

[48] Shuvalov, V.A., Ke, B. and Dolan, E. (1979) ***FEBS Lett.*** 100, 5-8.

[49] Sauer, K., Mathis, P., Acker, S. and Van Best, J.A. (1978) ***Biochim. Biophys. Acta*** 503, 120-134.

[50] Golbeck, J.H., Velthuys, B.R. and Kok, B. (1977) ***FEBS Lett*** 82, 183-186.

[51] Hiyama, T. and Fork, D.C. (1980) ***Arch. Biochem. Biophys.*** 199, 488- 496.

[52] Evans, E.H., Dickson, D.P.E., Johnson, C.E., Rush, J.D. and Evans, M.C.W. (1981) ***Eur. J. Biochem.*** 118, 81-84.

[53] McDermott, A.E., Yachandra, V.K., Guiles, R.D., Britt, R.D., Dexheimer, S.L., Sauer, K. and Klein, M.P. ***Proc. 7th International Congress on Photosynthesis*** (in press).

[54] Ke, B., Hansen, R.E. and Beinert, H. (1973) ***Proc. Nat. Acad. Sci.*** 70, 2941-2945.

[55] Evans, M.C.W., Reeves, S.G. and Cammack, R. (1974) ***FEBS Lett*** 49, 111-114.

[56] Hiyama, T. and Ke, B. (1971) ***Arch. Biochem. Biophys.*** 147, 99-108.

[57] Malkin, R. and Bearden, A.J. (1978) ***Biochim. Biophys. Acta*** 505, 147- 182.

[58] Warden, J.T. and Golbeck, J.H. (1986) ***Biochim. Biophys. Acta*** 849, 25-31.

[59] Golbeck, J.H. and Cornelius, J.M. (1986) ***Biochim. Biophys. Acta*** 849, 16-24.

[60] Bonnerjea, J., Ortiz, W. and Malkin, R. (1985) ***Arch. Biochem. Biophys.*** 240, 15-20.

[61] Colman, P.M., Freeman, H.C., Guss, J.M., Murata, M., Norris, V.A., Rawshaw, J.A. and Venkatappa, M.P. (1978) ***Nature*** 272, 319-324.

[62] Haehnel, W., Pröpper, A. and Krause, H. (1980) ***Biochim. Biophys. Acta*** 593, 384-399.

[63] Reinman, S. and Mathis, P. (1981) ***Biochim. Biophys. Acta*** 635, 249-258.

[64] Bowes, J.M., Crofts, A.R. and Itoh, S. (1979) ***Biochim. Biophys. Acta*** 547, 336-346.

[65] Haehnel, W., Nairn, J.A., Reisberg, P. and Sauer, K. (1982) ***Biochim. Biophys. Acta*** 680, 161-173.

[66] Mauzerall, D.C. (1985) ***Biochim. Biophys. Acta*** 809, 11-16.

[67] Kamogawa, K., Morris, J.M., Takagi, Y., Nakashima, N., Yoshihara, K. and Ikegami, I. (1983) ***Photochem. Photobiol.*** 37, 207-213.

[68] Il'ina, M.D., Krasanskas, V.V., Rotomskis, R.J. and Borisov, A.Y. (1984) ***Biochim. Biophys. Acta*** 767, 501-506.

[69] Shuvalov, V.A., Klevanik, A.V., Sharkov, A.V., Kryukov, P.G. and Ke, B. (1979) ***FEBS lett.*** 107, 313-316.

Chapter Two: Energy Transfer and Fluorescence

2.1 Introduction

In higher plants excitation is absorbed by the antenna chlorophyll and transferred to the reaction center which acts as an energy trap and produces chemical energy. The mechanisms of excitation transfer within the antenna and energy trapping by the reaction center are important in understanding the high efficiency of energy conversion in photosynthesis. Little is known about the specific orientations of the chlorophyll molecules in the antenna of higher plants. As a result, it is difficult to develop models for the mechanisms and rates of excitation transfer. It is widely accepted that excitation migrates through the antenna chlorophyll by two mechanisms [1]. (1) Excitation can spread across closely coupled chromophores by exciton coupling. (2) Excitation transfer between more loosely associated chlorophyll molecules occurs by the Forster mechanism. This chapter describes these excitation migration mechanisms. Experimentally, time-resolved fluorescence is an important spectroscopic tool for measuring rates of energy transfer and excitation quenching.

2.2 Excitation Migration

Proteins define the antenna structure which confines the chlorophyll molecules to a densely packed environment. As a result, when an absorbed photon produces an electronic excited singlet state in one Chl a molecule the excitation delocalizes through a dipole-dipole coupling mechanism to another closely associated Chl a molecule. This exciton coupling can be observed by circular dichroism studies which monitor the relative orientation and number of interacting molecules [2]. Exciton coupling is present only when the chromophores are separated by less than 20A [3]. This can be put in the perspective of an individual Chl a molecule whose conjugated porphyrin ring is 10A square by 4A. Exciton delocalization among antenna Chl a occurs in less than one picosecond [4].

Excitation migrates between Chl a molecules separated by greater than 20A by the Forster resonance interaction. This is an electric dipole oscillation mechanism [5] where the rate of energy transfer (K_T) is described by:

$$K_T = \frac{3\phi_D \kappa^2}{4\tau_D \pi R^6} \int_0^\infty \frac{F_D(\omega)\sigma_A(\omega)}{(2\pi n)^4 \omega^4} \, d\omega$$

ϕ_D and τ_D are the quantum yield and lifetime of the donor in the absence of the acceptor. R is the distance between the donor and acceptor. n is the refractive index of the medium. σ_A is the acceptor's absorbance cross section and F_D is donor's emission intensity. κ defines the relative orientation and positions of the donor and acceptor transition dipoles. The rate of Forster energy transfer depends upon two important factors. (1) K_T is directly proportional to the overlap integral, which is the degree of spectral overlap between the donor's emissive and acceptor's absorptive spectra. (2) K_T is inversely proportional to R^6. Therefore, Forster energy transfer is most effective when Chl a molecules separated by 20-100A. These distances include the separation of two Chl a molecules in adjacent pigment protein complexes or the separation between antenna Chl a and the reaction center primary donor Chl a (P680 or P700).

2.3 Fluorescence

One can gain insight into energy transfer rates and mechanisms by monitoring the fluorescence yield and kinetics. The excitation and emission spectra describe the absorbing and fluorescing species in addition to detecting energy transfer between pigments. The fluorescence yields and lifetimes obtained from time-resolved measurements can provide rates of energy transfer and efficiencies of non-radiative excitation quenching. The fluorescence yield, ϕ_f, depends upon the rate constants of competing deexcitation processes:

$$\phi_f = \frac{K_f}{K_f + K_q}$$

K_f is the rate constant of fluorescence alone and is inversely dependent upon the intrinsic lifetime, τ_0, ($K_f = \frac{1}{\tau_0}$) which for chlorophyll a is about 15ns. K_q is the sum of the rate constants of all non-radiative deexcitation processes. Quenching mechanisms of singlet excited antenna or reaction center Chl a include intersystem crossing to a triplet state (K_{isc}), production of heat by internal conversion (K_{ic}), photochemical charge separation (K_p) and fluorescence (K_f). Thus, for Chl a in a photochemically active complex:

$$\phi_f = \frac{K_f}{K_f + K_{isc} + K_p + K_{ic}}$$

Changes in any of the deexcitation rate constants results in a change in fluorescence yield. Thus, the fluorescence yield is a measure of the photochemical efficiency of the reaction

center. If all competing deexcitation processes remain constant, inhibition of photochemistry is observed as an increase in the fluorescence yield.

2.4 Instrumentation

Our instrumentation for measuring picosecond fluorescence kinetics is diagrammed in Fig. 2.1 [6]. The excitation source consists of an acoustooptically mode locked (Spectra Physics SP 362 Ultrastable Mode Locker) argon ion laser (Spectra Physics SP 171) which pumps a Rhodamine 6G dye laser (Spectra Physics SP 375) producing a train of pulses, at 83MHz, with a FWHM of about 8ps. The jitter in the excitation pulses is 5ps. After passing through a beam splitter, an interference filter and a light pipe, the excitation pulse reaching the sample is 1-50mW. Because of the low excitation intensity, about 10^{6}-10^{8} photons per cm^2 per pulse, singlet-singlet annihilation is minimized. The detector is at a right angle from the excitation pulse. The excitation wavelength is determined by laser tuning and an interference filter; the emission wavelength is set by an interference filter.

Two types of detectors are employed, a microchannel plate detector (ITT F4129f), MCP, or a photomultiplier tube (RCA 31034A), PMT. Most measurements are made on the PMT with which the instrument response has a FWHM of 320-340ps and a time resolution of 50ps. Samples with lifetimes less than 70ps are remeasured and the decay rates confirmed with the MCP detector. The MCP is comprised of a photocathode (18mm diameter) located 0.3mm from an array of hundreds of thousands of hexagonally packed microchannels (12.5μm diameter, 2mm length) which merge into a single microchannel at the anode. The MCP operates at 2400V. The microchannels are parallel and aligned in a Z formation to obtain a higher gain (2×10^{6}) as the photoelectron can produce three cascade effects. Fluorescence photons are absorbed by the photocathode, ejecting a photoelectron which produces an amplified voltage while passing through the microchannels. The result is a high gain and a much shorter transit time than the PMT. The instrument response with the MCP has a FWHM of about 175ps and a time resolution of 20ps.

Both the PMT and MCP detectors employ the reverse single-photon counting timing mechanism outlined in Fig. 2.1. The fluorescence photon produces a voltage output which performs three functions: it triggers a count ratemeter allowing one to monitor the fluorescence intensity

Figure 2.1 Instrumentation for Prompt Fluorescence Kinetics. Abbreviations: M.L., Spectra Physics PS 362 Ultrastable Mode Locker; BS, beam splitter; P.D., Texas Instruments 55 photodiode; lev. disc., level discriminator; F1, excitation wavelength interference filter; F2, emission wavelength interference filter; P.M., photon detector- either MCP (ITT F4129f) or PMT (RCA 31034A); CFD, constant fraction discriminator; TAC, Canberra 2043 time to amplitude converter; ADC, Northern 1024 analog to digital converter; MCA, Northern NS636 multichannel analyzer. [6]

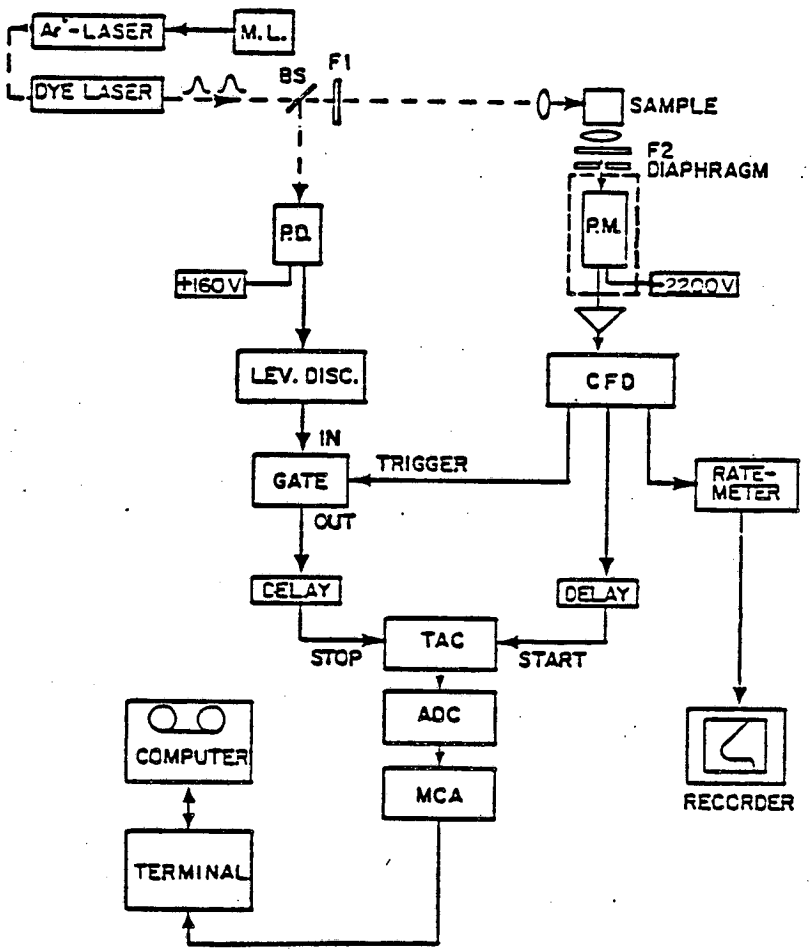

PHOTON TIMING SYSTEM

XBL 811-4422

during a measurement; it starts a voltage ramp in the time-to-amplitude converter (Canberra 2043 TAC); it signals the gate box to allow the next laser excitation pulse to stop the voltage ramp in the TAC. The laser repetition rate is too high for the TAC to be triggered on each pulse. However, a fluorescence photon is detected once in about 10^3 laser pulses and the gate box prevents laser pulses from affecting the TAC unless it has been triggered by a fluorescence photon. Thus, we start our timing with the fluorescence photon and stop it with the next laser flash. The voltage output from the TAC is proportional to the time between the fluorescence photon and the excitation pulse. It is converted to a digital signal by an analog-to-digital converter and stored in the appropriate channel of a multichannel analyzer (Northern NS636 MCA). The kinetic measurements are continued until the peak channel records 10^4 events. This can take 15sec to 15min depending on experimental conditions. The count rate meter is monitored throughout a measurement to be sure the fluorescence intensity remains constant. The MCA has 1024 channels, averaging 7.5ps each; lifetimes between 50ps and 4.0ns can be resolved.

2.5 Deconvolution and Kinetic Analysis

Ideally fluorescence kinetic data would be most easily analysed if the excitation source was a delta function. Experimentally this is not possible, and the observed fluorescence, I(t), is a convolution of the instrument response, E(u), and the actual fluorescence, F(t-u), where:

$$I(t)= \int_0^t E(u)\ F(t-u)\ du$$

E(u) is determined by using a scattering solution and is recorded often throughout an experiment since the excitation profile can change.

The fluorescence decay law, F(t), is assumed to be a sum of exponentials:

$$F(t)= \sum_{i=1}^{N} \alpha_i \exp^{-t/\tau_i}$$

where α_i and τ_i are the relative amplitudes ($\sum_{i=1}^{N} |\alpha_i| = 1$) and lifetimes, respectively, of the individual components. The relative yield ϕ_i, is defined as $\phi_i = \tau_i \alpha_i$. For given values of α_i and τ_i, a non-linear least squares routine calculates a sum of exponentials fluorescence decay law, convolutes the calculated decay with E(t) to obtain a calculated data profile $I_{calc}(t)$, compares $I_{calc}(t)$ with I(t) and varies α_i and τ_i to obtain the best fit. The goodness of the fit is given by:

Figure 2.2 CP1 Prompt Fluorescence Decay Kinetics. The log of intensity is displayed vs. time. The narrower trace is the laser excitation profile, E(t); the slower decay is the raw data, I(t). The smooth curve through I(t) is the fit, assuming the sum of three exponential components (listed above) to describe the fluorescence, F(t). Each component is characterized by its lifetime (τ), relative amplitude (α) and relative yield (ϕ), where $\phi = (\alpha)(\tau)$. The lower plot is the weighted difference between I(t) and the fit. $\chi^2 = .97$. The sample conditions are excitation wavelength, 620nm, and temperature, 298K.

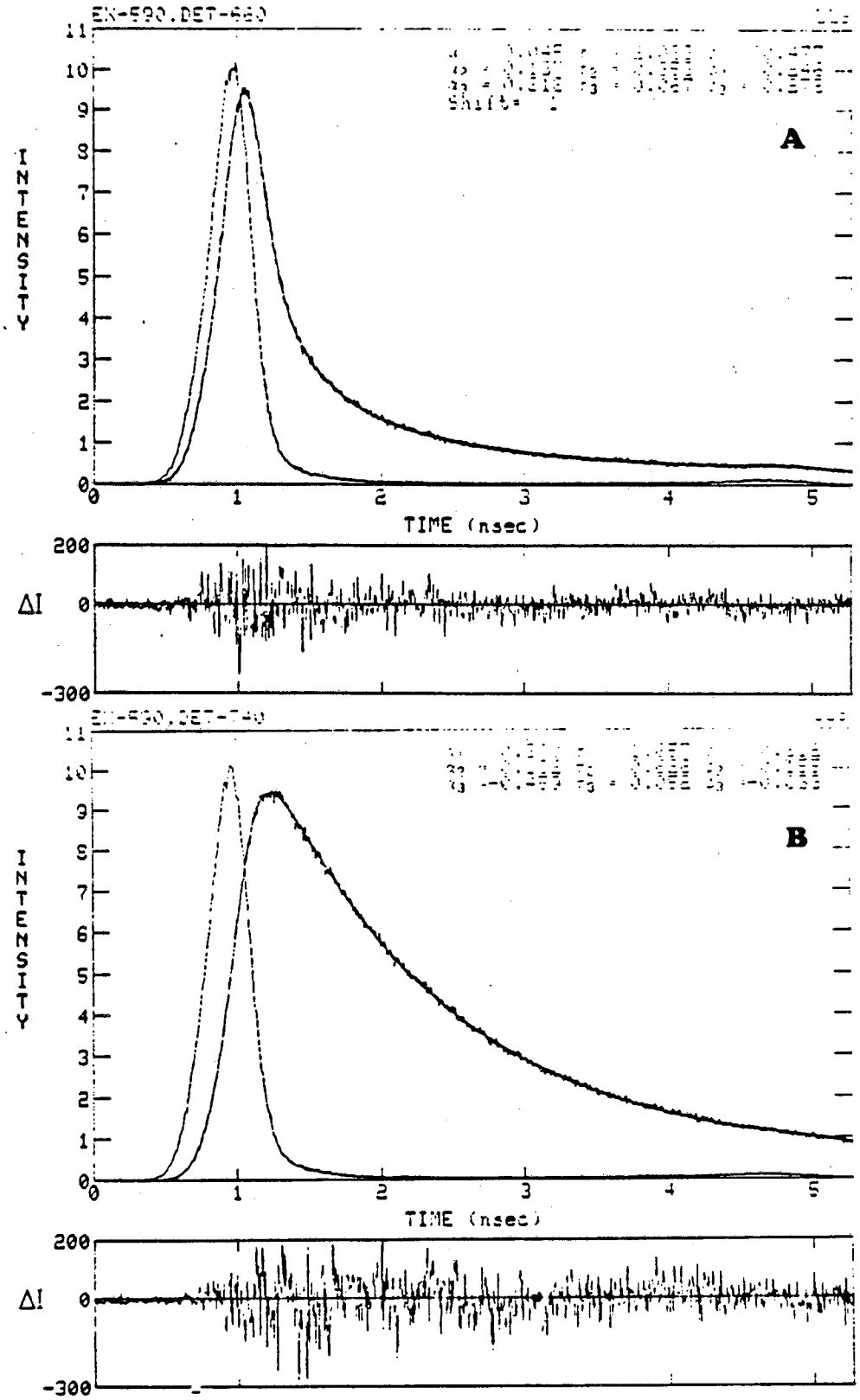
A
INTENSITY
TIME (nsec)
ΔI
B
INTENSITY
TIME (nsec)
ΔI

$$\chi^2 = \sum_{i=1}^{N} \omega_i \, [I(t) - I_{calc}(t)]^2$$

where ω_i is a statistical weighting factor, $\omega_i = 1/I(t)$. A χ^2 value of 1.0 is a perfect fit and 1.0 $\pm$ .2 is considered to be a good fit. Fig. 2.2 shows an example of the data analysis. The kinetic traces are log of fluorescence intensity vs. time. E(t) is the narrower trace; it reflects the excitation pulse. The wider trace showing noise is I(t). The fit $I_{calc}(t)$, is represented by the smooth line through I(t). The weighted difference between the data and the fit is shown at the bottom. The three components' α_i, τ_i and ϕ_i are listed and χ^2 is .97.

Data demonstrating a measurable fluorescence rise time are presented in Fig. 2.3. In Fig. 2.3A the fluorescence rise is instrument limited. Fig. 2.3B shows a fluorescence rise of 52ps. The amplitudes are measured at t=0, thus a rise component appears as a negative amplitude. Risetimes are not assumed when analyzing fluorescence data. Only positive α_i values are input as initial guesses, but the only way the non-linear least squares routine can fit some data is with risetimes. Most fluorescence traces can be fit to three exponentials; however, at temperatures below 260K, fluorescence from the 722nm emission band requires four components, 3 decays and 1 rise.

Time resolved data taken as a function of emission wavelength are also fit by a deconvolution analysis based on a global optimization algorithm provided by A.R. Holzwarth [7]. This procedure simultaneously analyzes the fluorescence decay curves at all measured emission wavelengths. The fluorescence decay law is described by the sum of exponentials explained above. It is assumed that the component lifetimes are independent of emission wavelength while the amplitudes, α_i, may vary. The lifetime constraint reduces the number of floating parameters and results in increasing the accuracy of the resolved component yields and amplitudes [8].

Finally, it is important to recognize that almost any fluorescence decay can be fit to a sum of three exponentials [9]. The motivation for applying a sum of exponentials to describe photosynthetic fluorescence is based on the expected exponential fluorescence decay predicted by the energy transfer theories outlined earlier in this chapter.

Figure 2.3 Picosecond Fluorescence Kinetics at 77K; instrument-limited vs. measurable rise times. The kinetic profiles are fluorescence intensity vs. time (ns). The narrow trace is the excitation pulse, E(t); the wider trace is the raw data, I(t). The line thru I(t) is the fit described by the sum of the exponential components listed. Each component is presented by its lifetime (τ), relative amplitude (α) and relative yield (ϕ), where $\phi = (\alpha)(\tau)$. The lower plots are the log of the difference between the data and the fit. The excitation wavelength is 590nm.

A. The emission wavelength is 660nm. χ^2 is 1.09. The rise is instrument limited and the decay is best fit to the sum of three exponential components with lifetimes of 2.1ns, 350ps and 70ps.

B. The emission wavelength is 740nm. χ^2 is 1.16. The rise is 52ps and the decay is fit to two components with lifetimes of 1.66ns and .63ns.

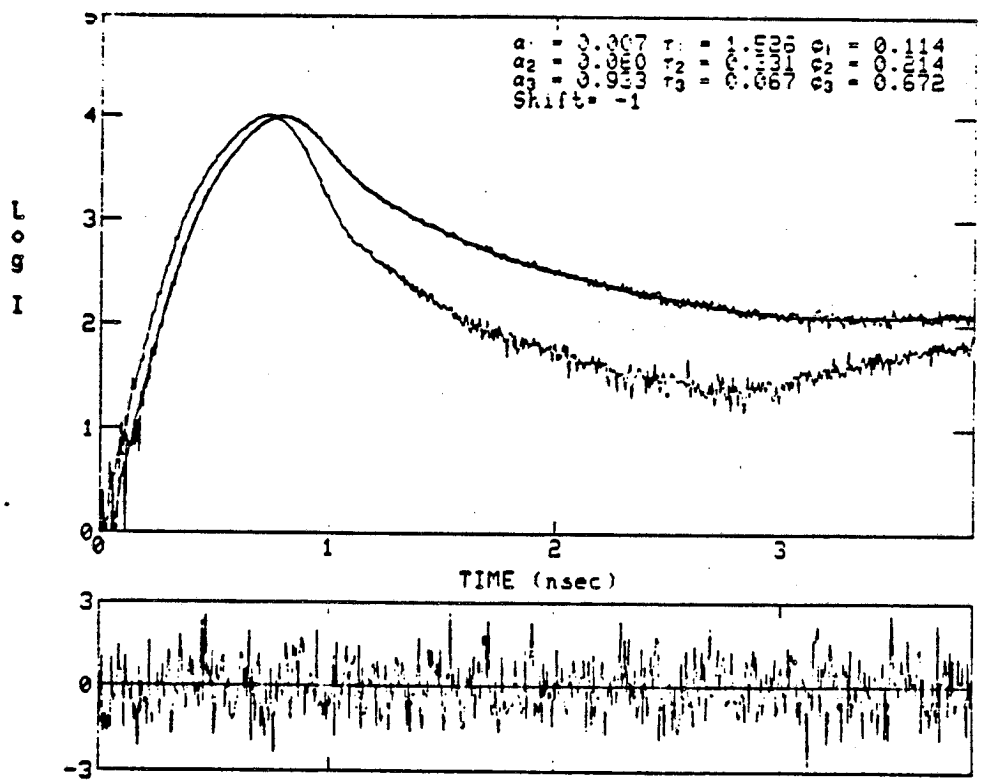
a1 = 0.307 τ1 = 1.526 φ1 = 0.114
a2 = 0.060 τ2 = 0.331 φ2 = 0.214
a3 = 0.933 τ3 = 0.067 φ3 = 0.672
Shift= -1
Log I
TIME (nsec)

2.6 References

[1] Sauer, K. (1981) ***Photosynthesis III. Structure and Molecular Organization of the Photosynthetic Membrane*** ed. G. Akoyunoglou, Balaban International Science Services, Philadelphia. pp. 685-699.

[2] Sauer, K. (1978) ***Accts. Chem. Res.*** 11, 257-264.

[3] Sauer, K. (1975) ***Bioenergetics of Photosynthesis*** ed. Govindjee, Academic Press, NY. pp. 118-181.

[4] Knox, R.S. (1977) ***Topics in Photosynthesis, Vol. II*** ed. J. Barber, Elsevier, Amsterdam. pp 55-97.

[5] Forster, T. (1965) ***Modern Quantum Chemistry, Part III*** ed. O. Sinanoglu, Academic Press, NY. pp. 93-137.

[6] Nairn, J.A. (1981) Ph.D. Thesis, University of California, Berkeley. p.77.

[7] Holzwarth, A.R., Max-Planck-Institut, Munich, West Germany.

[8] Wendler, J., John, W., Scheer, H. and Holzwarth, A.R. (1986) ***Photochem. Photobiol.*** 44, 79-85.

[9] Lakowicz, J. R. (1983) ***Principles of Fluorescence Spectroscopy*** Plenum Press, New York, ch. 3.

Chapter Three: Fluorescence and EPR Characterization of Linolenic Acid Inhibition in PS II

3.1 Acknowledgements

The work in this chapter was done in collaboration with Prof. John Golbeck (Portland State University). John provided the preliminary motivation for the experiments, participated in the initial sample preparation and data collection, and was continually encouraging in contributing insight into the analysis.

3.2 Introduction

Alteration of chloroplast membrane structure [1] and inhibition of photosystem II (PSII) electron transfer [2] are important effects of the unsaturated fatty acid, linolenic acid, upon photosynthetic systems. Both effects occur at μM concentrations of linolenic acid.

Electron microscopy revealed that the addition of 20-60μM linolenic acid to spinach chloroplasts results in the unfolding of grana stacks, and 100μM linolenic acid divides the chloroplasts into smaller vesicles. These transformations are reversible by bovine serum albumin (BSA) [1]. Linolenic acid has been reported to decrease the 77K chloroplast emission intensity at 735nm (F_{735}) relative to 698nm (F_{698}) in the presence of greater than 120μM linolenic acid (greater than a 3:1 molar ratio of linolenic acid to chlorophyll) [3].

I also see a linolenic acid-induced decrease of F_{735}/F_{698} in the emission spectra of chloroplasts at 77K. In addition, I observe dramatic changes in the 77K fluorescence spectra of digitonin-isolated PSII subchloroplast particles (D-10) produced by 66μM linolenic acid. Further, linolenic acid changes the room temperature absorption spectra of chloroplasts and D-10 particles. The fluorescence and absorption spectra are compared to identical measurements made in the presence of DCMU alone. DCMU had no effect on the absorption or emission spectra of chloroplasts or D-10 particles. Thus, the spectral changes due to linolenic acid do not arise only from electron transfer inhibition; they are more likely due to structural changes in the photosynthetic membranes.

In light of the structural changes induced by linolenic acid, it is important to determine that PSII is not photochemically inactivated. I observe, by EPR, a P680 spin-polarized radical pair

triplet (RPT) in D-10 particles treated with linolenic acid. The presence of the RPT confirms that charge separation and recombination occur in linolenic acid treated PSII particles.

Although it does not prevent primary photochemistry, linolenic acid does inhibit electron transfer in PSII. The photosystem II (PS II) reaction center consists of a primary electron donor, P680, a secondary donor, Z, and an electron acceptor complex composed of a molecule of pheophytin and a bound iron-quinone, Q_A [4]. A secondary quinone, Q_B, serves as a gate, accepting, in sequence, two electrons from Q_A and two protons before entering as plastohydroquinone into the mobile PQ/PQH_2 pool [5]. Q_B-site inhibitors, such as DCMU and atrazine, function by occupying the mobile quinone binding site on the 32-kD protein, thereby preventing electron flow from Q_A to the plastoquinone pool [6].

There is a growing body of evidence implicating inhibition by linolenic acid at the site of Q_A in PS II. Linolenic acid treatment is characterized by: (1) high initial fluorescence yield; (2) inhibition of electron flow from DPC to DCPIP; (3) absence of flash-induced P680 optical absorption changes on the microsecond timescale; (4) absence of EPR Signal II_f (Z^+) and Signal II_s. Linolenic acid affects components on both the oxidizing (Signal II) and the reducing (Q_A) sides of PS II [2,7,8].

The most characteristic attribute of linolenic acid is its ability to induce a rapid rise in the fluorescence from the F_0 level to the F_{max} level upon excitation. According to the model that variable fluorescence is a consequence of charge recombination between $P680^+$ and Ph^- [9], a blocked pathway for electron flow between Ph and Q_A should mimic the effect of the presence of Q_A^-. This chapter describes the fluorescence decay kinetics of stacked spinach chloroplasts and of digitonin-isolated PS II particles (D-10) in the presence of linolenic acid using a mode-locked dye laser with low-intensity excitation pulses and a single-photon timing detection system. The fluorescence decay characteristics of D-10 particles and chloroplasts at room temperature are best described by three exponential phases [10,11]. The fast phase appears to originate from both PS I and PS II; the middle phase may represent several different unresolved decay processes and probably has multiple origins [12,13]. The slow phase, however, is attributed to fluorescence from the radical pair recombination between $P680^+$ and Ph^-, which increases in yield as Q_A^- accumulates [14,15]. The use of extremely low laser excitation intensity allowed us to differentiate effects caused by inhibitors acting at the secondary quinone site, Q_B, or at the primary quinone site, Q_A.

3.3 Materials and Methods

Chloroplasts were isolated by grinding spinach for 10s in 400mM NaCl, 2mM $MgCl_2$, 1mM EDTA and 20mM Tris at pH 7.5, followed by straining through miracloth. The suspension was centrifuged at 12,000xg for 8min, and the pellet was washed in 150mM NaCl, 4mM $MgCl_2$, and 20mM Tris at pH 7.5. The resulting chloroplasts were suspended in 15mM NaCl, 5mM $MgCl_2$, and 50mM Tris at pH 7.5 for fluorescence measurements. D-10 particles were isolated by the method of Boardman [16] and suspended in the chloroplast buffer.

Room temperature absorption and 77K steady state emission measurements were made on chloroplasts and D-10 particles with an absorbance at 678nm of 0.4 and 0.5, respectively. Samples were buffered in 50mM Tris (pH 7.5), 10% glycerol, 10mM $MgCl_2$ and 15mM NaCl. The inhibitor concentrations were: linolenic acid, 66μM; DCMU, 20μM; and NH_2OH (hydroxylamine), 1mM. The inhibitors were added to the samples 3 min prior to absorption measurements, and 3 min prior to freezing at 77K in NMR tubes for the fluorescence measurements.

Steady state fluorescence measurements were performed on a SPEX Fluorolog 212T with a RCA photon-counting photomultiplier tube (RCA: C31034A; spectral response, 60ERX). Right angle detection was used, no filters were present, the excitation was at 438nm, and emission was corrected for monochromator and PMT wavelength dependence. The scan rate was 2.0nm/sec, and the instrument response was 0.5nm. For 77K measurements, the NMR tube was immersed in a liquid nitrogen dewar with an optically transparent finger. Condensation was prevented by passing nitrogen gas over the outside of the dewar. Absorption measurements were made on a Varian 2300 spectrophotometer. The instrument settings were: scan rate, 2nm/sec; response time, 1sec; and pathlength, 1cm.

EPR measurements were performed on D-10 particles, with a chlorophyll concentration of 4mg/ml [17], suspended in 15mM NaCl, 5mM $MgCl_2$ and 50mM Tris (pH 7.5). Linolenic acid was added to 4mM and dithionite was added under nitrogen gas to 50mM. The samples were dark adapted 5min and frozen at 77K in complete darkness. EPR samples were excited with white light modulated at 33Hz with the phase set to maximize the z peak of the radical pair spin-polarized triplet of *R. capsulata* chromatophores. EPR measurements were made on a Varian E-109 spectrometer operating at X-band and equipped with a liquid transfer Heli-Tran Cryostat (Air Products, Model LTR) and a TE_{102} cavity fitted with an 100% transmitting optical flange for

the exciting light. The instrument settings were: temperature, 6-8K; modulation amplitude, 32G; microwave frequency, 9.18GHz; microwave power, 0.1mW; modulation frequency, 100kHz; time constant, 1s; scan rate, 6.8G/s; spectrometer gain, x32000. Spectra were recorded on a digital oscilloscope (Nicolet Explorer IIIa), stored on a home-built signal averager and transferred to a VAX 11/780 computer. Field scans were signal averaged and normalized to the number of passes; signal amplitudes in all EPR spectra presented are directly comparable.

The fluorescence excitation source consisted of a Spectra Physics acoustooptically mode-locked argon ion laser pumping a Rhodamine 6G dye laser (SP171 ion laser, SP362 mode locker and SP375 dye laser). The system produces a train of pulses at 83MHz with a FWHM of 10ps. The maximum excitation intensity was 10^6 photons cm^{-2} per pulse. To measure the decay kinetics at F_0, the intensity was attenuated to 1-3% of the F_{max} excitation intensity with neutral density filters, and fluorescence was determined at room temperature with a 1-cm path cuvette. Interference filters (10nm bandwidth) were employed to detect 680nm emission photons at a right angle from the 620nm excitation pulses. The single-photon timing system and numerical analysis methods are described in Chapter Two. Fluorescence decays were fit to a sum of exponentials with a time resolution of about 50ps.

Fluorescence decay kinetics were recorded with a chlorophyll concentration of 10μg/ml. Inhibitor concentrations were 66μM for linolenic acid and 10μM for DCMU. Inhibitors were added in darkness 15s before measuring, and samples were stirred during measurements. Under F_{max} exciting conditions, measurements were begun after the fluorescence yield steadied at the maximum level. BSA was added to 1% (w/v) 15s after the addition of linolenic acid and 2min before the fluorescence decay was recorded.

Continuous illumination fluorescence rise curves were measured on D-10 particles at 10μg Chl/ml in 15mM NaCl, 5mM $MgCl_2$, 50mM Tris (pH 7.5). Inhibitor concentrations were 10μM DCMU and 100μM linolenic acid. Excitation was at 440nm (10nm bandwidth) and emission was detected at 690nm (10nm bandwidth) by a Hamamatsu (R928) photomultiplier tube and recorded on a digital oscilloscope (Nicolet Explorer IIIa). There was some scattering, which appears as a time independent contribution to the fluorescence level. The samples were dark adapted 10min, and inhibitors were added 1min prior to illumination.

3.4 Absorption and Emission Spectra

Linolenic acid affects the room temperature optical absorbance of D-10 particles and chloroplasts, Fig. 3.1. The absorption values at the wavelengths indicated with arrows are listed in the figure legend. The absorption values relative to the long wavelength peak at 678nm are given in Table 3.1. The absorption at 655nm, 620nm, 470nm and 438nm all increase 8-10% relative to that at 678nm in the presence of linolenic acid. DCMU has no effect on the absorption spectra of chloroplasts or D-10 particles, Fig. 3.1 and Table 3.1. Thus, the changes produced by linolenic acid in the absorption spectra of chloroplasts and D-10 particles are not simply a result of inhibition of electron transfer in PSII.

Linolenic acid has a more dramatic effect upon the 77K emission of chloroplasts and D-10 particles, Fig. 3.2. Due to the shattered state of the frozen sample, the chlorophyll absorption can vary depending upon the position of the sample relative to the excitation beam. Therefore, the emission spectra have been normalized at 685nm to facilitate comparing the spectra. Linolenic acid (66μM) produces two major effects upon the 77K emission spectra of chloroplasts (5μg Chl/ml). (1) There is a loss of the trough between the 685nm peak and the 698nm peak. This may arise from a decrease in intensity and a shift to the blue of the 698nm emission band. (2) There is a decrease in F_{735}/F_{698} from 1.7 to 1.3. The two dominant effects of 66μM linolenic acid on the 77K emission spectra of D-10 particles (6.3μg Chl/ml) are a decrease in F_{695} and a blue-shift of the 735nm peak to 730nm. It has been suggested that the 77K fluorescence band at 693-698nm originates from the reaction center pigment of PSII [18]. If the relative decrease of F_{695} upon addition of linolenic acid reflects a decrease in PSII fluorescence, it is occurring under conditions where PSII primary photochemistry is active as observed by spin-polarized radical pair triplet formation (next section). DCMU has no effect on the emission spectra of chloroplasts or D-10 particles, confirming that the observed changes due to linolenic acid arise from its effect upon photosynthetic membrane structure and not its inhibitory role in PSII electron transfer.

3.5 Results of EPR Measurements: P680 Spin-Polarized Radical Pair Triplet

To confirm that linolenic acid does not inactivate PSII primary photochemistry, I measured the P680 radical pair spin-polarized triplet (RPT) by EPR in D-10 particles treated with linolenic

Figure 3.1: The effect of linolenic acid on the room temperature optical absorption of D-10 particles and chloroplasts. The experimental conditions are described in the Materials and Methods section. All measurements were made on aliquots of a single D-10 or chloroplast sample; the chlorophyll concentrations are directly comparable. Linolenic acid was added to 66μM and DCMU/NH_2OH to 20μM and 1mM, respectively. The arrows in the figure indicate the wavelengths listed below. The absorbance values are accurate to $\pm$0.003.

	A_{678}	A_{655}	A_{620}	A_{470}	A_{438}
Chloroplasts					
No Additions, Fig. 3.1A	0.395	0.155	0.092	0.395	0.571
DCMU, Fig. 3.1B	0.397	0.155	0.095	0.393	0.572
Linolenic Acid, Fig. 3.1C	0.401	0.175	0.110	0.422	0.621
D-10 Particles					
No Additions, Fig. 3.1D	0.495	0.224	0.119	0.547	0.773
DCMU, Fig. 3.1E	0.506	0.229	0.122	0.559	0.795
Linolenic Acid, Fig 3.1F	0.491	0.238	0.129	0.585	0.807

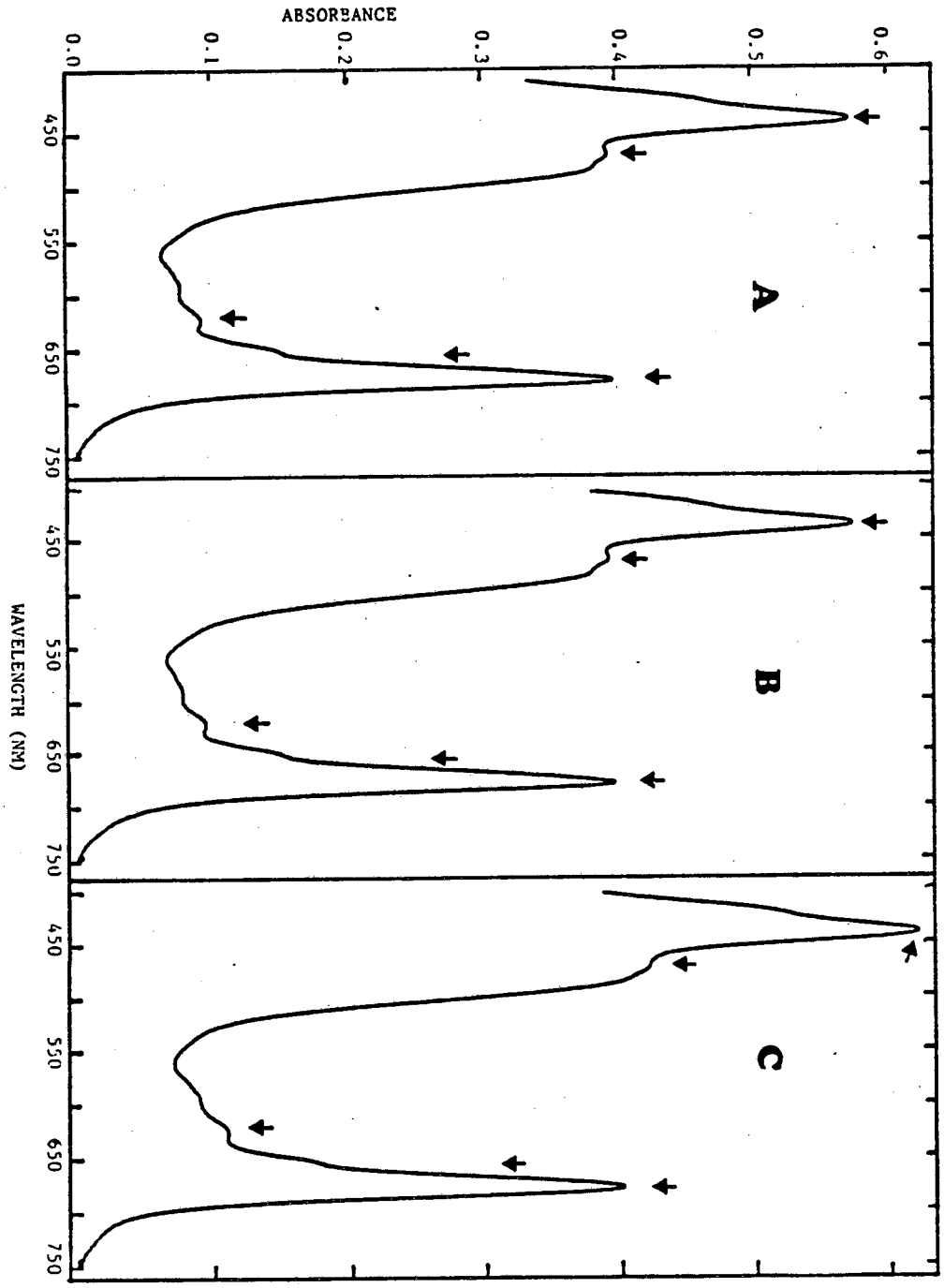
ABSORBANCE
0.0
0.1
0.2
0.3
0.4
0.5
0.6
A
B
C
450
550
650
750
WAVELENGTH (NM)

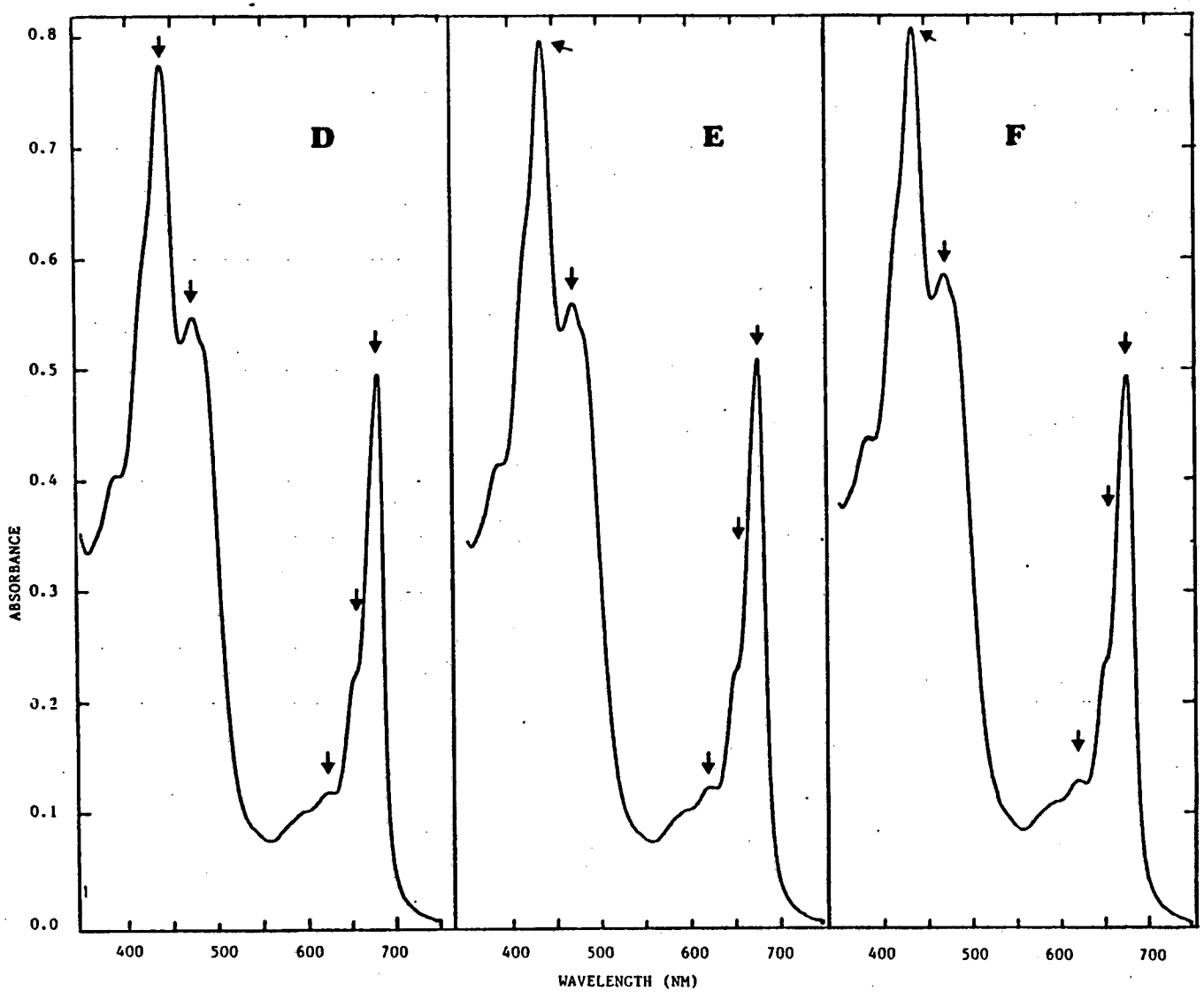
D
E
F
ABSORBANCE
0.0
0.1
0.2
0.3
0.4
0.5
0.6
0.7
0.8
400
500
600
700
WAVELENGTH (NM)

Figure 3.2: The effect of linolenic acid on the steady state emission of chloroplasts and D-10 particles at 77K. The sample and inhibitor concentrations are the same as in Figure 3.1. The experimental conditions are describes in the Materials and Methods section. The excitation wavelength is 438nm. The measurements were made on samples with the same concentration of chlorophyll. However, due to the shattered state of the frozen sample, the chlorophyll absorption can differ depending on the position of the sample relative to the excitation beam. Therefore, the emission spectra have been normalized at 685nm to facilitate comparing the spectra.

A. Chloroplast emission spectra at 77K with no additions (heavy line), with 20μM DCMU and 1mM NH_2OH (thin line) and with 66μM linolenic acid (heavy line).

B. D-10 particles emission spectra at 77K with no additions (heavy line), with 20μM DCMU and 1mM NH_2OH (thin line) and with 66μM linolenic acid (heavy line).

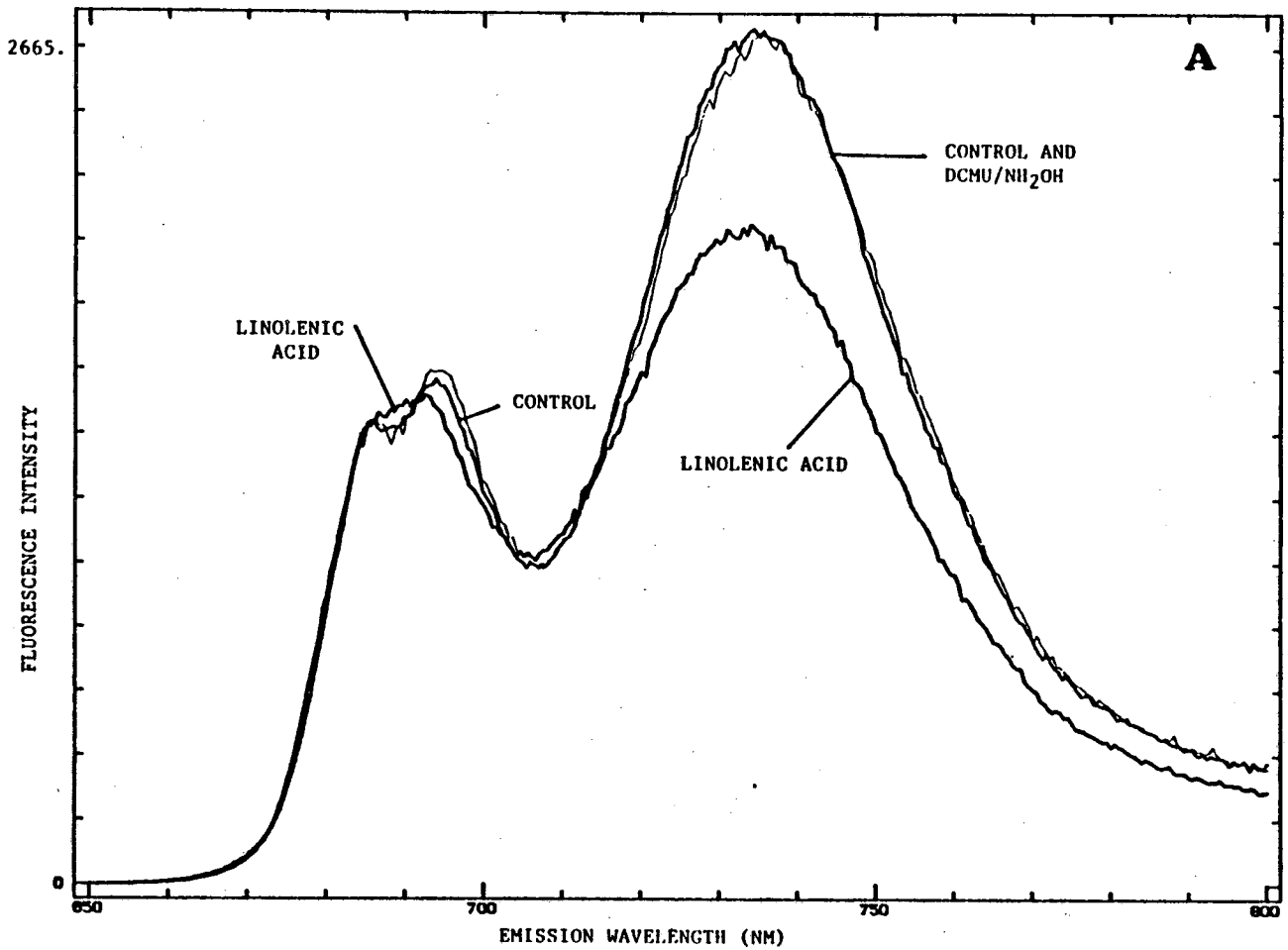
A
2665.
0
FLUORESCENCE INTENSITY
650
700
750
800
EMISSION WAVELENGTH (NM)
CONTROL AND
DCMU/NH2OH
LINOLENIC
ACID
CONTROL
LINOLENIC ACID

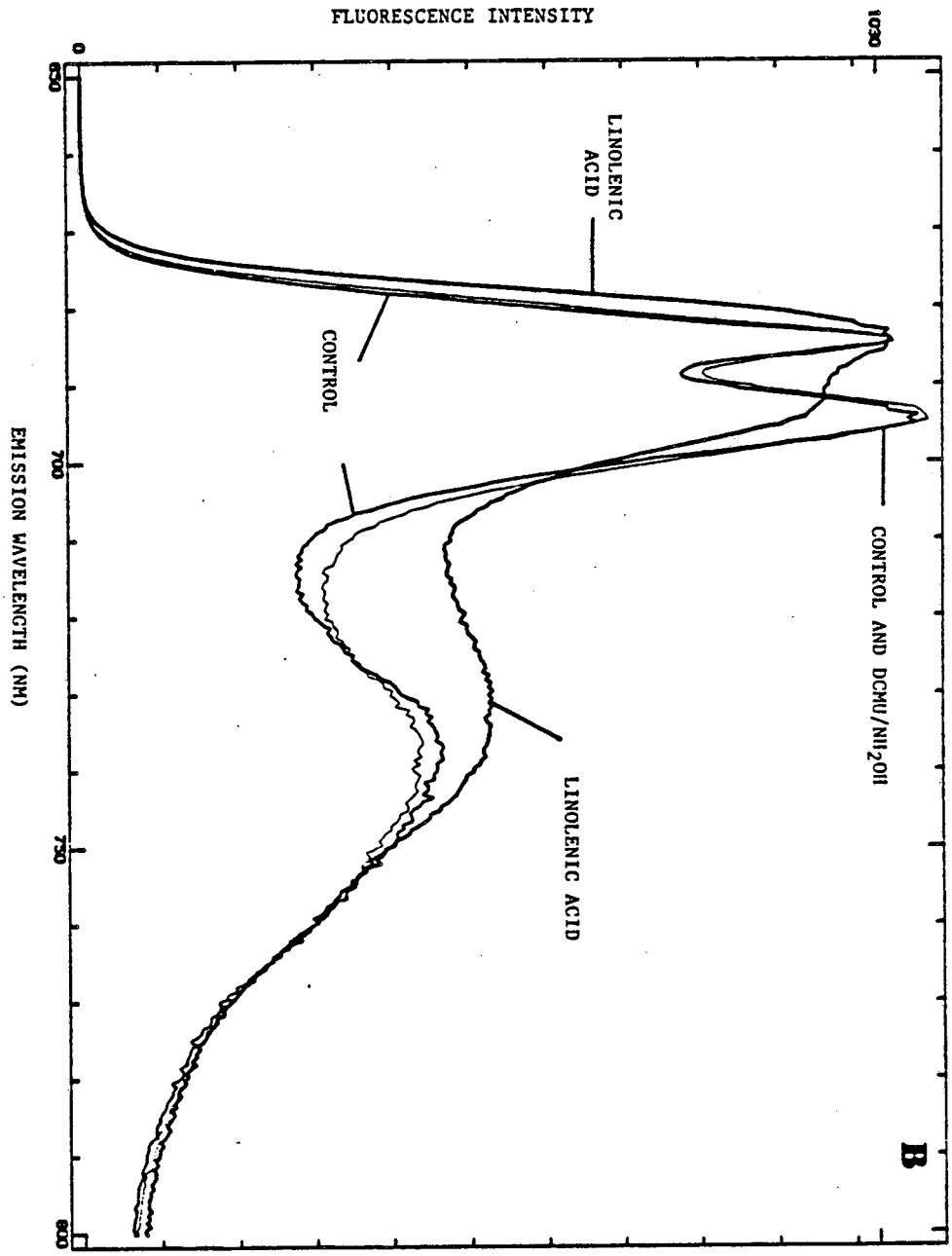
B
CONTROL AND DCMU/NH2OH
LINOLENIC ACID
CONTROL
LINOLENIC ACID
FLUORESCENCE INTENSITY
1000
0
650
700
750
800
EMISSION WAVELENGTH (NM)

acid. A RPT is indicative of charge separation and recombination in an active reaction center (described in Chapter Four).

Untreated samples exhibit no inhibition of electron transfer through the acceptors; charge recombination does not occur to a significant extent, and a RPT is not observed, (Fig. 3.3d). Addition of dithionite (pH 10) reduces Q_A, which prevents forward electron transfer and results in recombination, and a RPT is observed, (Fig. 3.3a). The zero field splittings of $|D|$ = .0284 cm^{-1} and $|E|$ = .0042 cm^{-1} $\pm$.0008 cm^{-1} are consistent with reported values for P680 RPT [19]. Addition of 4mM linolenic acid to dithionite-reduced PS II particles does not inhibit the RPT formation in D-10 particles under conditions that lead to a high fluorescence yield at F_0, (Fig. 3.3b). Although the chlorophyll concentrations necessary for EPR are considerably higher than those for fluorescence measurements, the same ratio of linolenic acid to chlorophyll was used in both studies. Thus, linolenic acid appears not to inactivate the primary photochemistry in the PS II reaction center.

D-10 particles in the presence of linolenic acid alone do not produce a RPT, (Fig. 3.3c). Similar results were observed by Warden et al. [20] and will be discussed later.

3.6 Results of Fluorescence Induction Curves

Although linolenic acid does not inactivate charge separation, it appears to inhibit electron transfer in PSII. The fluorescence behavior upon continuous illumination of D-10 particles before and after the addition of 10μM DCMU are shown in Fig. 3.4. Because the rate-limiting step in photosynthetic electron transport occurs between reduced plastoquinone and the cytochrome f/b_6 complex, the area over the rise curve (Fig. 3.4a) represents the photoreduction of Q_A and the plastoquinone pool. An inhibitor such as DCMU, which blocks electron flow from Q_A to Q_B, produces an abbreviated rise curve that reflects solely the reduction of Q_A (Fig. 3.4b). The fluorescence rise curve of chloroplasts inhibited with linolenic acid is shown in Fig. 3.4c. Even though the inhibitor was added in darkness, the initial level of fluorescence is at the level of the maximum fluorescence yield (F_{max}) observed in untreated D-10 particles (Fig. 3.4a). The complete absence of area over the rise curve after addition of linolenic acid is quite unlike the inhibition with DCMU and indicates that the photochemical traps are closed within the instrument response time (6msec). Assuming that variable fluorescence arises from $P680^+$

Figure 3.3. Light-modulated EPR detection of the P680 radical pair spin-polarized triplet in D-10 particles. The excitation light was modulated at 33Hz with the phase set to maximize the z peak of the radical pair spin-polarized triplet in ***R. capsulatus*** chromatophores. Instrument settings were: modulation amplitude, 32G; microwave power, .1mW; modulation frequency, 100kHz; time constant, 1s; scan rate, 6.8G/s; microwave frequency, 9.18GHz; temperature, 6-8K; spectrometer gain, x32000. All spectra are signal averaged and normalized to the number of passes so that all signal amplitudes are directly comparable. The samples were dark adapted 5min and frozen at 77K in complete darkness. The chlorophyll concentration was 4mg/ml.

The uncertainty in the zero field splitting parameters is .0008cm^{-1}.

A. ***Dithionite***: 50mM dithionite, $|D|$ = .0284cm^{-1}, $|E|$ = .0043cm^{-1}.

B. ***Dithionite and Linolenic Acid***: 4mM linolenic acid and 50mM dithionite, $|D|$ = .0284cm^{-1}. $|E|$ = .0041cm^{-1}.

C. ***Linolenic acid***: 4mM linolenic acid.

D. ***Control***: no additions.

Figure 3.5. Fluorescence decay of D-10 particles (top) and chloroplasts (bottom) in the presence of linolenic acid (66μM) or DCMU (10μM) at F_0 and F_{max}. All samples contain 10μg Chl/ml in 50mM Tris (pH 7.5), 15mM NaCl and 5mM $MgCl_2$. The excitation wavelength was 620nm; the emission wavelength was 680nm. The instrument time resolution of 50ps limited all fluorescence rises.

PS2 PARTICLES (D-10)

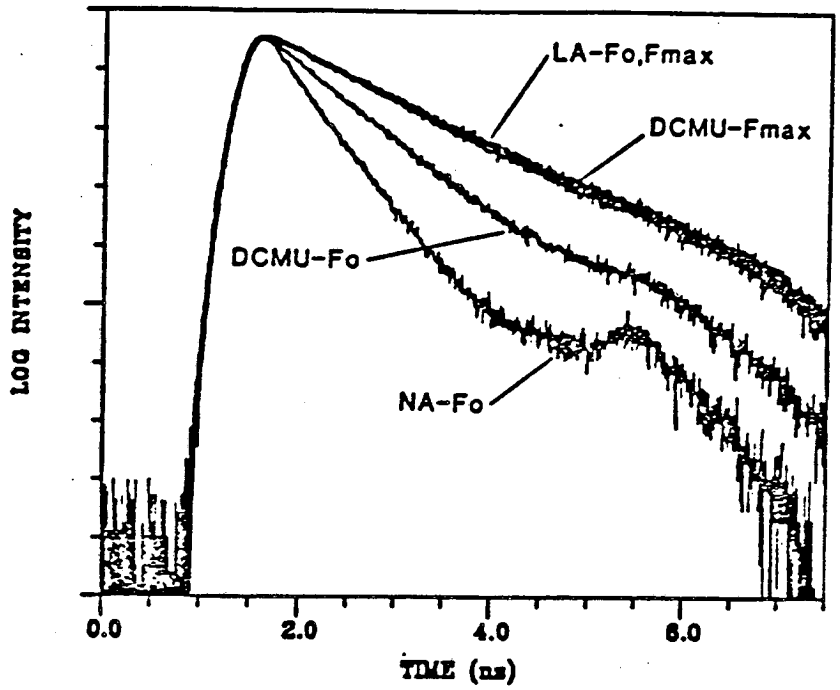

(a)

CHLOROPLASTS

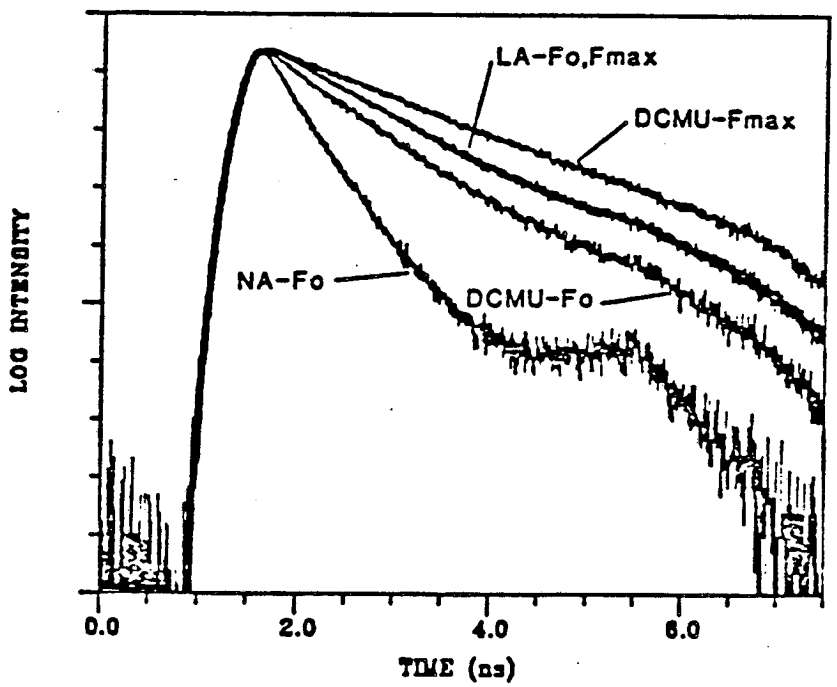

(b)

XBL 853-1550

increase in laser excitation intensity raises the fluorescence yield from F_0 to F_{max}. The lifetime and relative amplitude of the slow component increase in both preparations as the excitation intensity is raised, and the major contributor to the total fluorescence yield shifts from the middle to the slow component [10].

Addition of 66μM linolenic acid leads to an increase in the total fluorescence yield under low excitation intensity (F_0) reflecting an increase in the yield and lifetime of the slow kinetic component in both preparations (Tables 3.2 and 3.3). In the presence of linolenic acid the total fluorescence yield increases only 1.6-fold between F_0 and F_{max} in chloroplasts and D-10 particles. The identical fluorescence lifetime and relative yield of the slow kinetic component under high (F_{max}) and low (F_0) excitation conditions indicates that linolenic acid closes the photochemical traps prior to illumination.

Addition of DCMU to chloroplasts results in qualitatively different fluorescence decay characteristics. Under low-intensity excitation conditions (F_0) the intensity was sufficient to cause a somewhat higher total fluorescence yield than in control chloroplasts, owing to an accumulation of Q_A^-. There is, nevertheless, a 2.5-fold difference in the total fluorescence yield in chloroplasts and a 3.1-fold difference in the total fluorescence yield in D-10 particles between low-intensity (F_0) and high-intensity (F_{max}) excitation in the presence of DCMU. More importantly, the relative yield and lifetime of the slow component show a consistent increase between F_0 and F_{max} in both preparations. This is quite unlike the effect of linolenic acid, where the slow component showed the same relative yields and lifetimes at F_0 and F_{max}.

3.8 Reversibility of Fluorescence Decay Characteristics

The effects of linolenic acid on the fluorescence yield and decay kinetics are reversible in the presence of bovine serum albumin (BSA), Fig. 3.6. The addition of 1% BSA alone to chloroplasts (Table 3.2) causes a 2.2-fold increase in the lifetime of the slow component at F_0 without affecting the total fluorescence yield or the relative yields of the three decay components. In D-10 particles, at F_0, BSA has little effect on the lifetime of the slow component, but nearly doubles its yield, resulting in a small increase in the total fluorescence yield (Table 3.3).

BSA addition to chloroplasts and D-10 particles that have been incubated for 15s with 66μM linolenic acid results in a lowering of the total fluorescence yield (Tables 3.2 and 3.3).

Figure 3.6. Reversibility of linolenic acid effects in D-10 particles (top) and chloroplasts (bottom) by bovine serum albumin at F_0 exciting intensities. LA, linolenic acid (66μM); BSA, bovine serum albumin (1%). All curves are normalized at their maximum intensity. Linolenic acid was added 15sec before measurement (LA) or BSA addition (LA, BSA). BSA was added 2min before measurement. For the D-10 particles, addition of BSA to particles alone or to particles plus linolenic acid resulted in identical decay curves. All samples contained 10μg Chl/ml in 50mM Tris (pH 7.5), 15mM NaCl and 5mM $MgCl_2$. The excitation wavelength was 620nm; the emission wavelength was 680nm. The instrument time resolution of 50ps limited all fluorescence rises.

PS2 PARTICLES (D-10)

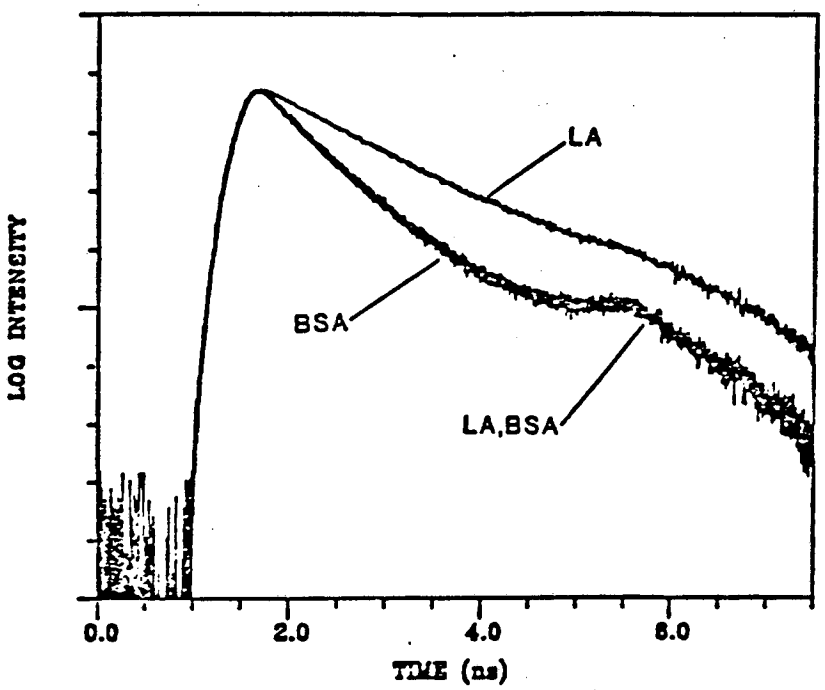

(a

CHLOROPLASTS

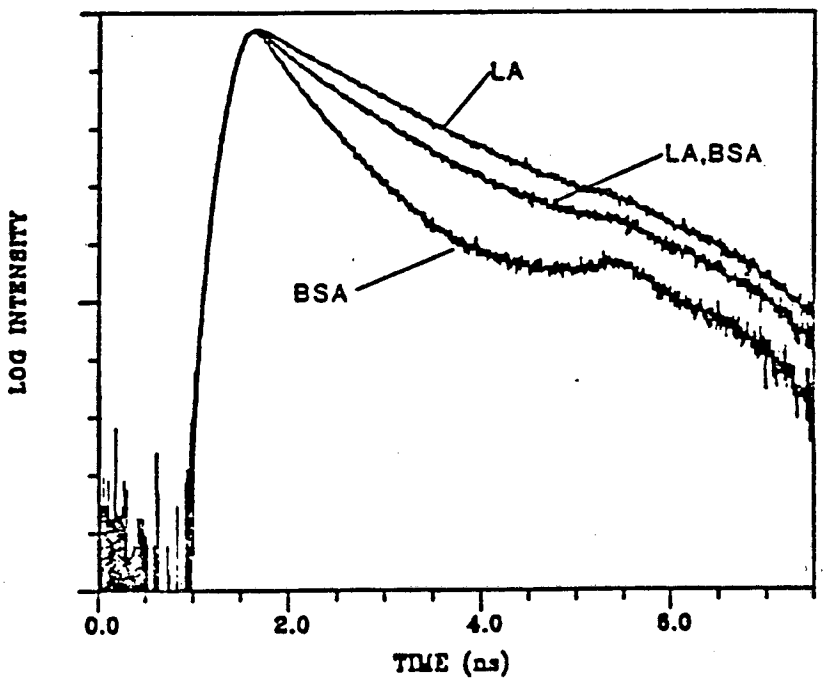

(b

XSL 853-1651

The decay kinetics in D-10 particles under low excitation intensity (F_0) after reversal (LA, BSA) is similar to the kinetics with BSA alone (Fig. 3.6a). In chloroplasts, the fluorescence behavior after BSA addition (LA, BSA) is only partially reversed (Fig. 3.6b). The lifetime of the slow component is appreciably shortened in chloroplasts after reversal compared with that in the presence of BSA alone (Table 3.2). In sum, the reversibility by BSA of the total fluorescence yield is 86% in D-10 particles and about 28% in chloroplasts.

3.9 Discussion

Our fluorescence induction and prompt fluorescence kinetic data indicate that linolenic acid acts as an inhibitor of PSII electron transfer. The yield of the slow fluorescence decay component in chloroplasts increases as Q_A is reduced chemically or with light [10,14]. Klimov, et al [9] proposed that the slow component originates from charge recombination between $P680^+$ and Ph^- and migration of the excitation back to the antenna before being emitted. When 66μM linolenic acid is added to spinach chloroplasts or to D-10 particles, the yield and lifetime of the slow fluorescence component are increased, and the yield of the middle component under low excitation intensities (F_0) is decreased. The lifetimes and relative yields of the fluorescence decay components at F_0 matched those obtained under high intensities, F_{max}, indicating that the inhibition leading to charge recombination in the reaction center occurs in the dark.

In the presence of DCMU, Q_A is not reduced prior to illumination, and the fluorescence yields and lifetimes under sufficiently low laser excitation intensity (F_0) should match those of the control chloroplasts and PS II particles. In practice, even at our lowest excitation intensity, we observed an increase in the total fluorescence yield during the first few seconds of illumination owing to the low rate of Q_A^- oxidation in the absence of a well-connected plastoquinone pool. This effect is more pronounced in stacked spinach chloroplasts than in D-10 particles.

Bovine serum albumin (BSA) affects the fluorescence decay kinetics causing an increase in the lifetime of the slow kinetic decay component at F_0 which is most pronounced in chloroplasts and hardly detectable in D-10 particles. The absence of a significant increase in the total fluorescence yield upon addition of BSA to either D-10 particles or chloroplasts indicates that the traps remained open under these conditions. As is the case with the steady-state fluorescence

yield [2], the effect of linolenic acid on the decay kinetics was partially reversed in chloroplasts and completely reversed in D-10 particles by addition of 1% BSA. Other than the ability of BSA to bind fatty acids, the mechanism of its effect upon fluorescence decay kinetics is not known.

The significant difference in the fluorescence induction rise curves and the decay kinetics between linolenic acid-treated and DCMU-treated chloroplasts or D-10 particles confirm that the two inhibitors block electron transfer at different sites. DCMU inhibits electron flow from Q_A to Q_B, which we observe as an abbreviated rise curve to F_{max} and an increase in the lifetime and relative yield of the slow fluorescence decay component as Q_A becomes reduced under illumination. The fluorescence of linolenic acid treated samples rises immediately to F_{max} upon illumination and exhibit the same decay kinetics at low (F_0) and high (F_{max}) exciting light intensities. The linolenic acid induced fluorescence decay kinetics are similar to DCMU induced kinetics at F_{max} for chloroplasts and are identical for D-10 particles. We conclude that by blocking electron transfer at the primary quinone, P680 Ph // Q_A Q_B, linolenic acid in the dark produces a state similar to DCMU at F_{max}.

Using EPR at 6-8K, I observe a P680 spin-polarized radical pair triplet (RPT) upon illumination of dithionite reduced D-10 particles, with and without the addition of linolenic acid. The RPT arises from charge separation and recombination. Thus, linolenic acid does not inactivate primary photochemistry in PSII.

The RPT is not observed in D-10 particles treated with linolenic acid in the absence of dithionite. We propose two possible explanations for this unexpected behavior. (1) At cryogenic temperatures electron donation is slowed to a point where electrostatic interactions may have a significant effect on electron transfer rates. Specifically, recombination of $P680^+$ and Ph^- may have different kinetics depending on the oxidation state of Q_A. Addition of dithionite in the dark reduces Q_A and all subsequent electron acceptors, P680 Ph Q_A^- Q_B^-. Charge separation results in an unfavorable coulombic interaction between Ph^- and Q_A^-, and rapid $P680^+$ Ph^- recombination occurs to form the EPR detectable P680 RPT. Let us assume that linolenic acid blocks electron transfer at the primary quinone site without affecting the oxidation state of the acceptors, P680 Ph // Q_A Q_B. The charge separated state is electrostatically more stable, $P680^+$ Ph^- // Q_A Q_B than when Q_A is reduced, so that $P680^+$ reduction is dominated by electron donation from a secondary donor. At 7K we would not expect to see

a 2ns fluorescence component. This remains to be tested. (2) The absence of a P680 RPT in linolenic acid treated samples could also be explained by invoking an additional acceptor which shuttles electrons from Ph to Q_A. Such an acceptor has been proposed [21-23]; Evans et al. measured its reduction potential to be -430mV (pH = 10) and labeled it X [21]. In the presence of dithionite (pH 10) the dark state of PS II would be P680 Ph X^- Q_A^-, and light-induced charge separation/recombination would result in RPT formation. Assuming that linolenic acid inhibits at the primary quinone, linolenic acid treated samples will have electron transfer blocked between X and Q_A, P680 Ph X // Q_A. Illumination should produce the charge separated state $P680^+$ Ph X^- // Q_A, which does not recombine to form a P680 RPT.

Dithionite-treated: P680 Ph X^- Q_A^- $\xrightarrow{h\nu}$ $P680^+$ Ph^- X^- Q_A^- $\rightarrow$ RPT

Linolenic acid-treated: P680 Ph X // Q_A $\xrightarrow{h\nu}$ $P680^+$ Ph X^- // Q_A $\rightarrow$ no RPT

It is not easy to understand an instantaneous fluorescence rise if this model is correct, because the fluorescence should initially be low, and only rise as X becomes reduced upon illumination of linolenic acid-treated samples. There is much work to be done employing EPR to study the effects of linolenic acid on electron transfer, including the questions raised in this report: the absence of a RPT in the PS II particles treated with linolenic acid alone and the increase in the amplitude of the RPT when linolenic acid is added to dithionite reduced PS II particles. However, the EPR measurements described in this chapter are fundamental in confirming that linolenic acid does not inhibit PSII primary photochemistry.

While the fluorescence kinetic data indicate that linolenic acid plays a role as an inhibitor of PSII electron transfer, dramatic changes in the room temperature absorption and 77K emission spectra of chloroplasts and D-10 particles indicate that linolenic acid also plays a role in structural transformations of the photosynthetic membranes. I find that linolenic acid decreases the relative long wavelength absorption maxima in chloroplasts and D-10 particles. Similar spectral changes in linolenic acid-treated chloroplasts have been reported [24]. This long wavelength bleaching induced by linolenic acid treatment originates predominantly from PSII and is independent of photochemical activity [25]. Linolenic acid (66μM) induces a decrease in intensity and a shift to the blue of the 698nm emission band, and a decrease in F_{735}/F_{698} from 1.7 to 1.3 in chloroplasts (5μg Chl/ml) at 77K. These changes are similar to a previous report that

at 77K F_{735}/F_{698} in chloroplasts decreases from 2.17 with 40μM Chl and 120μM linolenic acid to 1.1 with 40μM Chl and 400μM linolenic acid; the spectral changes are reported to reflect unstacking of the grana [1]. A more dramatic effect is found in D-10 particles, where I observe a large decrease in the relative intensity of F_{695} in the presence of linolenic acid. F_{695} is thought to arise from a PSII reaction center chromophore [18]. However, the linolenic acid-induced spectral changes, observed in my measurements, do not inhibit PSII primary photochemistry as confirmed by the presence of a RPT in linolenic acid-treated PSII particles.

In conclusion, we have shown that while linolenic acid does not inactivate the primary charge separation and recombination in PS II, it does play several roles in the photosynthetic system. (1) Linolenic acid induces structural transformations in the chloroplast membranes, including unstacking of the grana. (2) Linolenic acid decreases the relative long wavelength absorbance of chloroplasts and D-10 particles. This bleaching, in chloroplasts, has been reported to be associated primarily with PSII [25]. (3) Linolenic acid decreases the relative 77K emission intensity at 695nm, which is thought to be associated with a PSII reaction center chromophore. (4) Linolenic acid inhibits PS II electron transfer in a manner different from that of DCMU. DCMU suppresses electron flow from Q_A to Q_B (P680 Ph Q_A // Q_B). In contrast, our results support the conclusion that linolenic acid effectively closes the traps by blocking electron transfer from pheophytin to Q_A (P680 Ph // Q_A Q_B). It is important to recognize these widespread effects when observing linolenic acid treated photosynthetic complexes.

Table 3.1: The Effect of Linolenic Acid on Optical Absorbance.

	A_{655}/A_{678}	A_{620}/A_{678}	A_{470}/A_{678}	A_{438}/A_{678}
Chloroplasts				
No additions, Fig. 3.1A	0.39	0.23	1.0	1.45
DCMU, Fig. 3.1B	0.39	0.24	1.0	1.44
Linolenic Acid, Fig. 3.1C	0.44	0.27	1.1	1.55
D-10 Particles				
No additions, Fig. 3.1D	0.45	0.24	1.11	1.56
DCMU, Fig. 3.1E	0.45	0.24	1.11	1.57
Linolenic Acid, Fig. 3.1F	0.49	0.26	1.19	1.64

These are the results of the room temperature absorption spectra of several chloroplast and D-10 particle preparations. The values are accurate to ±0.01. The experimental conditions are given in the Materials and Methods section and the caption of Fig. 3.1.

TABLE 3.2

CHARACTERISTICS OF THE FLUORESCENCE DECAY IN SPINACH CHLOROPLASTS

Chloroplasts were freshly prepared and suspended at 10μg Chl/ml in 50mM Tris (pH 7.5), 15mM NaCl and 5mM $MgCl_2$. τ, 1/e lifetime in ns; φ(i), relative yield of the ith component, where $\sum_i \varphi(i)=1$; φ(T), the total fluorescence yield measured during lifetime measurements and normalized to DCMU at F_{max}.

	No Additions			Linolenic Acid			DCMU			BSA			Linolenic acid, BSA		
	τ(ns)	φ(i)	φ(T)	τ(ns)	φ(i)	φ(T)	τ(ns)	φ(i)	φ(T)	τ(ns)	φ(i)	φ(T)	τ(ns)	φ(i)	φ(T)
F_0	1.09	.16	16	1.47	.81	41	1.36	.84	41	2.43	.20	16	1.51	.79	34
	.42	.73		.53	.16		.54	.13		.45	.70		.49	.17	
	.11	.12		.11	.03		.11	.03		.10	.11		.07	.03	
F_{max}	1.86	.94	98	1.46	.87	65	1.69	.96	100						
	.69	.05		.42	.11		.62	.02							
	.13	.02		.08	.02		.13	.02							

The standard deviations, based on repeated measurements, are 80ps, τ(slow); 50ps, τ(middle); 20ps, τ(fast); <.05 φ(i); 2.5 φ(T).

TABLE 3.3

CHARACTERISTICS OF THE FLUORESCENCE DECAY IN SPINACH D-10 PARTICLES

D-10 particles were suspended at 10μg Chl/ml in 50mM Tris (pH 7.5), 15mM NaCl, and 5mM $MgCl_2$. τ, 1/e lifetime in ns; φ(i), relative yield of the ith component where $\sum\phi(i)=1$; φ(T), total fluorescence yield measured during lifetime measurements and normalized to DCMU at F_{max}.

	No Additions			Linolenic Acid			DCMU			BSA			Linolenic Acid, BSA		
	τ(ns)	φ(i)	φ(T)	τ(ns)	φ(i)	φ(T)	τ(ns)	φ(i)	φ(T)	τ(ns)	φ(i)	φ(T)	τ(ns)	φ(i)	φ(T)
F_0	.86	.24	18	1.22	.79	47	1.24	.55	32	.97	.45	24	1.15	.57	22
	.40	.66		.46	.18		.60	.41		.38	.51		.47	.38	
	.09	.10		.07	.03		.09	.05		.05	.04		.11	.05	
F_{max}	1.12	.67	55	1.29	.79	77	1.39	.82	100						
	.48	.29		.51	.19		.57	.15							
	.05	.03		.04	.03		.07	.03							

The standard deviations, based on repeated measurements, are 80ps, τ(slow); 70ps, τ(middle); 20ps, τ(fast); .09, φ(slow); .08, φ(middle); .01, φ(fast); 6.0, φ(T).

3.10 References

[1] Okamoto, T., Katoh, S. and Murakami, S. (1977) ***Plant Cell Physiol.*** 18, 551-560.

[2] Golbeck, J.H., Martin, I.F. and Fowler, C.F. (1980) ***Plant Physiol.*** 65, 707-713.

[3] Cohen, W.S., Nathanson, B., White, J.E. and Brody, M. (1969) ***Arch. Biochem. Biophys.*** 135, 21-27.

[4] Vermaas, W.F.J. and Govindjee (1981) ***Photochem Photobiol*** 34, 775-793.

[5] Cramer, W.A. and Crofts, A.R. (1982) in ***Photosythesis*** (Govindjee, ed) Volume 1, pp 387-467, Academic Press, New York.

[6] Mullet, J.E. and Arntzen, C.J. (1981) ***Biochim. Biophys. Acta*** 635, 236-248.

[7] Golbeck, J.H. and Warden, J.T. (1984) ***Biochim. Biophys. Acta*** 767, 263-271.

[8] Vernotte, C., Solis, C., Moya, I., Maison, B., Briantais, J.M., Arris, B. and Johannin, G. (1983) ***Biochim. Biophy. Acta*** 725, 376-383.

[9] Klimov, V.V., Klevanik, A.V., Shuvalov, N.A. and Krasnovsky, A.A. (1977) ***FEBS Lett.*** 82, 183-186.

[10] Haehnel, W., Nairn, J.A., Reisberg, P. and Sauer, K. (1982) ***Biochim. Biophys. Acta*** 680, 161-173.

[11] Nairn, J.A., Haehnel, W., Reisberg, P. and Sauer, K. (1982) ***Biochim. Biophys. Acta*** 682, 420-429.

[12] Green, B., Karukstis, K.K. and Sauer, K. (1985) ***Biochim. Biophys. Acta*** 767, 574-581.

[13] Karukstis, K.K. and Sauer, K. (1984) ***Biochim. Biophys. Acta*** 766, 148-155.

[14] Karukstis, K.K. and Sauer, K. (1983) ***Biochim. Biophys. Acta*** 722, 364-371.

[15] Karukstis, K.K. and Sauer, K. (1983) ***Biochim. Biophys. Acta*** 725, 264-253.

[16] Boardman, N.K. (1971) ***Methods in Enzymology*** 23A, 269-276.

[17] Arnon, D.I. (1949) ***Plant Physiol.*** 24, 1-15.

[18] Krey, A. and Govindjee (1966) ***Biochim. Biophys. Acta*** 120, 1-9.

[19] Rutherford, A.W., Paterson, D.R. and Mullet, J.E. (1981) ***Biochim. Biophys. Acta*** 635, 205-214.

[20] Warden, J.T. and Csatorday, K. (1986) ***Biophys. J.*** 49, 486a.

[21] Evans, M.C.W., Atkinson, Y.E. and Ford, R.C. (1985) ***Biochim. Biophys. Acta*** 806, 247-254.

[22] Hoff, A.J. and Proskuryakov, I.I. (1985) ***Biochim. Biophys. Acta*** 808, 343-347.

[23] Warden, J.T. Personal communication.

[24] Luthy, B., Martinoia, E., Matile, P. and Thomas, H. (1984) ***Z. Pflanzenphysiol.*** 113, 423-434.

[25] Luthy, B., Thomas, H. and Matile, P. (1986) ***J. Plant Physiol.*** 123, 203-209.

Chapter Four: Preparation and Characterization of the PS I Reaction Center Complex, CP1

4.1 Introduction

Isolation of reaction center complexes is an important technique for studying the photochemical properties of individual photosystems. In higher plants, the similarity between many of the characteristics (e.g. peptide composition, electron paramagnetic resonance (EPR), absorption, fluorescence) of photosystem one (PS I) and photosystem two (PS II) makes it difficult to assign experimental results to a particular photosystem. It is common to prepare samples containing the fewest components sufficient to carry out the photochemistry in question.

Several PS I reaction center complex preparations have been developed using a variety of techniques. I have focused on isolating a reaction center complex CP1 that has few components while maintaining the *in vivo* primary photochemical reactions and kinetics. CP1 consists of an apoprotein with reported molecular weight values varying from 110 to 160kD which is thought to contain an oligomer of one or two peptides in the 58-70kD range, a small pool of antenna chlorophyll a molecules, and a primary donor, P700, and acceptor, A_0, capable of charge separation [1-4]. The presence of phylloquinone as a secondary acceptor, A_1, has been suggested [5] while subsequent acceptors (X, Fd_A, Fd_B) are inactive or absent. This chapter describes the preparation and characterization of the CP1 complex.

4.2 Materials and Methods

CP1 can be isolated from crude PS I particles extracted with the detergent Triton X-100 from spinach thylakoids. The isolation technique involves non-denaturing sodium dodecyl sulfate polyacrylamide gel electrophoresis (SDS-PAGE).

The entire preparation of CP1 particles is carried out on ice or at 277K with minimal exposure to light. Spinach leaves are ground in a high salt buffer (400mM NaCl, 2mM $MgCl_2$, 1mM EDTA, 20mM Tris, pH 7.5) and passed sequentially through 2-fold then 32-fold cheesecloth layers. The suspension is then concentrated (12,000xg for 10min) and resuspended (150mM NaCl, 4mM $MgCl_2$, 20mM Tris, pH 7.5). Soluble components are removed by centrifugation (12,000xg for 10min). The pellet is resuspended to

1 mg Chl/ml (15mM NaCl, 5mM $MgCl_2$, 50mM Tris, pH 7.5). Triton X-100 is added, 20:1 (w/w) detergent to chlorophyll, to separate PS I and the light harvesting complex (LHC) from the thylakoid membrane following centrifugation (39,000xg for 30min).

The supernatant is diluted in a buffer compatible with the SDS-PAGE system onto which it is loaded (gel conditions below). Gels are run in the dark until the slowest migrating dark green band is sufficiently separated from other bands to be cut out. The electrophoresis separates the PS I reaction center from the LHC and nonpigmented membrane proteins. A Coomassie-Blue stained denaturing SDS-PAGE (gel conditions below) of this PS I reaction center shows a diffuse band from 62 to 65kD, plus two faint bands around 20-25kD. The smaller peptides are the light harvesting complex associated with PS I. Further purification of the PS I reaction center is obtained by loading the initial gel band onto a second, identical non-denaturing SDS-PAGE system. The slowest migrating green band from this gel is cut out, homogenized, and incubated in buffer (15mM NaCl, 5mM $MgCl_2$, 50mM Tris, pH 7.5) with .1% (w/v) SDS, in the dark, at 277K for 12hrs. The eluted CP1 is separated from the acrylamide by centrifugation (35,000xg for 15min) and dialyzed (against 50mM Tris, pH 7.5), with a 10-12kD cutoff, to remove free SDS and chlorophyll.

The sample can be stored at 253K, in the dark, for at least two weeks without any change in the P700 photobleaching (kinetics or quantity), the steady state fluorescence or absorption spectra, or the prompt fluorescence decay kinetics.

All SDS-PAGE is done by the methods of Laemmli [6]. Only Bio-Rad electrophoresis-grade reagents are used and all solutions are filtered (Whatman #1). The following SDS-PAGE systems are employed: the tank buffer contains 0.1% (w/v) SDS, 192mM glycine, 250mM Tris, pH 8.3; the stacking gel is made up of 0.1% SDS, 123mM Tris, 4% (w/v) acrylamide with 0.35% (w/w) bis-acrylamide crosslinker, 0.05% (w/v) ammonium persulfate, 0.05% (w/v) TEMED, pH 6.8; the running gel is similar except that it is 10% acrylamide, 500mM Tris, pH 8.8. The sample buffer is 62.5mM Tris, 10% (v/v) glycerol, 0.1% SDS, pH 6.8; for denaturing gels it contains 2% SDS plus 5% (v/v) 2-mercaptoethanol. Sample prep gels are 9x16x0.6cm, have no wells and are precooled to 277K; denaturing gels are 18x16x0.15cm. Denaturing gels are run at a constant power of 5W to stack, then 25W (at 295K); prep gels are run at a constant current of 100mA to stack, then 190mA (at 277K).

All steady state absorption measurements are made using a Varian 2300 Spectrophotometer. The pathlength is 10mm. Steady state fluorescence measurements are performed on a SPEX Fluorolog 212T with a RCA photon-counting, photomultiplier tube (RCA: C31034A; spectral response, 60ERX). All excitation scans are corrected for the lamp and monochromator wavelength dependence; all emission scans are corrected for the emission monochromator and photomultiplier tube wavelength dependence. Front face detection is used to minimize self-absorption. A 389nm cut-off filter is placed in front of the photomultiplier tube to eliminate second harmonic peaks.

Measurements at 77K are made in a liquid nitrogen-filled, cylindrical, pyrex dewar placed directly in the excitation beam. Dry nitrogen gas is blown over the outer dewar surface to prevent condensation. The sample suspension contains 30-50% (w/v) glycerol and is frozen slowly in a 4mm diameter NMR tube or a 2mm EPR tube to a uniformly finely shattered state. Active samples are dark adapted and frozen in the dark, unless otherwise noted.

Light-induced absorption changes at 699nm are used to determine the number of active primary donors, P700. An AMINCO DW-2 Spectrophotometer is set up with a tungsten lamp side illumination as the excitation source. The excitation beam is limited to 330-660nm (Corning filter 4-96), and passes through a water bath and focusing lens, before entering the sample compartment via a fiber optic cable. A 700nm interference filter, with a 10nm bandpass, is placed in front of the detector. The pathlength is 10mm and the instrument response is 100ms. The measurements are made, with 10 μg Chl/ml, in 5mM ascorbate.

EPR measurements are performed on a Varian E-109 spectrometer operating at X-band and equipped with an Air Products Helitran cryostat. The sample cavity, with a 100% optically transmitting flange, is kept at a constant temperature in the range 8 to 12K, and monitored with a gold-chromel thermocouple.

For steady state scans, a home-built signal averager triggers the field sweep, and the EPR spectrum is recorded on a digital oscilloscope (Nicolet Explorer IIIA with a model 204 plug-in). The EPR spectra are signal averaged to improve the signal-to-noise. To observe the radical pair spin polarized triplet (RPT) a light minus dark spectrum is obtained by chopping a white, tungsten exciting light (50-100 mW cm^{-2}) at 33.5 Hz, and passing the light through a 5cm water bath and light pipe before reaching the sample. The phase of the exciting light

modulation is set to maximize the z peak of the RPT from *Rps. capsulata* chromatophores. All scans are transfered to a VAX 11/780 computer for analysis.

4.3 Peptide Composition

There is considerable controversy over the peptide composition of the CP1 apoprotein. The discrepancies are highly dependent upon sample and gel conditions (i.e., SDS concentration, presence of dithiothreitol or 2-mercaptoethanol, heating, percent acrylamide). Some workers observe a single polypeptide at 65kD [7], 68kD [2,8] or 70kD [9]. Others report doublets at 58 and 62kD [1] or 62 and 65kD [4]. Peptide digests (CNBr cleavage or *S. aureus* proteolysis) produce homologous peptide fragments [1]. The possibility of one polypeptide being a degradation product of the other is unlikely, because the presence of the protease inhibitor phenylmethanesufonyl fluoride (PMSF) throughout the prep and gel has no effect on the doublet ratios [1]. It had been previously proposed that the two peptides arise from a post-translational modification of polypeptides with identical primary structure [10]. However, a recent report indicates that two partially homologous genes encode two CP1 core proteins which are not subject to extensive post-translational processing [11].

A denaturing (2% SDS, 5% 2-mercaptoethanol, at 295K) SDS-PAGE comparing spinach chloroplasts to isolated CP1 complex is shown in Fig 4.1. Lane 2 contains chloroplast thylakoid membranes. The dark band at about 50kD is from coupling factor CF-1, and the band at 25kD is the light harvesting complex. Lane 3 contains the isolated CP1 reaction center complex. We observe a diffuse band at 65kD with perhaps a faint band at 62kD, but no additional detectable bands at lower molecular weights.

4.4 Absorption and Emission Spectra of the CP1 Complex

The absorption spectrum of CP1 at room temperature is shown in Fig 4.2. The long wavelength absorption maximum is at 675nm. The lack of chlorophyll b is apparent from the missing absorbance peaks around 650nm and 470nm. The complete absence of chlorophyll b from CP1, as determined by chromatography, has been reported [4].

A 735nm emission band has been reported to dominate the 77K PS I fluorescence spectrum [12-14]. More recently, it has been shown that removal of the peripheral PS I associated light harvesting complexes (designated LHC or LHCP1) coincides with the following effects: a

Figure 4.1 A denaturing SDS-PAGE showing the peptide composition of spinach chloroplasts and the isolated CP1 complex. The samples are solubilized in 2% SDS and 5% 2-mercaptoethanol. The gel is 15% acrylamide. The SDS-PAGE conditions are detailed in Methods.

Lane 1,4	protein standards: phosphorylase B, 92.5kD; bovine serum albumin, 66.2kD; ovalbumin, 45.0kD; carbonic anhydrase, 31.0kD; soybean trypsin inhibitor, 21.5kD; lysozyme, 14.4kD. These water soluble protein standards have different migration behavior different from those of membrane proteins; molecular weights are only approximate.
Lane 2	chloroplast thylakoid membranes
Lane 3	purified CP1 complex

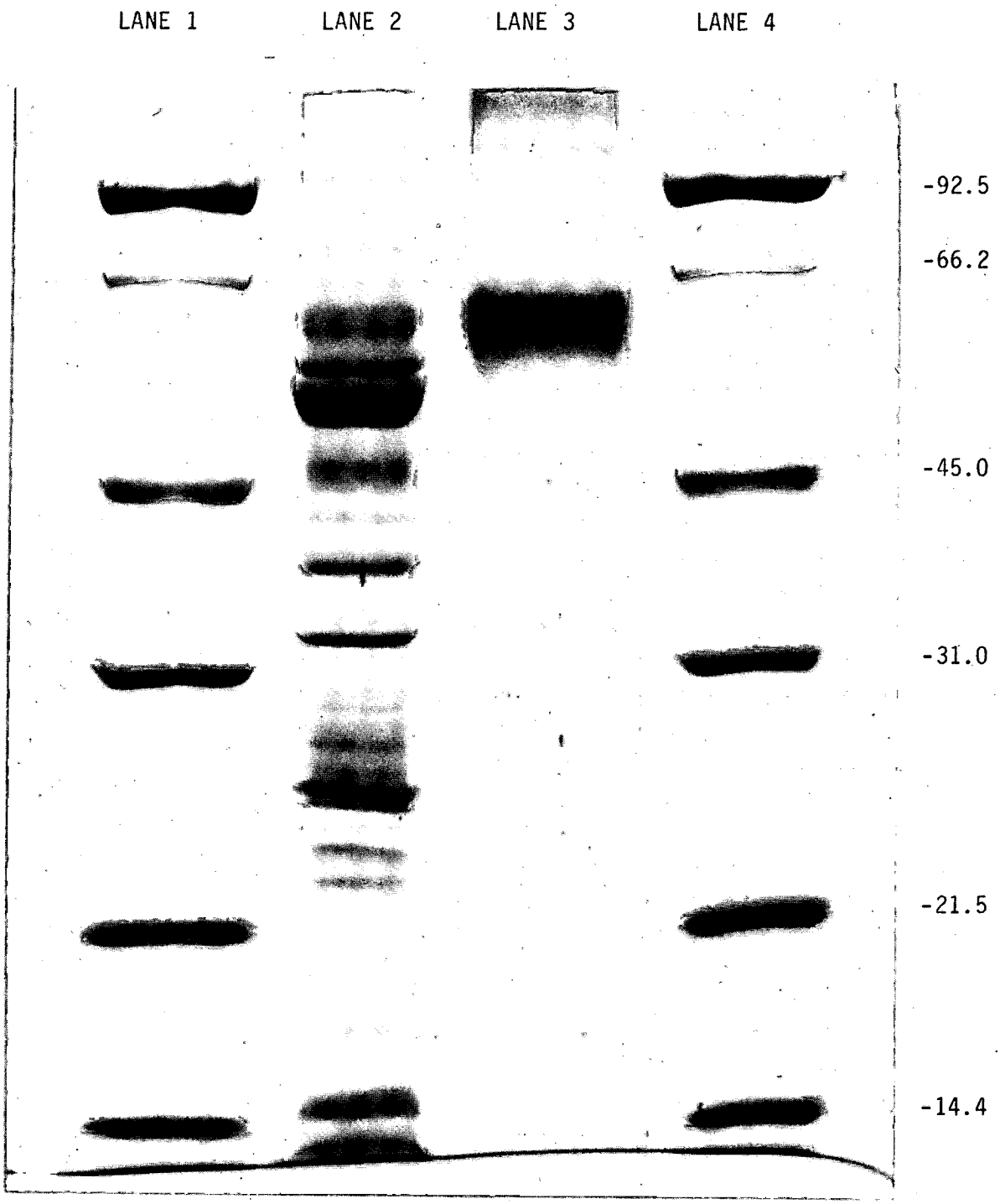

XBB 832-1180

Figure 4.2 An optical absorption spectrum of the CP1 complex. T, 298K; pathlength, 10mm; scan rate, 2nm/s; response time, 500ms.

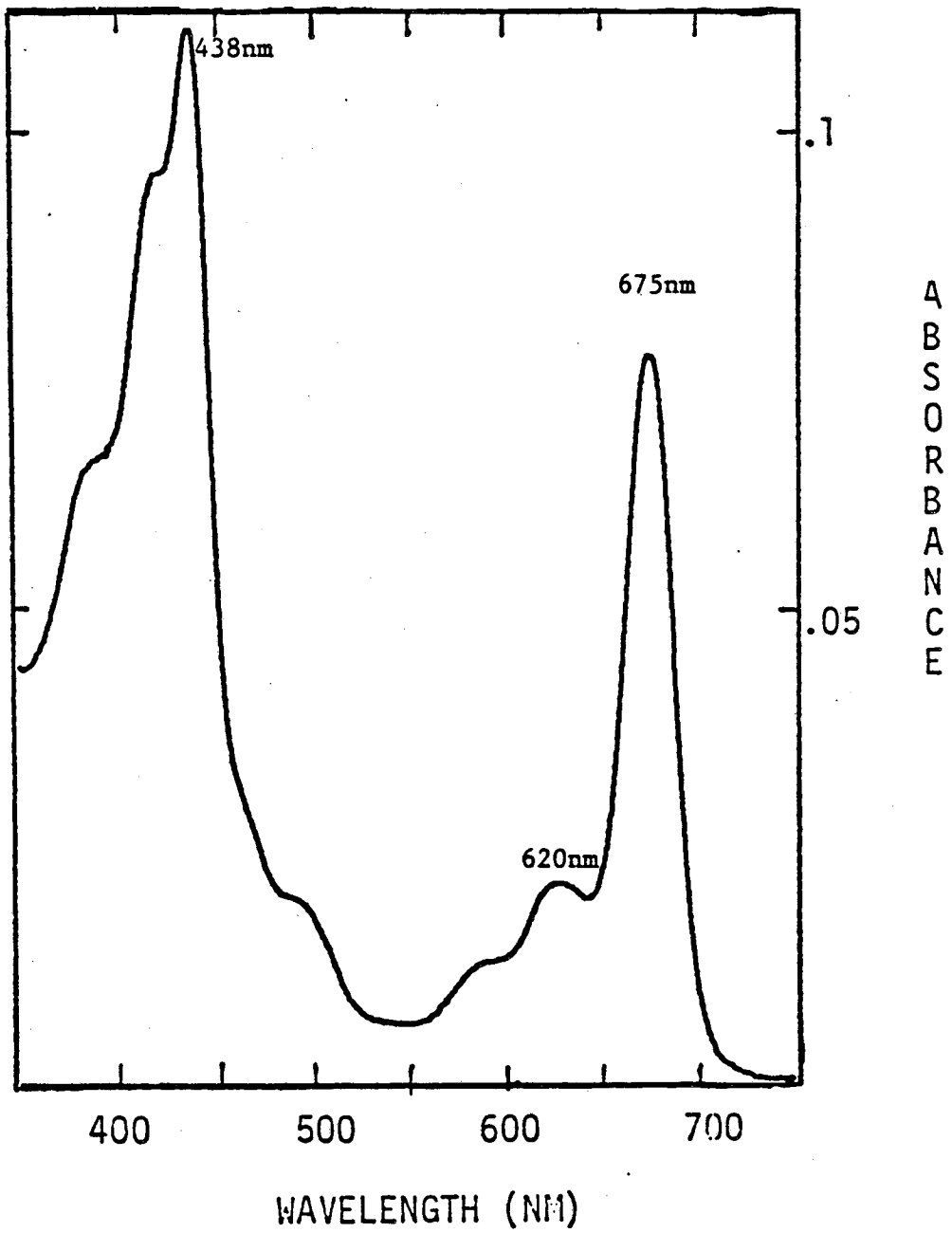
438nm
675nm
620nm
.1
.05
ABSORBANCE
400
500
600
700
WAVELENGTH (NM)

Figure 4.3 The fluorescence emission spectra of the CP1 complex at 77K and 295K. The CP1 particles are suspended in 15mM NaCl, 5mM $MgCl_2$, 50mM Tris, pH 7.5, 50% glycerol) with A_{675} = 0.2. The excitation wavelength is 438nm. The slits are set with a 4nm bandpass. The spectra are corrected for the wavelength dependence of the emission monochromator and the detector. The emission maxima are 690nm at T = 295K and 722nm at T = 77K.

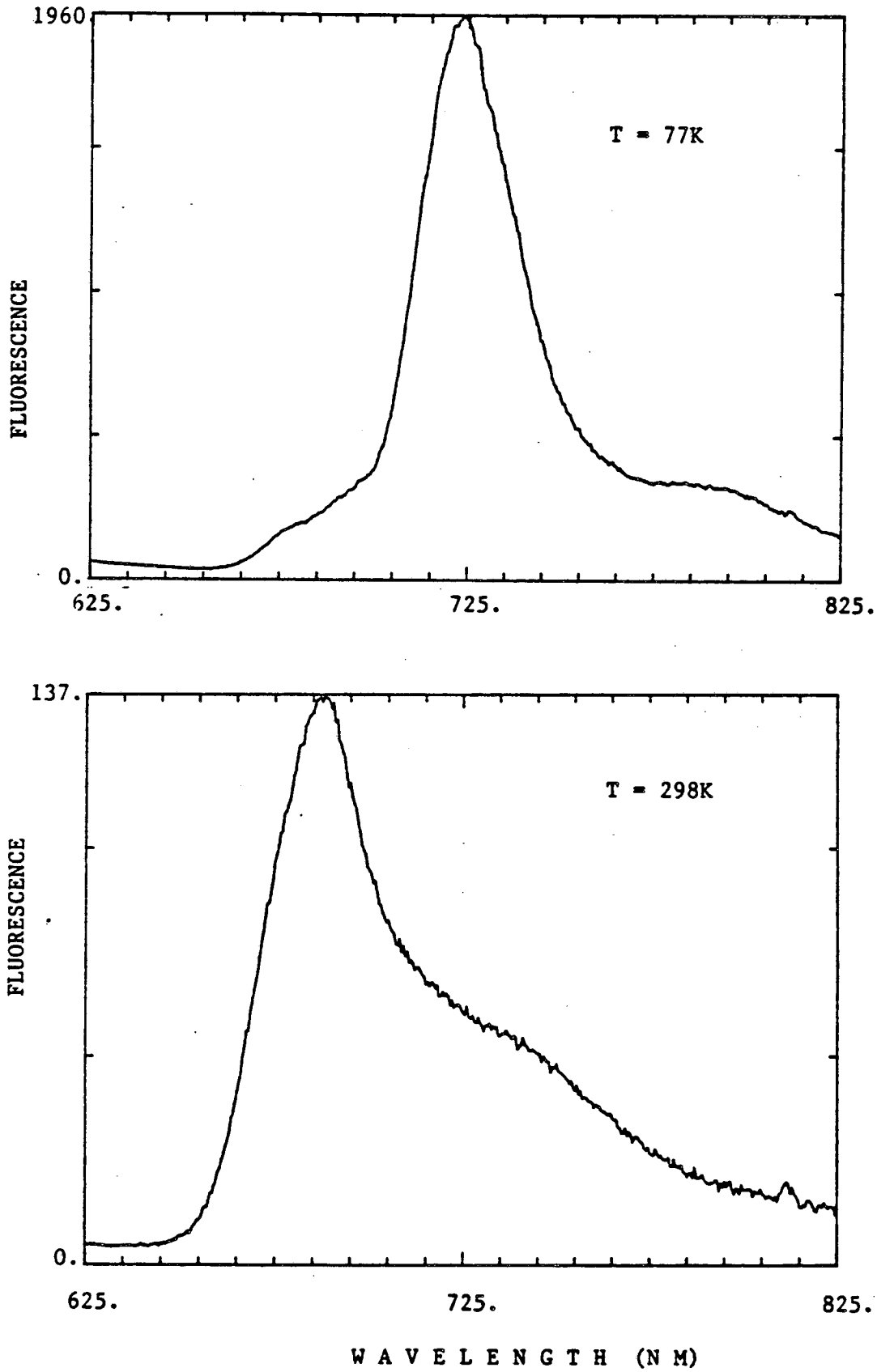
1960
T = 77K
FLUORESCENCE
0.
625.
725.
825.
137.
T = 298K
FLUORESCENCE
0.
625.
725.
825.
W A V E L E N G T H (N M)

shift of the long wavelength emission maximum at 77K to 720-722nm [8,15]; the removal of all Chl b [7,16]; and the loss of three [17] or four [8] polypeptides in the molecular weight range 20-24kD (determined by SDS-PAGE). I find the CP1 emission spectra, Fig. 4.3, to be consistent with the literature. At 295K, the maximum occurs at 690nm with a shoulder at 720nm. At 77K, the maximum occurs at 722nm with a shoulder at 695nm. The ratios of the fluorescence intensities are F_{690}/F_{722} = 2.1 at 295K and F_{695}/F_{722} = 0.16 at 77K.

4.5 EPR Spectroscopy of the CP1 Complex

EPR spectroscopy is an important tool for monitoring photochemistry. Charge separation and electron transfer can be observed by the EPR signals of oxidized donors and reduced acceptors. Charge recombination can be detected by the presence of a radical pair spin polarized triplet (RPT) thought to be located on the primary donor [18-20].

EPR has been employed to show the inactivation of the PS I acceptors X, Fd_A and Fd_B in the presence of SDS [21]. Chloroplasts reduced with ascorbate (50mM) and frozen under illumination exhibit the EPR signals of $P700^+$ (g=2.0025), X^- (g_x=2.08, g_y=1.87, g_z=1.76), Fd_A^- (g_x=2.05,g_y=1.94, g_z=1.86) and Fd_B^- (g_x=2.07, g_y=1.93, g_z=1.88) at 10K, [22], Fig 4.4A. Under these same conditions, the CP1 reaction center complex shows only an EPR signal in the g=2.0 region arising from $P700^+$, A_0^- and/or A_1^-, Fig 4.4B. This result is not surprising concerning the absence of Fd_B and Fd_A, because they are thought to be associated with a 19kD polypeptide [23] not present in CP1. However, it has recently been proposed that X is associated with the 64kD PS I reaction center peptide [24]. The absence of an X^- EPR signal is most likely a result of damaging the X center with 0.1% SDS [25] treatment during the CP1 isolation procedure. CP1 particles prepared with 2-5% lithium dodecyl sulfate (LDS) showed no active, EPR detectable A_1^- [26].

Although the secondary acceptors (X, Fd_A, Fd_B) are inactive in the CP1 complex, primary photochemistry does occur. Upon illumination at cryogenic temperatures, an EPR triplet signal is observed with a distinctive spin polarization pattern that arises from radical pair charge recombination. Fig 4.5 shows this radical pair spin polarized triplet (RPT) in CP1 particles in the absence of any exogenous donors or acceptors. The zero field splitting parameters, $|D|$ = .0277 cm^{-1} and $|E|$ = .0038 cm^{-1} ($\pm$ .0008 cm^{-1}), are characteristic of the P700 RPT

Figure 4.4 Steady State EPR of Reduced PS1 Electron Acceptors

The spectra are recorded in the dark at 11-12K. The instrument settings are: microwave frequency, 9.2GHz; microwave power, 20mW; modulation amplitude, 12.5G; modulation frequency, 100kHz; scan rate, 2.1Gs^{-1}; instrument response, 500ms.

A. Chloroplasts (4mg Chl/ml) reduced with 50mM ascorbate, illuminated 30s prior to cooling and frozen under illumination. The gain is 20,000.

B. CP1 (1mg Chl/ml) reduced with 15mM ascorbate, illuminated 30s prior to cooling and frozen under illumination. The gain is 3,200.

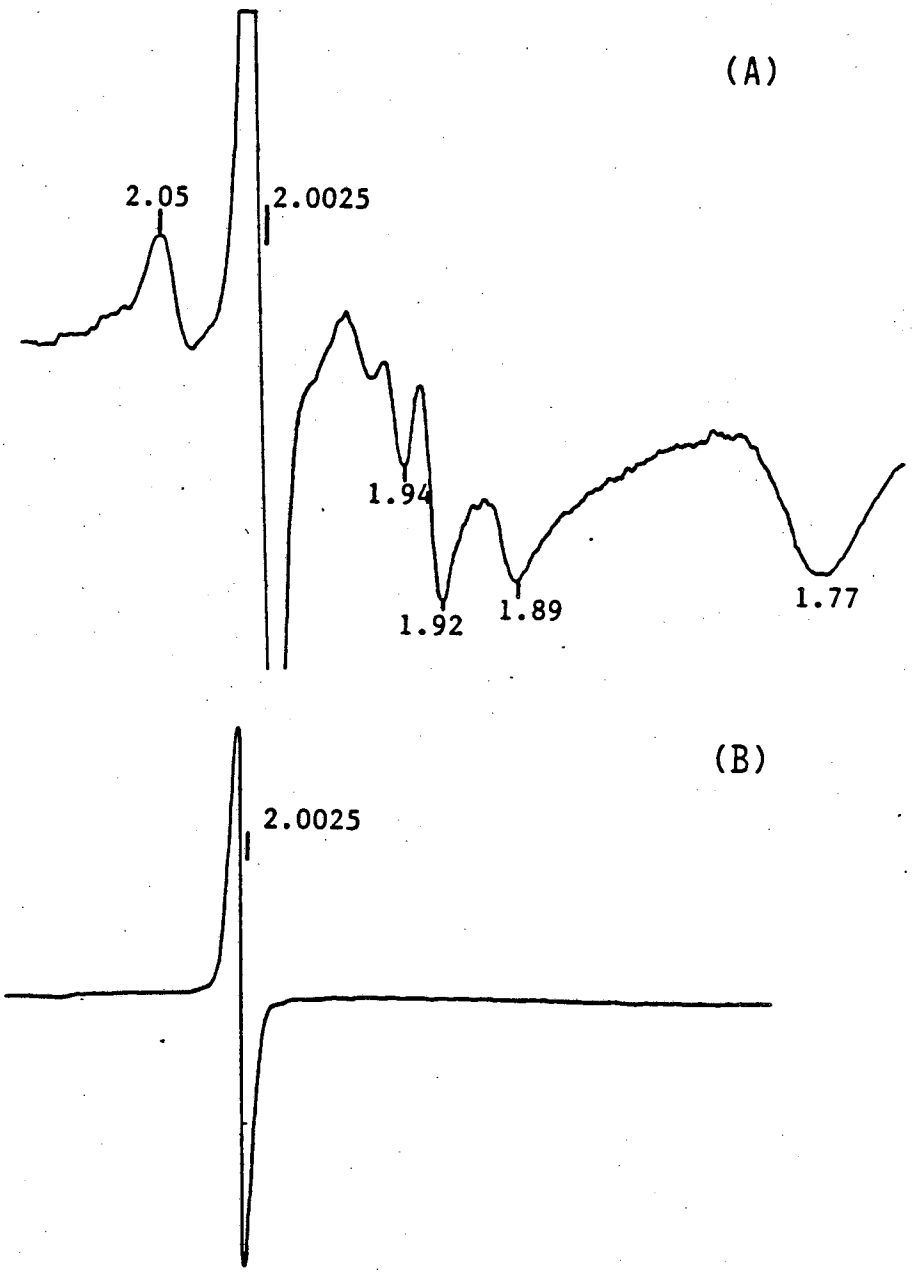
(A)
2.05
2.0025
1.94
1.92
1.89
1.77
(B)
2.0025

Figure 4.5 An EPR spectra showing the radical pair spin polarized triplet in CP1 particles. CP1 particles were concentrated to 0.52mg Chl/ml and frozen to 77K in the dark. The light modulation conditions are described in Methods. The instrument settings are: 32G modulation amplitude, 100kHz modulation frequency, 100μW microwave power, 9.18GHz microwave frequency, x4000 spectrometer gain, 3.4G/s scan rate, and 1s time constant. Zero field splitting parameters are $|D|$ = .0277 cm^{-1} and $|E|$ = .0038 cm^{-1} $\pm$.0008 cm^{-1}.

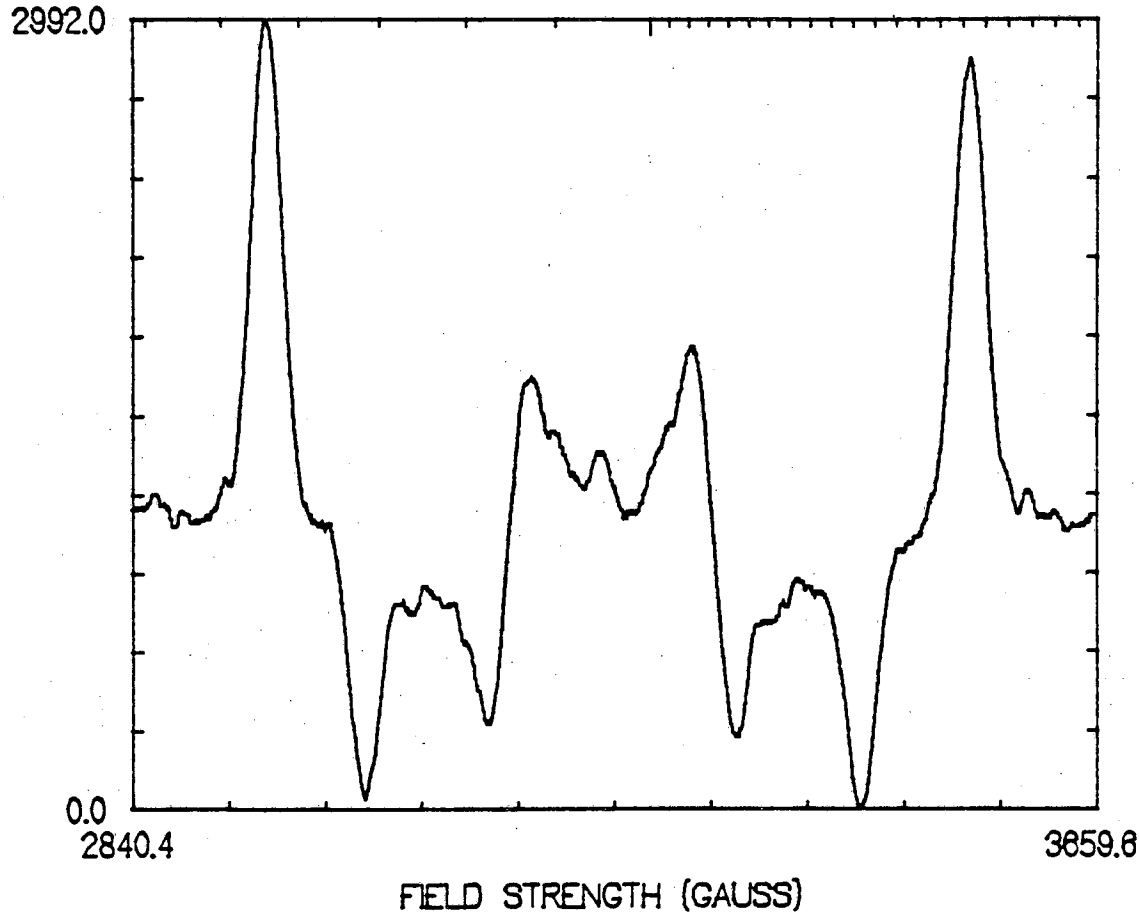
2992.0
0.0
2840.4
3659.6
FIELD STRENGTH (GAUSS)

[27]. This spin polarization pattern, aeeaae (a = absorptive, e = emissive) indicates electron population of only the high field T_0 triplet sublevel. Intersystem crossing population of the triplet sublevels cannot result in an electron distribution of solely or predominantly the T_0 level. Ion pair recombination best explains the aeeaae spin polarization pattern. The primary donor, P, is initially excited in a singlet state, and electron transfer produces a singlet excited radical pair state, $^1(P^+ A_0^-)$. Different Larmor frequencies of the two unpaired electrons results in dephasing of the spin angular momentum and mixing into the triplet state, $^3(P^+ A_0^-)$. The spin-spin interaction is small because the electrons are sufficiently separated, and at high magnetic field ($J << g\beta H$) only the T_0 sublevel is populated. Recombination results in a RPT on P:

$$P\ A_0 \rightarrow^{h\nu}\rightarrow {}^1(P^+ A_0^-) \rightarrow^{\Delta\omega}\rightarrow {}^3(P^+ A_0^-) \rightarrow\rightarrow {}^3P_{RPT}\ A_0$$

Therefore, an EPR detected RPT is indicative of charge separation and recombination, an active donor (P700) and acceptor (A_0). Thus, the CP1 reaction center complex is capable of primary photochemistry.

4.6 Photobleaching of the CP1 Complex

Charge separation and recombination can also be observed in CP1 in the form of a light induced absorption change. In the presence of ascorbate, the optical bleaching is completely reversible. The light-induced absorption difference spectrum of CP1 has a maximum at 698nm and appears to be identical to the absorption difference spectrum due to the chemical oxidation of P700 with ferricyanide (Fig. 4.6). The bleaching maxima are at 677nm and 698nm, and above 722nm the absorption increases. The bleaching and recovery kinetics are the same at all wavelengths measured (Chapter Five). The chemically induced absorption changes can be reversed with 5-10mM ascorbate. This agrees with the reported $P700^+$ minus P700 absorption difference spectrum [28-30]. The absorption difference spectrum is not that of $P700^+A^-$ minus P700A which has an absorption increase at 672nm. In addition, $P700^+A^-$ recombination has been measured at 295K in PS1 poised at -625mV ($P700AX^-Fd_B^-Fd_A^-$) as biphasic in 10ns and 3μs [31] which is much faster than our 100ms instrument response. Under continuous illumination CP1 forms the state $P700^+A$.

Light-induced bleaching of CP1 at 698nm measures $\Delta A_{698nm}/A_{675nm}$ = 0.012, Fig. 4.6B. In the presence of 5mM ascorbate the bleaching is completely reversible. A more common

Figure 4.6. CP1 Absorption Difference Spectra.

A. The chemically induced absorption difference spectra of $P700^{+}A$ minus P700A in CP1. The absorbance at 675nm is 0.48. The spectrum is sample minus reference where the sample is CP1 in 1mM potassium ferricyanide and 0.05mM potassium ferrocyanide and the reference is CP1 in 1mM ascorbate. Both are incubated for 10min prior to measurements. The optical changes are reversed upon addition of ascorbate.

B. The light induced absorption difference spectra of CP1. CP1 with an absorbance at 675nm of 0.5 is treated with 30μM methyl viologen and 1mM ascorbate. Excitation is through a 406nm interference filter with a 10nm bandwidth. Light induced absorption changes are monitored at the designated wavelength until a steady state level is reached and ΔA is recorded. All optical changes are completely reversed in the dark.

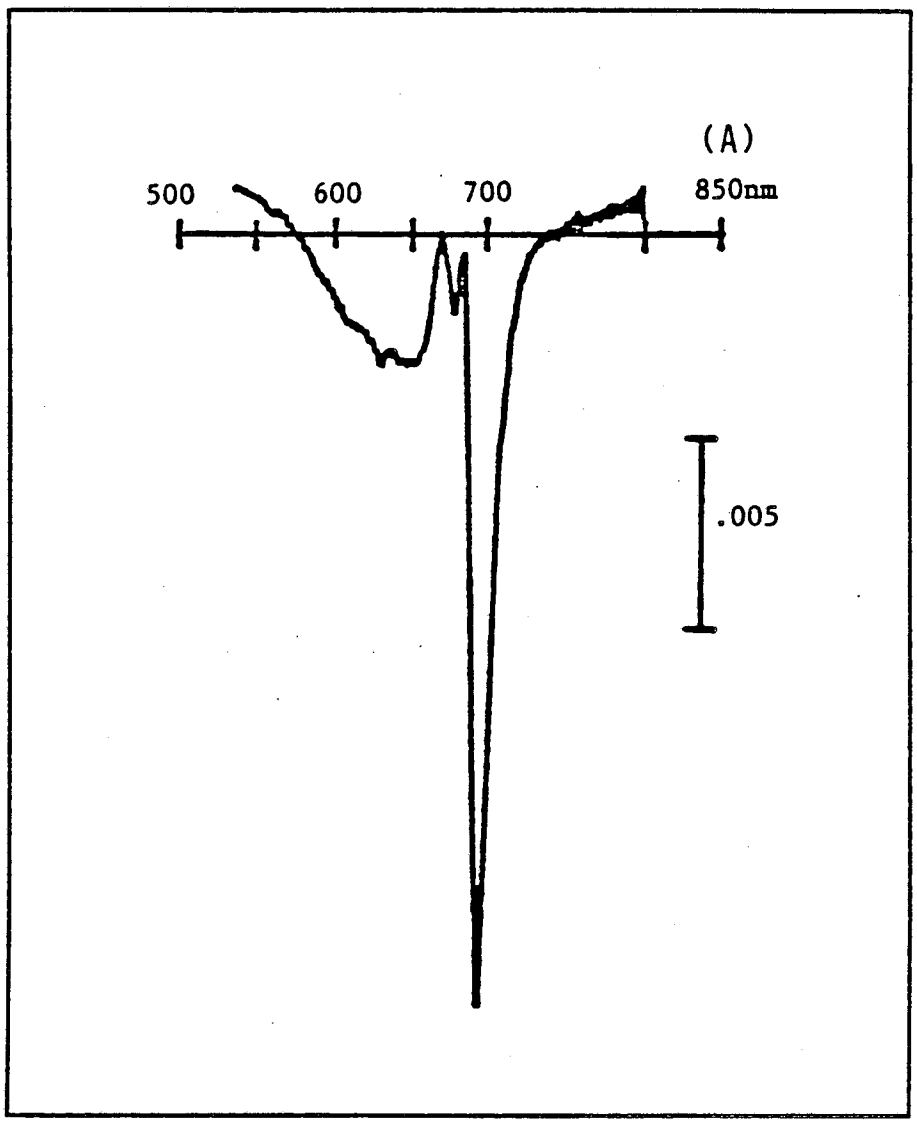
(A)
500
600
700
850nm
.005

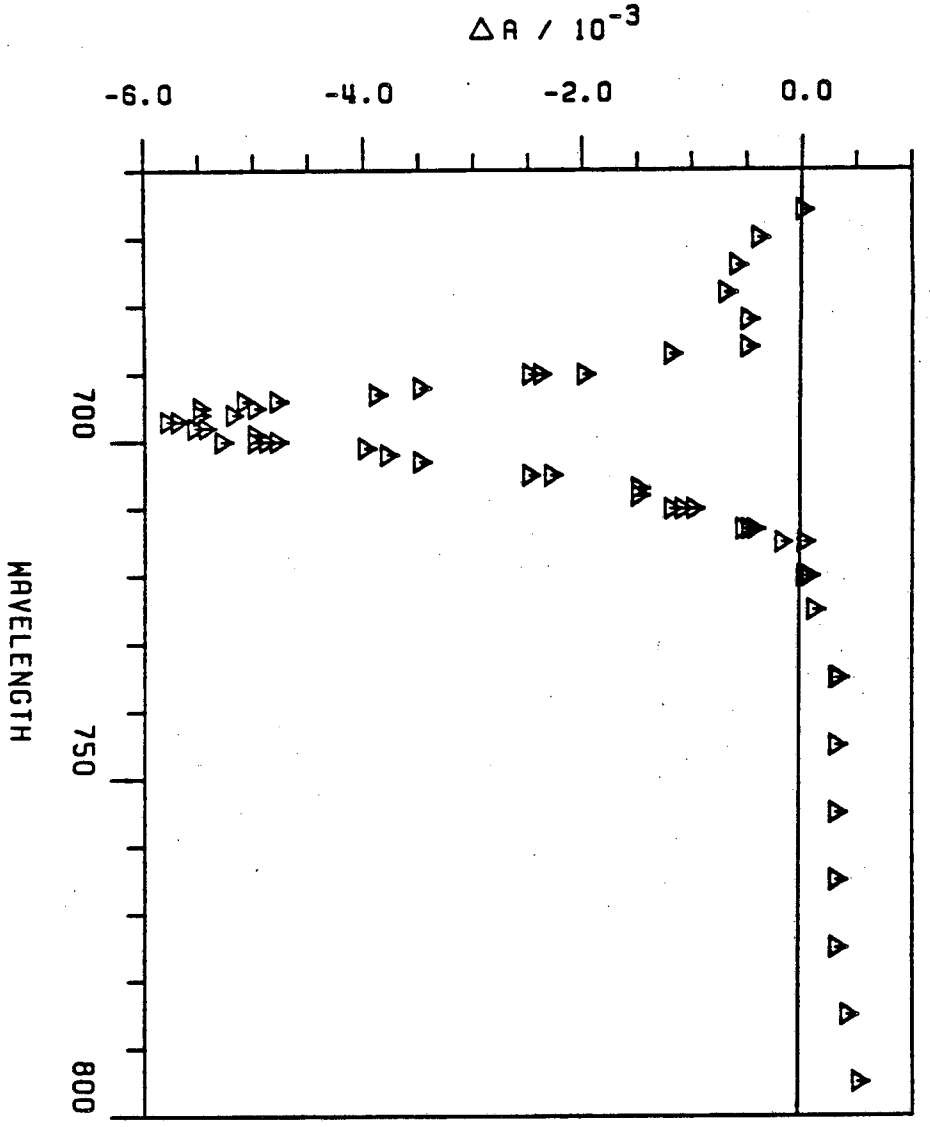

(B)

expression is chlorophyll per active P_{700}. Using a spectrophotometric assay for chlorophyll [32] and an extinction coefficient of $\Delta\epsilon$ = 64mM^{-1} cm^{-1} [33], I measure 75 Chl per active P700. Reversible chemical bleaching of CP1 produces $\Delta A_{698}/A_{675}$ = 0.04, Fig. 4.6A. This difference in the light-induced and chemically induced Chl/P700 ratios of PS1 centers has been reported by others [34,35]. The larger absorption change my be due in part to optical bleaching of chemically oxidized antenna Chl a [35].

4.7 Summary

CP1 is a stable, photochemically active PS I reaction center complex isolated from spinach thylakoids by non-denaturing SDS-PAGE. This chlorophyll-protein complex shows a single, diffuse polypeptide band from 62-65kD on a denaturing SDS polyacrylamide gel. It has an antenna pool of 40-50 chlorophyll a molecules per active reaction center.

CP1 has a long wavelength absorption maximum at 675nm. The fluorescence spectrum is temperature dependent. At T = 77K, the emission maximum is at 722nm with a shoulder at 695nm and at T = 298K, the emission maximum is at 690nm with a 720nm shoulder.

Light-induced bleaching at 698nm, and the EPR detected RPT confirm that CP1 contains the active electron transfer components, P700 and A_0. At 298K, in the presence of ascorbate, P700$^+$ A is produced under illumination; presumably as A$^-$ passes its electron to an exogenous acceptor (probably oxygen). This formation of the P700$^+$ A state is determined by comparing the light-induced optical difference spectrum to the chemically induced difference spectrum of P700$^+$ minus P700. The bleaching is reversible and P700$^+$ is reduced, in the dark, with a halftime of 50s.

As a result of its stability, its small and fairly homogeneous antenna pool, and the presence of only a a primary donor and acceptor, the CP1 reaction center complex is an excellent sample for monitoring the energy transfer and initial photochemistry of PS I.

4.8 References

[1] Vierling, E. and Alberte, R. (1983) *Plant Physiol.* 72, 625-633.

[2] Kuang, T., Argyroudi-Akoyunoglou, J.H., Nakatani, H.Y., Watson, J. and Arntzen, C.J. (1984) *Arch. Biochem. Biophys.* 235, 618-627.

[3] Setif, P., Acker, S., Lagoutte, B. and Duranton, J. (1980) *Photosyn. Res.* 1, 1-27.

[4] Lagoutte, B., Setif, P. and Duranton, J. (1981) *Photosynthesis III* ed. G. Akoyunoglou, Balaban International Sci. Serv., Philadelphia, PA. pp. 237-243.

[5] Schoeder, H.U. and Lochau, W. (1986) *FEBS. Lett* 199, 23-37.

[6] Laemmli, U.K. (1970) *Nature* 227, 680-685.

[7] Lam, E., Ortiz, W., Mayfield, S. and Malkin, R. (1984) *Plant Physiol.* 74, 650-655.

[8] Argyroudi-Akoyunoglou, J. (1984) *FEBS Lett.* 171, 47-53.

[9] Anderson, J.M. (1980) *Biochim. Biophys. Acta* 591, 113-126.

[10] Nechushtai, R. and Nelson, N. (1981) *J. Biol. Chem.* 256, 11624-11628.

[11] Fish, L.E. and Bogorad, L. (1986) *J. Biol. Chem.* 261, 8134-8139.

[12] Campillo, A.J., Shapiro, S.L., Geacintov, N.E. and Swenberg, C.E. (1977) *FEBS Lett.* 83, 316-320.

[13] Avarmaa, R.A., Kochubey, S.M. and Tamkivi, R.P. (1979) *FEBS Lett.* 102, 139-142.

[14] Butler, W.L., Tredwell, C.J., Malkin, R. and Barber, J. (1979) *Biochim. Biophys. Acta* 545, 309-315.

[15] Mullet, J.E., Burke, J.J. and Arntzen, C.J. (1980) *Plant Physiol.* 65, 823-827.

[16] Anderson, J.M., Brown, J.S., Lam, E. and Malkin, R. (1983) *Photochem. Photobiol.* 38, 205-210.

[17] Lam, E., Ortiz, W. and Malkin, R. (1984) *FEBS Lett.* 168, 10-14.

[18] Levanon, H. and Norris, J.R. (1978) *Chemical Reviews* 78, 185-198.

[19] Thurnauer, M.C., Katz, J.J. and Norris, J.R. (1975) *Proc. Nat. Acad. Sci.* 72, 3270-3274.

[20] Hoff, A.J. (1979) *Physics Reports* 54, 75-200.

[21] Malkin, R., Bearden, A.J., Hunter, F.A., Alberte, R. and Thornber, J.P. (1976) *Biochim. Biophy. Acta* 430, 389-394.

[22] Malkin, R. and Bearden, A. (1978) *Biochim. Biophys. Acta* 505, 147-182.

[23] Bonnerjea, J., Ortiz, W. and Malkin, R. (1985) ***Arch. Biochem. Biophys.***240, 15-20.

[24] Warden, J.T. and Golbeck, J.H. (1986) ***Biochim. Biophys. Acta*** 849, 25-31.

[25] Golbeck, J.H. and Cornelius, J.M. (1986) ***Biochim. Biophys. Acta*** 849, 16-24.

[26] Gast, P., Swarthoff, T., Ebskamp, F.C.R. and Hoff, A.J. (1983) ***Biochim. Biophys. Acta*** 722, 163-175.

[27] Frank, H.A., McLean, M.B. and Sauer, K. (1979) ***Proc. Nat. Acad. Sci.*** 76, 5124-5128.

[28] Setif, P., Acker, S., Lagoutte, B. and Duranton, J. ***Photosynthesis III*** ed. G. Akoyunoglou (1981) Balaban International Sci. Serv., Philadelphia, PA, pp. 503-511.

[29] Shuvalov, V.A., Klevanik, A.V., Sharkov, A.V., Kryukov, P.G. and Ke, B. (1979) ***FEBS Lett*** 107, 313-316.

[30] Shuvalov, V.A., Dolan, E. and Ke, B. (1979) ***Proc. Nat. Acad. Sci.*** 76, 770-773.

[31] Shuvalov, V.A., Ke, B. and Dolan, E. (1979) ***FEBS Lett.*** 100, 5-8.

[32] Arnon, D.I. (1949) ***Plant Physiol.*** 24, 1-15.

[33] Hiyama, T. and Ke, B. (1972) ***Biochim. Biophys. Acta*** 267, 160-171.

[34] Mathis, P., Sauer, K. and Remy, R. (1978) ***FEBS Lett*** 88, 275-278.

[35] Markwell, J.P., Thornber, J.P. and Skrdla, M.P. (1980) ***Biochim. Biophys. Acta*** 591, 391-399.

Chapter Five: Variable Fluorescence in CP1

5.1 Introduction

The decrease in optical absorbance at 700nm due to $P700^+$ formation in PS1 upon illumination is well documented [1-3]. In contrast, variable fluorescence of PS I has been difficult to observe because of the overwhelming fluorescence from PS II and light harvesting complexes which dominates most preparations. Only recently with the isolation of PS1 reaction center particles with low Chl a to P700 ratios has variable fluorescence associated with PS1 been observed. Telfer et al. have reported light induced variable fluorescence in Triton prepared PS I particles with 30-50 Chl per P700 [4]. However, fluorescence induction was reported only in the presence of dithionite or neutral red; no variable fluorescence was observed in the PS I particles in the absence of exogenous donors or acceptors. Variable fluorescence has also been observed by Ikegami in PS I particles with 6-9 Chl per P700 [5]. Ikegami compared variable fluorescence at 694nm to absorbance changes at 696nm and concluded that oxidized P700 and the primary electron acceptor ($P700^+A$) acts as a quencher of fluorescence, but they did not analyse the kinetics.

PS1 variable fluorescence is of particular interest because it differs from PSII variable fluorescence. In PSII the fluorescence intensity increases with illumination, Fig. 3.1, which is thought to reflect a closing of the reaction centers and an increase in fluorescence yield of the associated light harvesting complexes and antenna Chl a (Chapter Three). In contrast, the fluorescence intensity of particles enriched in PS1 decreases upon illumination [5]. The PS1 behavior is similar to ***Chromatium Minutissiumum*** where a reversible light-induced decrease in fluorescence is observed in chromatophores poised in the state PIQ^- (-450mV) [12]. This chapter focuses on identifying the fluorescence quenching state of PS1.

I have been able to detect variable fluorescence from PS I by monitoring the reaction center complex CP1, isolated from spinach chloroplasts by non-denaturing sodium dodecyl sulfate polyacrylamide gel electrophoresis (SDS-PAGE). The preparation and characterization of CP1 is described in Chapter Four. Briefly, CP1 has a small pool of antenna Chl a molecules per photochemically active P700 ($\Delta A_{699}/A_{675}$ = 0.012.) and has neither secondary donors nor the secondary acceptors X, Fd_A or Fd_B. The room temperature absorption maximum of CP1

is 675nm and the emission maximum is 690nm (Fig. 4.3). As a result of its low concentration of pigment per reaction center, CP1 is a prime candidate for observing PS I fluorescence.

In this chapter I demonstrate a correlation between the kinetics and magnitudes of light-induced absorbance changes (ΔA) and fluorescence changes (ΔF) in the PS I reaction center complex CP1. The light induced absorption difference spectrum of CP1 reflects the oxidation of P700 with a maximum at 699nm, Fig. 4.6, and is completely reversed in the dark at room temperature in the presence of added electron donors to $P700^+$. The fluorescence intensity of CP1 decreases upon illumination with similar kinetics to the photobleaching. I support Ikegami's proposal that the state $P700^+A$ quenches fluorescence. In addition, I have determined the rate constants of decreasing absorption and fluorescence upon illumination and find they have similar two component kinetics. I have measured and compared the changes in the magnitudes and kinetics of ΔA and ΔF under a variety of sample conditions, including: excitation intensity, ferricyanide/ferrocyanide redox titration, phenazinemethosulfate (PMS) concentration and ascorbate concentration.

5.2 Materials and Methods

All measurements are performed on the PS I reaction center complex, CP1, isolated from spinach chloroplasts by non-denaturing SDS-PAGE. The preparation is described in Chapter Four. Samples are suspended in 15mM NaCl, 5mM $MgCl_2$ and 50mM Tris (pH 7.5). The only variation among samples is in terms of exogenous donors and acceptors added in the specified amounts. The sample absorbance at 674nm is 0.9-1.0 unless noted. The CP1 particles are photochemically stable in the dark at 277K for hours. The magnitude and kinetics of light induced optical bleaching at 699nm is used to monitor the sample stability at 295K. Ascorbate (5-10mM) is necessary for complete reversibility and consistent reproducibility under repeated illumination. Unless noted, a fresh sample is used for each illumination.

The excitation source for both the variable fluorescence and optical bleaching is a 120V, 650W white light filtered for 330-650nm (Corning 4-96) and varied from 400-7000μEinstein m^{-2} s^{-1} (μ E $m^{-2}s^{-1}$). For ferri/ferrocyanide titrations 530-650nm is used for the excitation beam to avoid ferricyanide absorption. The excitation is at a right angle to the detection direction. The sample cuvette has a 10mm pathlength. The sample volume is 1.0-2.5ml and is specified in the figure legends.

The fluorescence is detected by a Hamamatsu R-928 photomultiplier tube through a 690nm interference filter (10nm bandwidth). The instrument response is 20ms. The kinetic traces are collected on a Nicolet Explorer 111A digital oscilloscope, added on a home-built signal averager and transferred to a VAX 11/780 computer for storage and analysis.

The optical changes are measured at 699nm with an Aminco DW-2 spectrophotometer with an EMI GENCOM 9684 (S1 type) photomultiplier tube. The instrument response time is 100ms.

The photobleaching kinetics are determined with a semi-log plot of ΔA_{max} (ΔA at the steady state level) minus ΔA at time t (where t=0 at the onset of illumination) vs. time. The slow component is fit to the linear region at longer times (usually t=10-40s) where the slope is $-K_S$ and the intercept is the amplitude. The slow component is extrapolated and subtracted at shorter times resulting in another linear region which represents K_F. The fluorescence kinetics are fit on the computer by an iterative sum of exponentials routine from the onset of illumination, F_{max}, to a steady state fluorescence level, F_0.

5.3 Photobleaching and Variable Fluorescence

Upon illumination at room temperature, the optical absorbance at 700nm of PS1 decreases as P700 becomes oxidized, Fig. 5.1. The PS1 reaction center complex, CP1, lacks endogenous secondary donors and acceptors (Chapter Four). Thus, exogenous electron donors to $P700^+$ (e.g. ascorbate, potassium ferrocyanide, PMS) are necessary for complete optical absorbance recovery in the dark.

The CP1 fluorescence spectrum at room temperature has an emission maximum at 690nm, Fig. 4.3. Upon illumination of CP1 at room temperature, the fluorescence intensity at 690nm exhibits a rapid rise to a maximum intensity, F_{max}, followed by a slow decrease to a steady state level, F_0, Fig. 5.2. After a dark adaption period that corresponds to a complete optical bleaching recovery time (5min in the presence of mM ascorbate or μM potassium ferrocyanide) the variable fluorescence measurement can be reproduced.

I find the magnitude of photobleaching at 699nm expressed as a percent of the long wavelength absorption maximum at 675nm ($\Delta A_{699}/A_{675}$), to have values up to 1.4%. The magnitude of variable fluorescence at 690nm expressed as a percent of the maximum fluorescence intensity at 690nm obtained at the onset of illumination, $\Delta F/F_{max}$, has values up to 25%.

Figure 5.1. Optical Photobleaching of CP1 at 699nm.

CP1 is suspended in 970μM potassium ferrocyanide, 4.8μM potassium ferricyanide ($[Fe^{+2}]$ / $[Fe^{+3}]$ = 202.), 15mM NaCl, 5mM $MgCl_2$ and 50mM Tris, pH 7.5. The absorbance at 675nm is 1.0. The excitation intensity is 2000μE m^{-2} s^{-1} in the wavelength range 330-650nm.

The figure displays the change in absorption at 699nm, ΔA, vs. time.

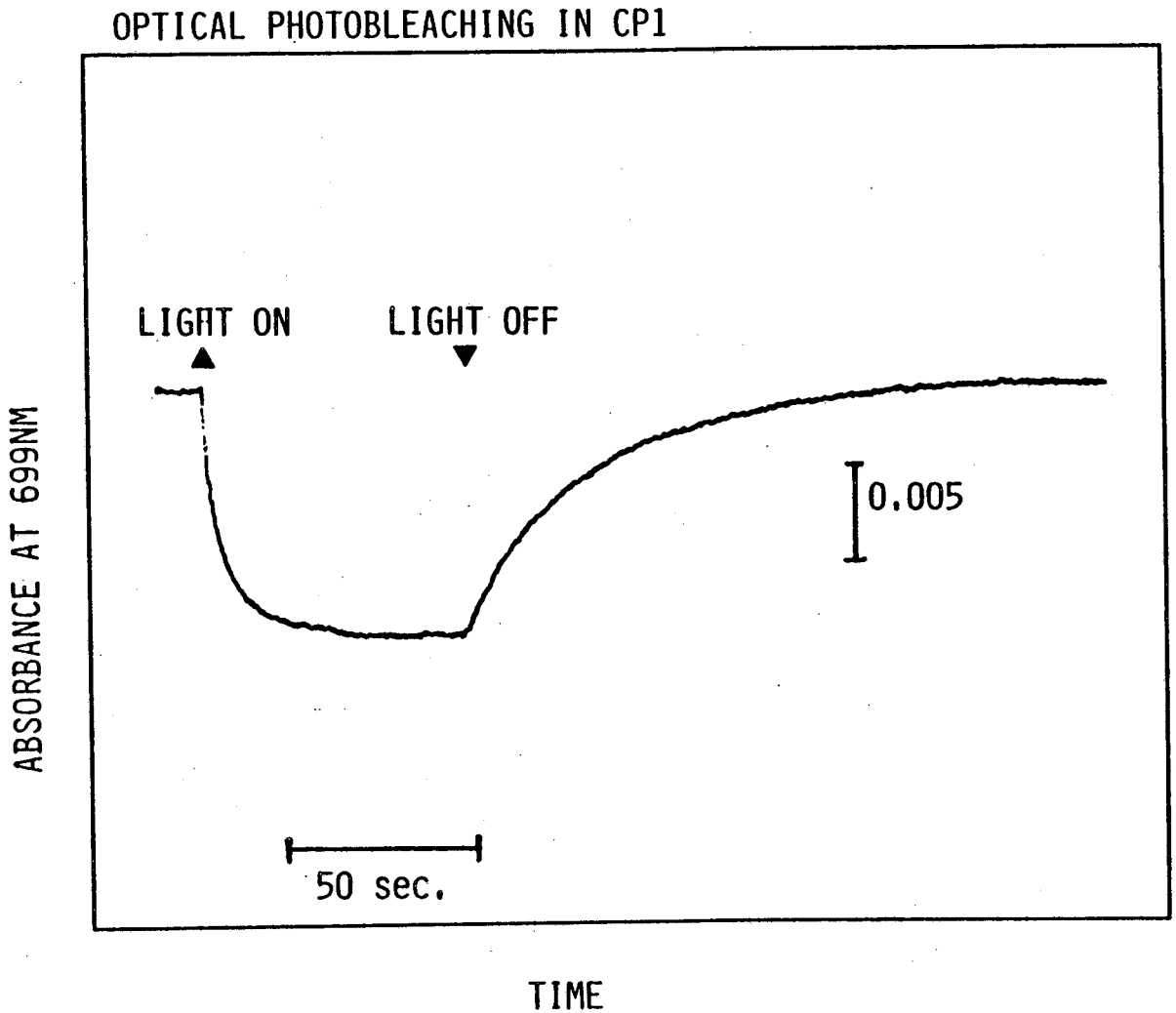
OPTICAL PHOTOBLEACHING IN CP1
LIGHT ON
LIGHT OFF
0.005
50 sec.
ABSORBANCE AT 699NM
TIME

Figure 5.2. Variable Fluorescence of CP1 at 690nm.

CP1 is suspended in 1.0μM potassium ferrocyanide, 15mM NaCl, 5mM $MgCl_2$ and 50mM Tris, pH 7.5. The absorbance at 675nm is 1.0. The excitation intensity is 1000μE m^{-2} s^{-1} and is 530-650nm.

The figure displays fluorescence intensity vs. time and is the sum of two kinetic traces. The fluorescence intensities are F_{max}, 42.1mV; F_0, 31.2mV; ΔF (F_{max} - F_0), 10.9mV and ΔF / F_{max}, 25%.

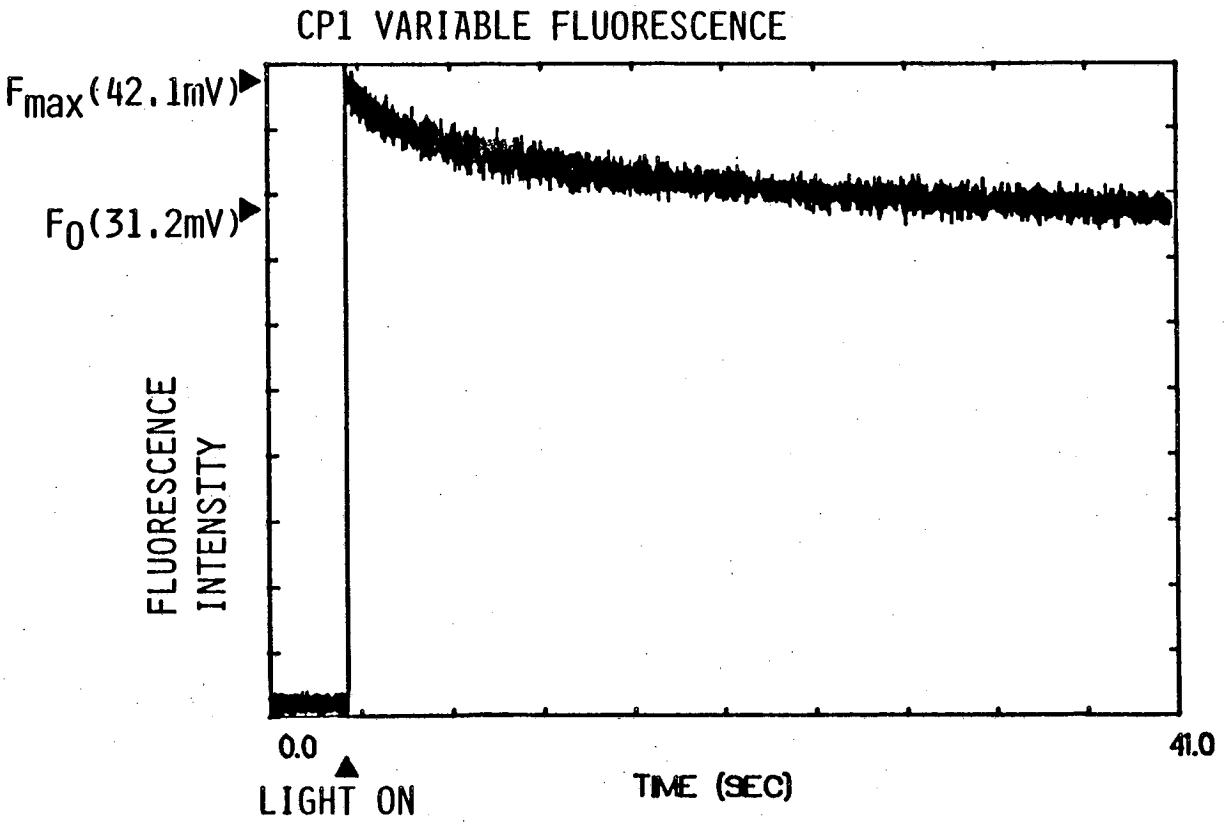
CP1 VARIABLE FLUORESCENCE
Fmax(42.1mV)
F0(31.2mV)
FLUORESCENCE INTENSITY
0.0
41.0
LIGHT ON
TIME (SEC)

Under most experimental conditions, the kinetics of decreasing absorption and fluorescence upon illumination in CP1 are best fit to the sum of two exponential components (exceptions are described later in this chapter). The rate constants vary considerably with excitation intensity, exogenous donors and acceptors. However, for most measurements, the rate constants for photobleaching and variable fluorescence are similar and are in the ranges of 0.2 - 1.6s^{-1} for K_F and 0.02 - 0.3s^{-1} for K_S. The relative amplitude of the fast component, α_F, is about 50% ($\alpha_F + \alpha_S = 100\%$) in the absence of exogenous donors or acceptors.

The similarity in the kinetics of light induced photobleaching and variable fluorescence indicate that the state $P700^+A$ may quench 690nm emission from CP1. I examined this question by comparing the magnitudes and kinetics during illumination of ΔA and ΔF under a variety of experimental conditions. The results of these studies are presented in subsequent sections of this chapter.

5.4 Excitation Intensity

The effects of excitation intensity upon the magnitudes and kinetics of variable fluorescence and photobleaching in CP1 are displayed in Fig. 5.3. Measurements are made in the presence of 5mM ascorbate. Thus, ΔA is completely reversed in the dark and both ΔF and ΔA measurements are reproducible.

The magnitudes of photobleaching and variable fluorescence increase with excitation intensity, Fig. 5.3A. ΔA which increases 2.5-fold and exhibits saturation behavior. The maximum fluorescence intensity at the onset of illumination, F_{max}, has a similar dependence on excitation intensity as ΔF, Fig. 5.3A. Thus, ΔF expressed as a percent of F_{max}, remains independent of excitation intensity at 15-25%.

Similar kinetic behavior is observed for both photobleaching and variable fluorescence. The rate constant of the fast component increases with excitation intensity, Fig. 5.3B. The rate constant of the slow component (about 0.07s^{-1}) is independent of excitation intensity within the signal-to-noise (data not shown). The relative amplitude of the fast component shows no excitation intensity dependence within our signal-to-noise (data not shown).

Figure 5.3. The Effects of Excitation Intensity upon the Variable Fluorescence and Photobleaching of CP1.

CP1 is suspended in 15mM NaCl, 5mM $MgCl_2$, 5mM ascorbate and 50mM Tris, pH 7.5. All samples are 1.0 or 2.5ml and have an absorbance at 675nm of 0.9-1.0. Similar results are obtained using two experimental techniques: repetitive illuminations of a single 1.0 or 2.5 ml sample with 5min dark adaptation (complete optical recovery) or using a batch sample with only a single illumination per aliquot. Photobleaching is measured at 699nm and fluorescence is measured at 690nm.

The kinetics of photobleaching and variable fluorescence are best fit to a sum of two exponential components. The exciting light intensity is measured at the sample and recorded in μEinstein m^{-2} s^{-1}. The fluorescence intensity is recorded in mV and the photobleaching is recorded in absorbance units.

A. The magnitude of photobleaching (ΔA), the magnitude of variable fluorescence (ΔF) and the maximum fluorescence intensity at the onset of illumination (F_{max}) vs. excitation intensity.

B. The rate constant of the fast component vs. excitation intensity.

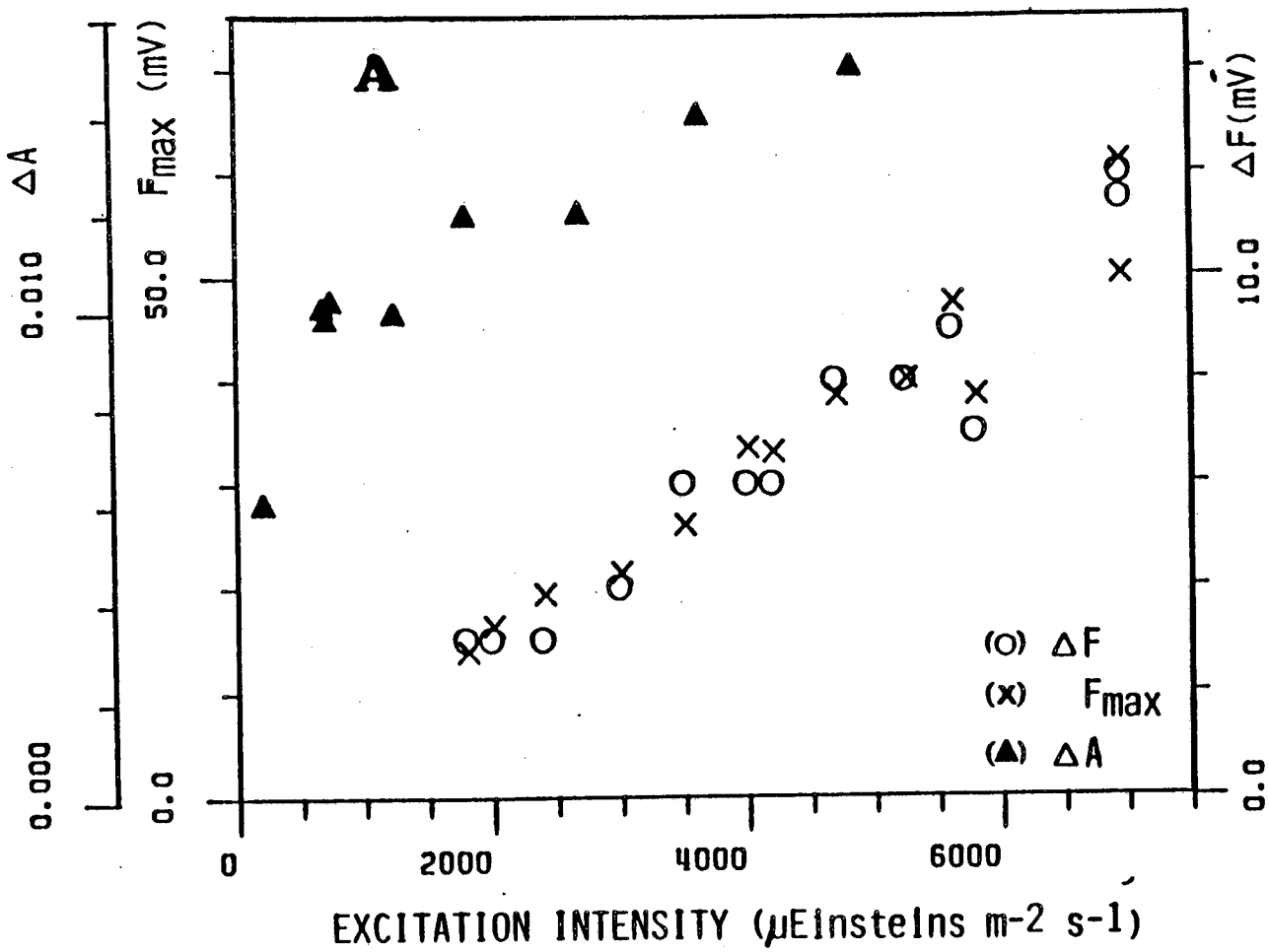
A
ΔA
0.010
0.000
Fmax (mV)
50.0
0.0
ΔF (mV)
10.0
0.0
0
2000
4000
6000
EXCITATION INTENSITY (μEinsteins m-2 s-1)
(O) ΔF
(X) Fmax
(▲) ΔA

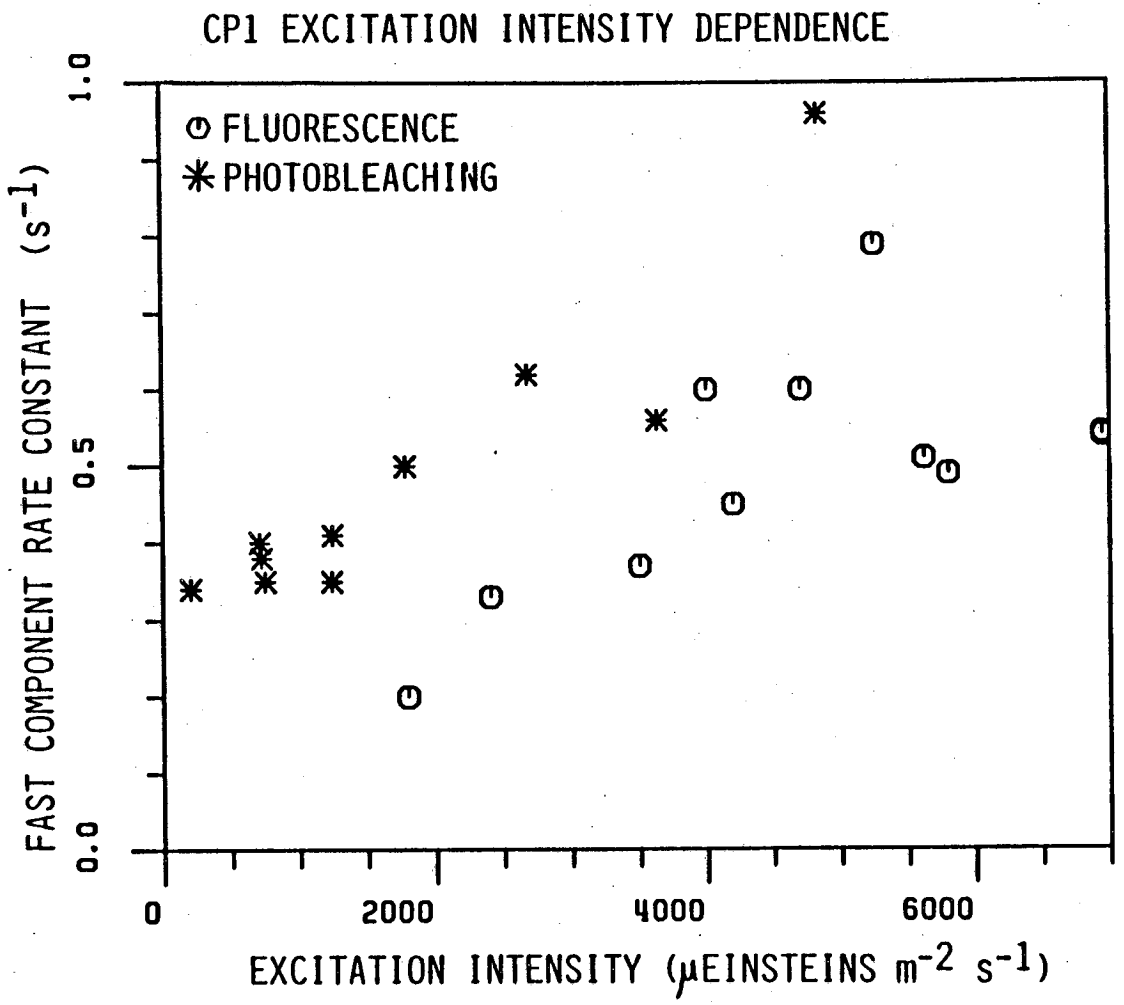
CP1 EXCITATION INTENSITY DEPENDENCE
FLUORESCENCE
PHOTOBLEACHING
FAST COMPONENT RATE CONSTANT (s-1)
0.0
0.5
1.0
0
2000
4000
6000
EXCITATION INTENSITY (μEINSTEINS m-2 s-1)

B

5.5 Ascorbate and PMS

Variations in ascorbate concentration produce changes in both the kinetics and magnitudes of variable fluorescence and photobleaching. Ascorbate measurements are made on CP1 samples with an excitation intensity of $750\mu Em^{-2}s^{-1}$. F_{max} is independent of ascorbate concentration. Over the concentration range of 0 to 5mM ascorbate ΔF decreases 2-fold while ΔA increases 2-fold (data not shown). This surprising result implies that ascorbate inhibits the fluorescence quenching mechanism without preventing light-induced $P700^+$ formation. Further experiments are necessary to understand this observation. The kinetics of photobleaching and variable fluorescence have similar dependence upon ascorbate concentration. The fast component increases from $0.33\pm.05s^{-1}$ in the absence of ascorbate to $0.6\pm.05s^{-1}$ in 12mM ascorbate. The slow component (about $0.05s^{-1}$) is independent of ascorbate concentration within the signal-to-noise. The relative amplitude of the fast component is independent of ascorbate.

Phenazinemethosulfate (PMS) acts as a rapid electron donor to P700. Since PMS shifts the level of $P700^+A$ formation under illumination, it is informative to compare the effects of PMS on the kinetics of photobleaching and variable fluorescence. Similar PMS dependence of the rate constants would support the proposal that the decrease in fluorescence of CP1 upon illumination reflects $P700^+A$ formation. The concentration of photochemically active P700 in the CP1 samples is $0.25\mu M$, using the 700nm absorption difference extinction coefficient for P700 of $64{,}000M^{-1}cm^{-1}$ [5]. Since low PMS concentrations (0.5 - $8.0\mu M$) are employed, the oxidation state of the reaction center will affect the equilibrium of reduced to oxidized PMS. Only the total PMS concentration is known. However, since all samples and experimental conditions are identical, the results of the PMS concentration dependence of variable fluorescence and photobleaching measurements are directly comparable.

Over the concentration range of 0.0 to $5.0\mu M$ PMS the following observations were made. (1) ΔA and ΔF decrease 3-4 fold, Fig. 5.4. (2) F_{max} is independent of PMS concentration. (3) The fast kinetic component of photobleaching and variable fluorescence increases 3 to 4-fold. (4) The slow kinetic component of photobleaching increases in rate while decreasing in relative amplitude so that at $5\mu M$ PMS a single kinetic component is present, $1.2s^{-1}$. (5) The kinetics of variable fluorescence also converge to a single component at greater than $5.0\mu M$ PMS,

Figure 5.4. The Effect of PMS upon the Variable Fluorescence and Photobleaching of CP1.

The magnitude of photobleaching, ΔA, and the magnitude of variable fluorescence, ΔF (mV), are displayed as a function of PMS concentration.

CP1 is suspended in 15mM NaCl, 5mM $MgCl_2$ and 50mM Tris, pH 7.5. All samples are 1.0 or 2.5ml and have an absorbance of 0.9-1.0 at 675nm. Similar results are obtained by two experimental techniques: repetitive illuminations of a single 2.5ml sample with 5min dark adaptions or using a batch sample with only a single illumination per aliquot. The exciting light intensity is 3000μEinstein m^{-2} s^{-1}. Fluorescence measurements are made at 690nm and photobleaching at 699nm.

The fluorescence intensity is recorded in mV, and the photobleaching is recorded in absorbance units. The PMS concentration units are the amount added and do not reflect the ratio of oxidized to reduced PMS in solution after equilibrium is reached. However, all sample conditions are the same so that the data can be directly compared as a function of PMS added.

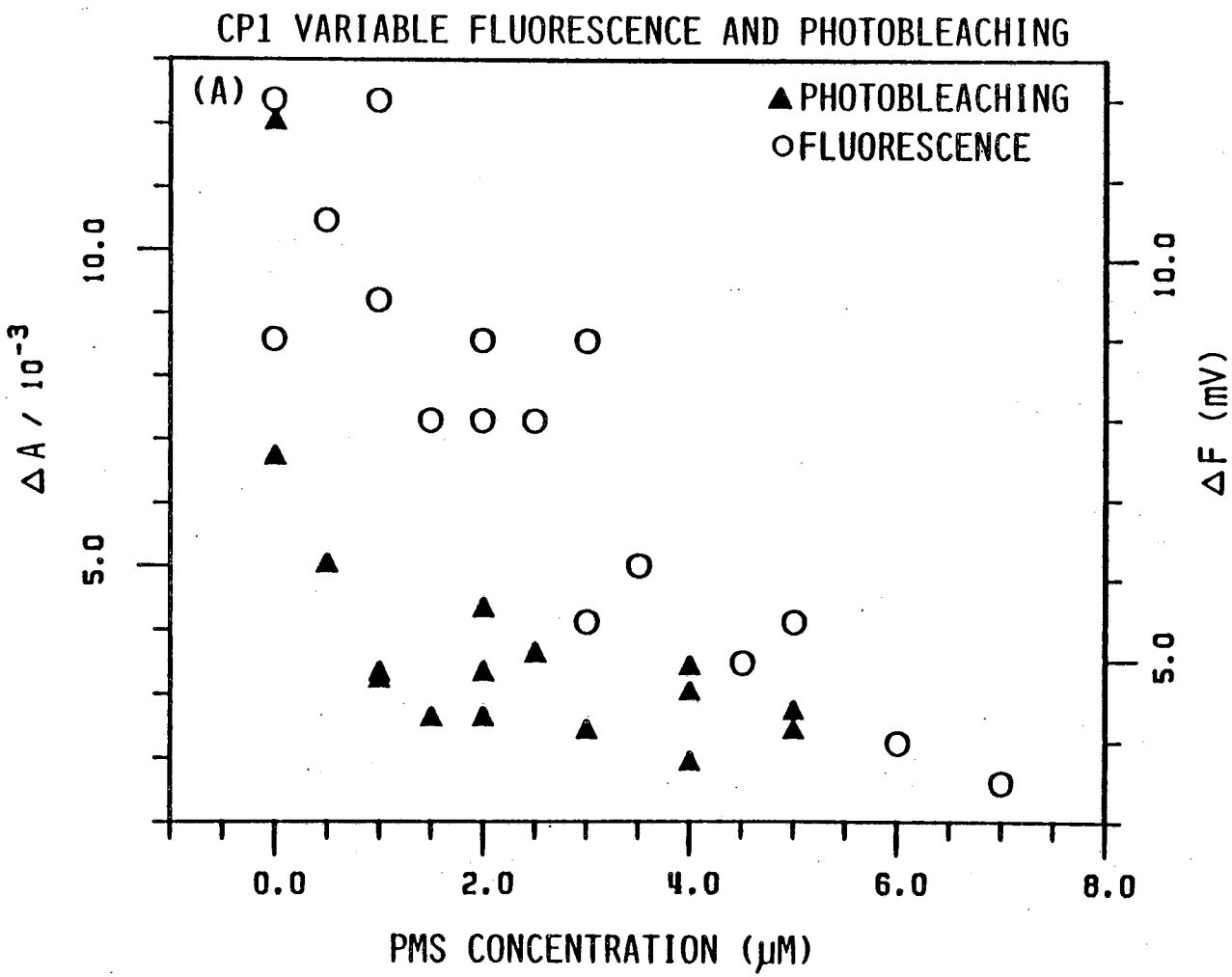
CP1 VARIABLE FLUORESCENCE AND PHOTOBLEACHING
(A)
▲PHOTOBLEACHING
○FLUORESCENCE
ΔA / 10^-3
10.0
5.0
ΔF (mV)
10.0
5.0
0.0
2.0
4.0
6.0
8.0
PMS CONCENTRATION (μM)

however, the kinetics are slower. The results of the ascorbate and PMS measurements are summarized in Table 5.1.

5.6 P700 Redox Titration

The oxidation state of P700 is altered by changing the potential of the sample with potassium ferricyanide and potassium ferrocyanide. The sample potential E_m, is calculated by:

$$E_m = E_m^0 - .059 \log([\text{ferrocyanide}] / [\text{ferricyanide}])$$

E_m^0 for ferro/ferricyanide in 50mM Tris, pH 7.0, was measured by O'Reilly to be 433mV [6]. The magnitude of light induced photobleaching at 699nm is a direct measure of the oxidation state of P700 (Chapter Four).

ΔA and ΔF are plotted vs. log([ferrocyanide] / [ferricyanide]) in Fig. 5.5. A potential of 450mV is indicated as a guideline. The reduction potential of $P700^+/P700$ has been previously reported and ranges from 400mV to 500mV [7]. ΔA and ΔF have the same potential dependence with an inflection point at 450mV, which reflects the reduction potential of $P700^+/P700$. F_{max} increases with increasing potential and also has an inflection point at 450mV (data not shown). All potential changes in ΔA, ΔF and F_{max} are reversed by returning the sample to the original concentration ratio of ferricyanide to ferrocyanide.

ΔA, ΔF and F_{max} decrease as P700 becomes oxidized. In the presence of ferrocyanide the CP1 reaction center is in the state P700A in the dark. Upon illumination the initial fluorescence intensity is high and maximum values of ΔF and ΔA are observed reflecting the light induced formation of $P700^+A$. In the presence of ferricyanide the state $P700^+A$ is present in the dark. Upon illumination the initial fluorescence intensity is at F_0 and ΔF and ΔA are absent, because the state of the reaction center is not affected by light. These measurements clearly indicate that $P700^+A$ quenches 690nm fluorescence from CP1.

5.7 Discussion

The measurements presented throughout this chapter are performed exclusively on the PS1 reaction center complex, CP1. CP1 is described in detail in Chapter Four. A few characteristics of CP1 must be kept in mind to understand the light induced variable fluorescence and optical absorption bleaching data. CP1 is a pigment-protein complex with 70 antenna

Figure 5.5. P700 Redox Titration.

CP1 is suspended in 15mM NaCl, 5mM $MgCl_2$ and 50mM Tris, pH 7.5. The absorbance at 675nm is 1.0. The sample volume is 2.0ml for photobleaching measurements and 1.0ml for variable fluorescence. The exciting light is 350-650nm and has an intensity of 1000μE m^{-2} s^{-1} for fluorescence measurements and 200μE M^{-2} s^{-1} for photobleaching.

The magnitude of variable fluorescence, ΔF (mV), and the magnitude of photobleaching, ΔA (absorbance units) vs. log ([ferrocyanide] / [ferricyanide]).

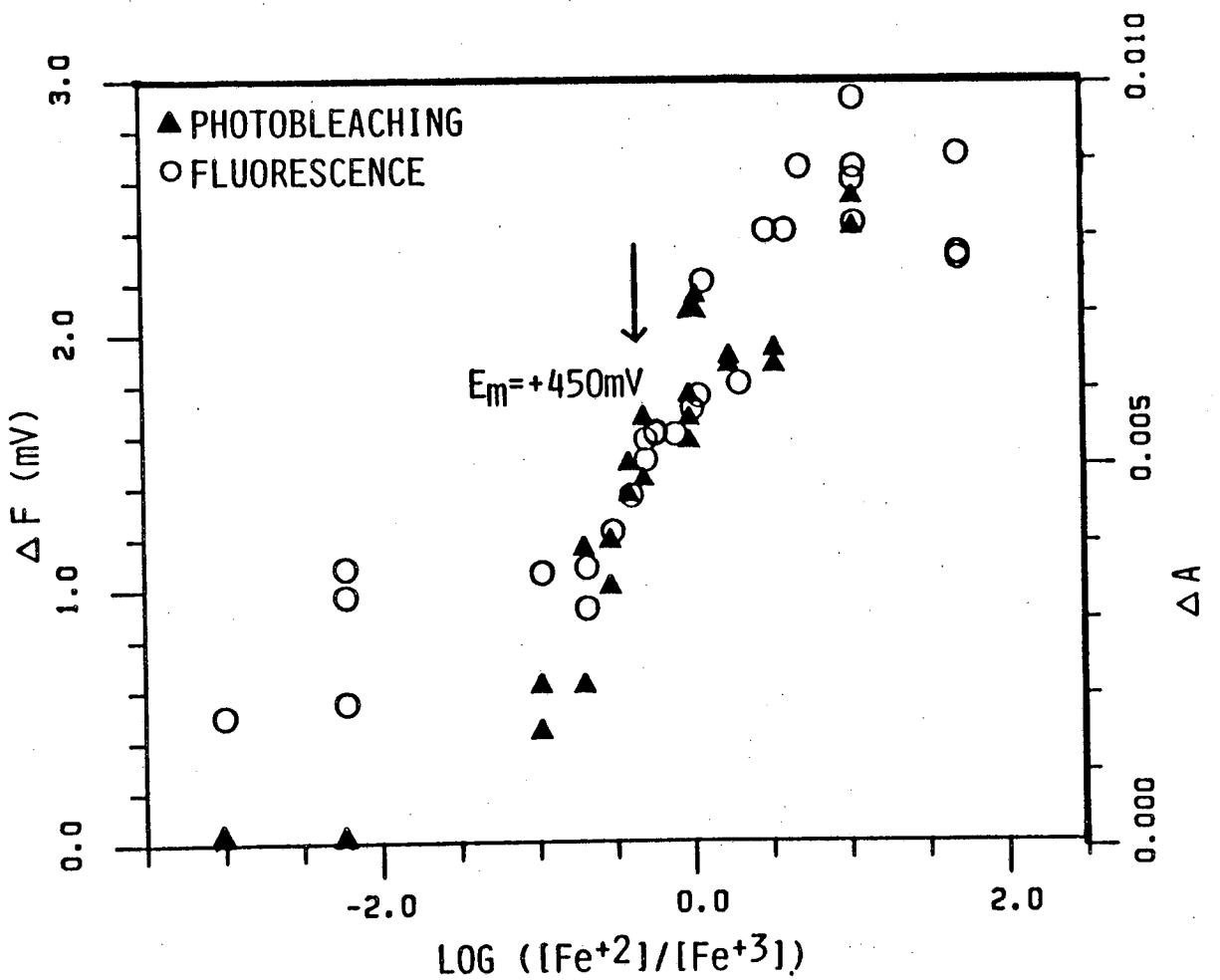
▲ PHOTOBLEACHING
○ FLUORESCENCE
Em=+450mV
ΔF (mV)
ΔA
LOG ([Fe+2]/[Fe+3])
3.0
2.0
1.0
0.0
0.010
0.005
0.000
-2.0
0.0
2.0

Chl a molecules per photochemically active PS1 reaction center (determined by light-induced optical bleaching at 699nm). CP1 lacks endogenous secondary donors and acceptors and is described by the notation P700A. The identity of A has not yet been determined; A is either a single acceptor A_0 (probably Chl a) or a composite of A_0 and A_1 (probably phylloquinone).

Photons are absorbed by the Chl a antenna pool, and excitation is transferred to the reaction center where charge separation occurs. The competing electron transfer reactions under illumination are presented in Fig. 5.6. R_1 is light induced charge separation which occurs in picoseconds [8]. R_{-1} represents two forms of recombination. (1) $P700^+A^-$ recombines to form an excited P700 which may transfer its excitation back to the antenna Chl a. The result is Chl a deexcitation (either the antenna or P700) by non-radiative decay or fluorescence. Although the recombination kinetics have not been reported for CP1, recombination of the PS1 state $P700^+A^-X^-Fd_{B,A}^{\equiv}$ occurs biphasically in 10ns and 3μs [9]. (2) $P700^+A^-$ also recombines to form a radical pair spin polarized triplet on P700 which relaxes non-radiatively in milliseconds (Chapter Four). R_2 and R_5 represent A^- passing its electron to exogenous acceptors. In the absence of added acceptors, the terminal electron acceptor present in the sample medium is most likely oxygen. Reduction of $P700^+$, R_3 and R_4, is slow in the absence of an added electron donor.

Some P700 remains oxidized in the dark. In the absence of added electron donors I find 20-25% of the P700 is oxidized prior to illumination and only 50% of the light induced $P700^+$ formation recovers in the 5min period following illumination. In most of the experiments described in this chapter the electron donors ascorbate, ferrocyanide and reduced PMS are employed. The more effective the electron donor, the more rapid the optical absorbance recovery at 700nm in the dark. This chapter does not discuss the behavior of the dark recovery of $P700^+A$ to P700A. However, most measurements are made in the presence of an electron donor to $P700^+$, and complete dark recovery to P700A is observed.

The oxidation state of P700 can be monitored by the CP1 optical absorbance at 699nm. Illumination of a PS1 reaction center in the state P700A causes a decrease in absorbance, with maxima at 677nm and 699nm, as P700 becomes oxidized. The light-induced absorption difference spectrum of CP1 in the presence of 30μM methyl viologen and 1.0mM ascorbate is the same as the chemically produced spectrum of $P700^+$ minus P700, Fig. 4.6, with the

Figure 5.6. A Model of the Light Induced Photochemistry of CP1.

P700 represents the primary donor which is thought to be a Chl a dimer. The identity of A has not yet been determined. A is either a single acceptor A_0, which is thought to a Chl a species, or A_0A_1, where A_1 is probably phylloquinone.

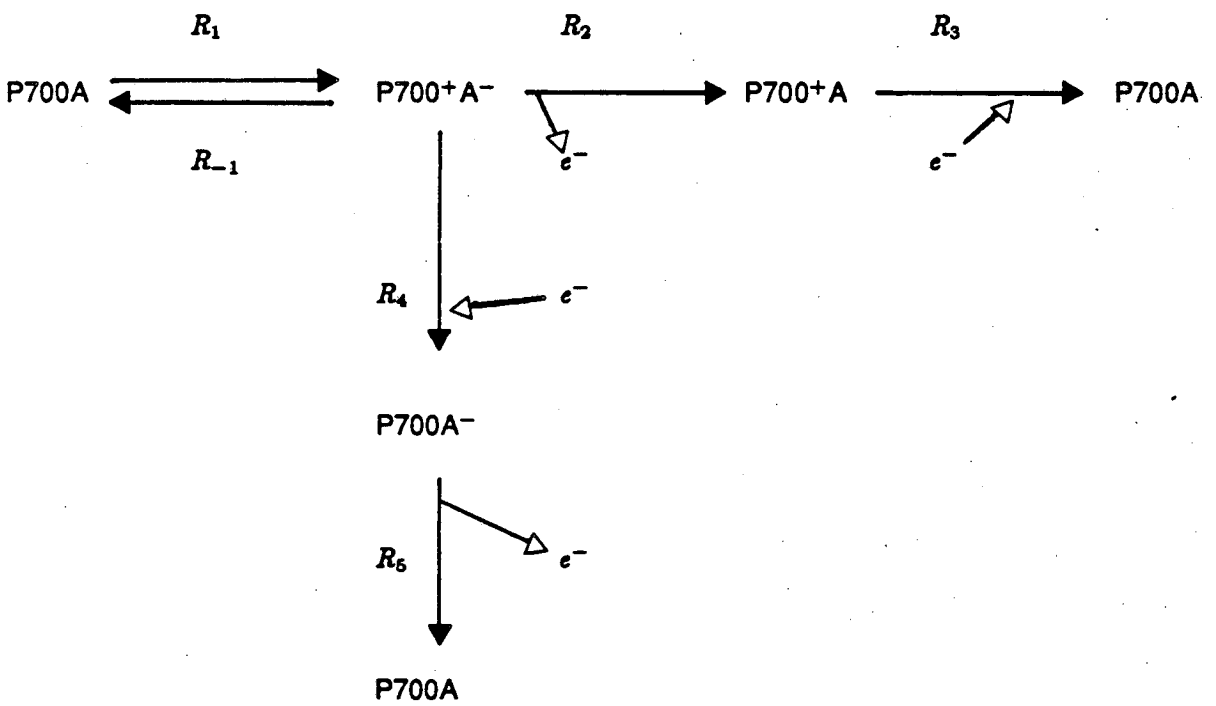

exception of the magnitude of the bleaching band at 699nm. The larger bleaching in the chemically (ferricyanide) treated sample is most likely due to contributions from oxidized antenna Chl a (Chapter Four). Identical light-induced optical difference spectra have been reported for CP1 particles suspended in 35μM methyl viologen and 3.0mM ascorbate [10]. This observed light-induced difference spectrum differs distinctly from the spectra of $P700^+A^-$ minus P700A or $P700A^-$ minus P700A [11]. Thus, the kinetics of optical bleaching in CP1 under continuous illumination represent the transition of P700A to $P700^+A$.

The CP1 emission maximum at room temperature is at 690nm. Upon illumination the fluorescence level decreases in seconds to a steady state level. The identity of the fluorescence quenching state is addressed in this chapter. There is significant similarity in the behavior of photobleaching and variable fluorescence. The magnitudes of variable fluorescence and photobleaching have different dependences upon excitation intensity. F_{max} and ΔF increase linearly with excitation. This behavior is characteristic of fluorescence. ΔA increases rapidly with excitation and then approaches saturation. At low excitation intensities the rate of the light induced charge separation, R_1, cannot compete with recombination, R_{-1}, and the reaction center remains primarily in the steady state, P700A. As the excitation increases so does R_1 and subsequently the rate of electron transfer from A^- to an exogenous acceptor, R_2, increases. Because R_{-1} and R_2 are fast, the steady state level of $P700^+A^-$ remains unobservable at all excitation intensities measured. However, $P700^+A$ is a long-lived state and as a result we observe an increase in ΔA which should saturate at higher intensities. At 5000$\mu Em^{-2}s^{-1}$, which corresponds to about 2000 photons per P700 per second, we still are not at saturation.

A significant aspect of the experiments in this chapter is the determination of the kinetics of variable fluorescence and photobleaching. The kinetics for both measurements are best fit, under most conditions, to two exponential components, K_F which ranges from 0.2 to 1.6s^{-1} and K_S which ranges from 0.02 to 0.3s^{-1}. The kinetic model, Fig. 5.6, does not predict a simple two exponential formation of $P700^+A$, rather a summation of several competing second order reactions. Most likely the two kinetic components represent an average of several unresolved components. However, comparing the kinetic trends as a function of excitation intensity, ascorbate concentration and PMS concentration between variable fluorescence and photobleaching is informative. When the excitation intensity is increased, K_F increases 2-fold

and K_S unchanged. In terms of the kinetic model only R_1 is dependent upon excitation intensity. Thus, K_F must include charge separation while K_S may represent electron transfer from A^- to exogenous acceptors, R_2.

I tested if $P700^+A$ is the fluorescence quenching state by observing whether ascorbate or PMS produce distinguishable effects upon photobleaching and variable fluorescence. Experimental results are summarized in Table 5.1 for reference. ΔA and ΔF decrease with PMS. Reduced PMS is an efficient donor to $P700^+$. Increasing PMS decreases the steady state concentration of $P700^+$ which we observe as a decrease in ΔA and ΔF. Within the signal-to-noise, the kinetics of photobleaching and variable fluorescence have similar dependence on ascorbate; the rates increase with increasing ascorbate. PMS increases the rates of photobleaching and variable fluorescence more dramatically than does ascorbate. Both PMS and ascorbate are electron donors to $P700^+$. It is possible that oxidized ascorbate or PMS act as electron acceptors from A^-, increasing R_2, or that they increase the concentration of P700A prior to illumination which subsequently increases the rate of $P700^+A$ formation. Whatever the mechanism, PMS is more lipid-soluble than ascorbate which may account for its more dramatic effect upon the kinetics. The present data do not justify further kinetic analysis. It is important to measure the light induced absorption difference spectrum of CP1 as a function of PMS or ascorbate concentration to confirm that the photobleaching to which we are comparing the variable fluorescence is actually $P700^+A$ formation under these conditions.

The most important similarity between variable fluorescence and photobleaching is seen in a redox titration of $P700^+/P700$ with ferro/ferricyanide. F_{max}, ΔF and ΔA have the same potential dependence, with inflection points at 450mV. This reflects the reduction potential of $P700^+/P700$, which has been reported to be in the range 400-500mV [7]. More specifically, Setif and Mathis measured the E_m of P700 in SDS isolated CP1 to be 431mV [3]. Treatment of CP1 particles with potassium ferrocyanide produces the dark state P700A. Upon illumination the initial fluorescence intensity is high and maximal ΔA and ΔF values are observed as the state $P700^+A$ is formed. Poising the reaction center in the state $P700^+A$ with potassium ferricyanide prior to illumination results in a lower initial fluorescence intensity and no photobleaching or variable fluorescence is observed. The $P700^+/P700$ redox titration supports the proposal that the state $P700^+A$ quenches CP1 fluorescence.

The results of the photobleaching and variable fluorescence experiments indicate that the predominant quencher of 690nm emission from CP1 is the state $P700^{+}A$. However, small differences in the behavior of variable fluorescence and photobleaching in the presence of ascorbate and PMS indicate there may be additional quenching states of CP1 fluorescence.

Table 5.1. Summary of Photobleaching and Variable Fluorescence

	ascorbate concentration 0-12mM	PMS concentration 0-7μM
ΔF	decrease 2-fold to 5mM 26 to 13mV	decrease 3-fold constant above 5mM 12 to 3.5mV
ΔA	increase 2-fold to 5mM 0.0055 to 0.01	decrease 3-fold constant above 5mM 0.012 to 0.003
F_{max}	independent	independent
$\Delta F/F_{max}$	decrease —	decrease 18% to 8%
$K_F(\Delta A)$	increase 0.38 to 0.6s^{-1}	increase 4-fold 0.4 to 1.6s^{-1}
$K_F(\Delta F)$	increase 0.35 to 0.55s^{-1}	increase 4-fold 0.35 to 1.2s^{-1}
$K_S(\Delta A)$	increase 3-fold 0.05 to 0.14s^{-1}	increase 4-fold 0.05 to 0.23s^{-1}
$K_S(\Delta F)$	0.031-0.085s^{-1}	0.02-0.06s^{-1}

5.8 References

[1] Kok, B. (1956) ***Biochim. Biophys. Acta*** 22, 399.

[2] Sauer, K. (1975) ***Bioenergetics of Photosynthesis*** ed. Govindjee, Acadmic Press, NY. 139-144.

[3] Setif, P. and Mathis, P. (1980) ***Arch. Biochem. Biophys.*** 204, 477-485.

[4] Telfer, A., Barber, J., Heathcote, P. and Evans, M.C.W. (1978) ***Biochim. Biophys. Acta*** 504, 153-164.

[5] Hiyama, T. and Ke, B. (1972) ***Biochim. Biophys. Acta*** 267, 160-171.

[6] O'Reilly, J.E. (1973) ***Biochim. Biophys. Acta*** 292, 509-515.

[7] Clayton, R.K. (1980) ***Photosynthesis: Physical Mechanisms and Chemical Patterns*** Cambridge University Press. p.182.

[8] Il'ina, M.D., Krasanskas, V.V., Rotomskis, R.J. and Borisov, A.Y. (1984) ***Biochim. Biophys. Acta*** 767, 501-506.

[9] Shuvalov, V.A., Ke, B. and Dolan, E. (1979) ***FEBS Lett*** 100, 5-8.

[10] Setif, P., Acker, S., Lagoutte, B. and Duranton, J. (1981) ***Photosynthesis III*** ed. G. Akoyunoglou, Balaban International Sci. Serv., Philadelphia, PA, pp. 503.

[11] Shuvalov, V.A., Dolan, E. and Ke, B. (1979) ***Proc. Nat. Acad. Sci.*** 76, 770-773.

[12] Shuvalov, V.A. and Klimov, V.V. (1976) ***Biochim. Biophys. Acta*** 440, 587-599.

Chapter Six: Temperature Dependence of CP1 Fluorescence

6.1 Introduction

An important focus of research in photosynthesis is understanding the mechanisms and kinetics of excitation transfer to the reaction center and the trapping of that energy by ion-pair formation. Chapter Two describes this entire process in depth for the PS1 reaction center complex CP1, and a brief synopsis is provided here. Photons are absorbed by the antenna Chl a molecules and excitation migrates to the reaction center where it is trapped as charge separation occurs to form the state $P700^+A_0^-$. Subsequent electron transfer can occur to form the state $P700^+A_0A_1^-$. Further electron acceptors (X, Fd_B and Fd_A) and secondary donors are absent (Chapter Four). I will denote the CP1 reaction center as P700A where A may represent A_0 or A_0A_1. The ion-pair $P700^+A^-$ can decay by the following mechanisms: recombination and deexcitation through fluorescence or non-radiative pathways from the reaction center or repopulated antenna Chl a, formation of a radical pair spin polarized triplet, or oxidation of A^- and reduction of $P700^+$ by exogenous acceptors and donors. Excitation transfer to and trapping by the reaction center occurs in less than 100ps [1-3]. Thus, the predominant experimental limitation is instrument response times. Recently absorption difference spectra have been reported by Il'ina et al., with 10ps time resolution, on Triton isolated PS1 particles (60 Chl per P700) [1]. They found an instrument limited rise in the optical bleaching at 676nm, ΔA_{676}, which they attribute to excitation of the antenna chl a, and a ΔA_{676} decay described by three components: 20-45ps, 100-300ps and >500ps. The optical bleaching at 704nm, ΔA_{704}, associated with $P700^+$ formation has a 15-30ps rise. They conclude that the 20-45ps decay of ΔA_{676} and the 15-30ps rise in ΔA_{704} reflect excitation transferred from the antenna chl a to P700. These optical kinetics can be constructively complemented by picosecond fluorescence kinetics.

A single-photon timing system (described in Chapter 2) enables us to measure fluorescence kinetics with lifetimes as short as 20ps. By varying the sample conditions (temperature, oxidation states) of the PS I reaction center complex CP1, and observing changes in the fluorescence kinetic lifetimes and yields, I have gained insight into energy transfer, charge separation and recombination rates on a rapid time scale.

The fluorescence emission of CP1 at 77K and 295K is shown in Fig. 4.3. At 295K the emission maximum is at 690nm with a shoulder at 720nm. At 77K the emission maximum is at 722nm with a 695nm shoulder. This dramatic temperature dependence raises several immediate questions that can be addressed with steady-state and picosecond kinetic fluorescence measurements. (1) How do the absolute fluorescence yields of the 690nm and 722nm peaks change with temperature? (2) Are the 690nm and 722nm bands comprised of different kinetic components? (3) What is the temperature dependence of the fluorescence kinetic components' lifetimes and yields? (4) Does oxidation of P700 alter the fluorescence emission characteristics? The answers to these questions will aid in characterizing the environments and identities of the species emitting at 722nm and 690nm. In addition, the mechanism and activation energies of excitation transfer into, out of, or between these chromophores can be elucidated.

This chapter addresses the above questions and presents the results of the temperature dependence of the steady state and picosecond kinetics of CP1 fluorescence.

6.2 Materials and Methods

All measurements are performed on the PS I reaction center complex CP1. CP1 is isolated from spinach chloroplasts by non-denaturing SDS-PAGE. Chapter 4 provides a complete description of the preparation and characterization of CP1. Briefly, the CP1 particles have a small pool of antenna chl a and are capable of primary photochemistry. Neither secondary donors nor the acceptors X, Fd_B, or Fd_A are present. CP1 is a prime candidate for studying energy transfer and characterizing the initial acceptors of PS I.

CP1 is very stable at room temperature. During fluorescence measurements, there is no change in the absorption spectra, the normalized emission spectra nor the fluorescence kinetics. Steady state spectra are recorded in 0.5 - 2.0min and prompt fluorescence kinetic measurements are made in 0.5 - 10.0min. After 4h at 295K, the absolute fluorescence yield decreases only 10-15%.

The steady state emission spectrometer is described in Section 4.2. The reverse single-photon counting detection system, deconvolution and kinetic analysis methods are detailed in Chapter 2.

Room temperature measurements are made in a fluorescence cuvette with a 10mm path. The sample is stirred during data collection. For temperatures below 295K, the CP1 sample suspension, containing 30-50% glycerol, is slowly frozen in a 4mm diameter NMR tube or a 2mm EPR tube to a uniformly finely shattered state. Active samples are dark adapted and frozen in the dark, unless otherwise noted. Measurements are made in a cylindrical, pyrex dewar placed directly in the excitation beam. For 77K the dewar is filled with liquid nitrogen. For temperatures between 77K and 295K, nitrogen gas is passed through liquid nitrogen and blown over the sample in the dewar. The temperature is regulated by the nitrogen flow rate and monitored by a thermocouple placed in the sample directly above the excitation beam. A second source of nitrogen gas is blown over the outer dewar surface to prevent condensation.

Fluorescence yields are obtained from analysis of the prompt fluorescence kinetic measurements. The sum of the component yields is the total fluorescence yield. The total relative fluorescence yield, ϕ_T(rel), is determined by numerical integration of the deconvoluted fluorescence decay, I(t),

$$\phi = \int_0^\infty I(t)\, dt$$

which is then corrected for differences in data collection time and filter transmission. The ϕ_T(rel) values from the temperature dependence measurements are scaled to 100 at the lowest measured temperature (103K). The absolute quantum yield, ϕ_T(abs), is proportional to ϕ_T(rel) for a given experimental measurement. ϕ_T(abs) can be expressed as the mean observed lifetime divided by the natural lifetime,

$$\phi_T(\text{abs}) = \tau_m \,/\, \tau_0.$$

For chlorophyll in solution, the natural lifetime is 15ns. The mean lifetime can be calculated from experimental lifetimes and yields,

$$\tau_m = \sum_{i=1}^{n} \phi_i\, \tau_i \,/\, \sum_{i=1}^{n} \phi_i$$

Thus, the proportionality constant can be calculated,

$$\phi_T(\text{abs}) = \tau_m/\tau_0 = M\phi_T(\text{rel})$$

For the temperature dependence measurements (see Figure 6.11), ϕ_i(abs) = 0.0011ϕ_i(rel).

Figure 6.1. Low temperature fluorescence excitation spectra of CP1. The CP1 sample is frozen in the dark in 50% glycerol, 5mM ascorbate, 15mM NaCl, 5mM $MgCl_2$, 50mM Tris, pH 7.5. The sample absorbance at 675nm is 0.2. The temperature is 77K. The excitation and emission bandwidths are 4nm.

The fluorescence intensity at 730nm (dark trace) and 680nm (light trace) are displayed vs. excitation wavelength. The spectra are normalized to their Soret maxima at 438nm.

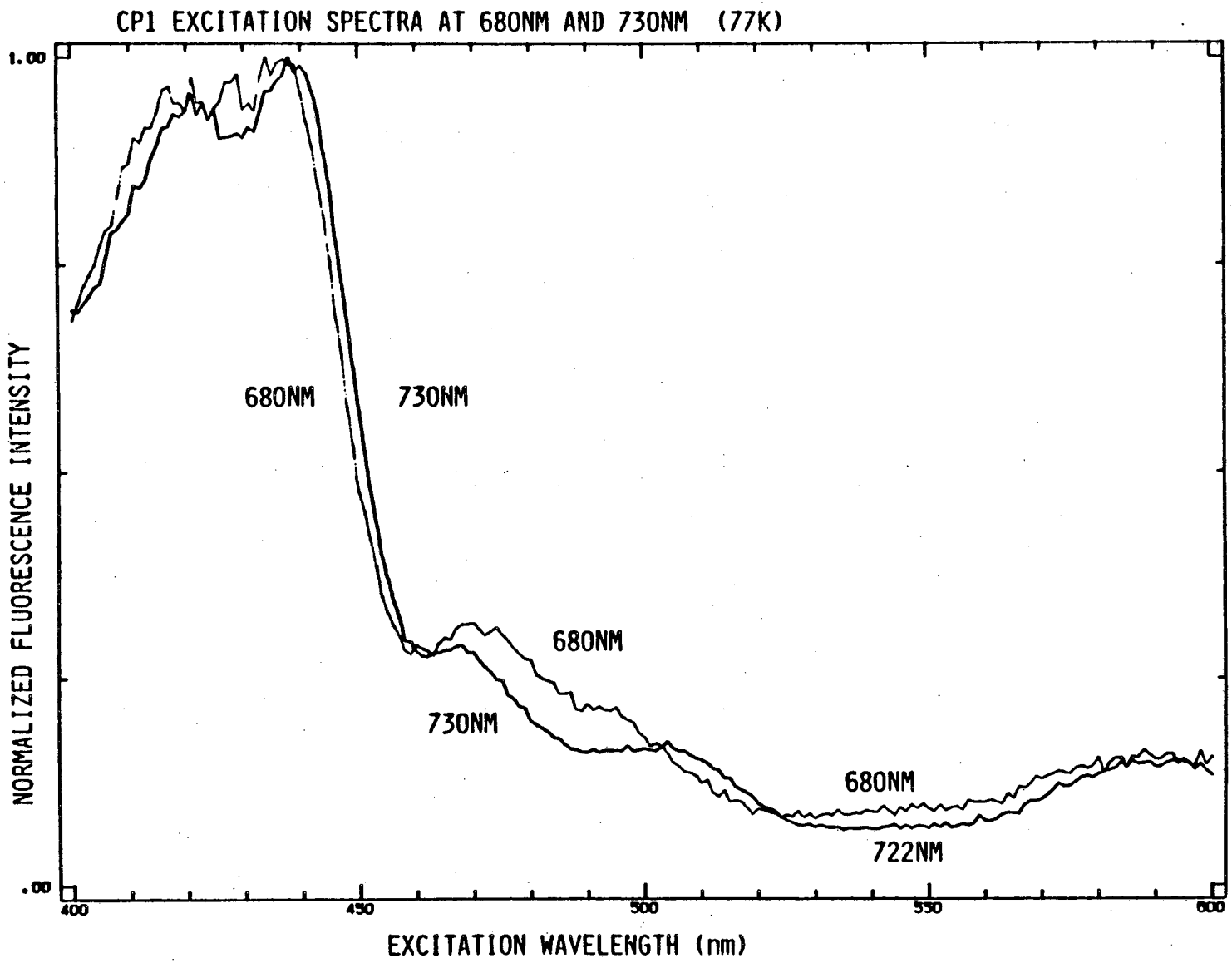
CP1 EXCITATION SPECTRA AT 680NM AND 730NM (77K)
1.00
.00
NORMALIZED FLUORESCENCE INTENSITY
680NM
730NM
680NM
730NM
680NM
722NM
400
450
500
550
600
EXCITATION WAVELENGTH (nm)

XBL 868-2894

6.3 Fluorescence Excitation Spectra

The fluorescence emission spectrum of CP1 particles excited at 438nm (Fig. 4.3) has two emission bands, 690nm and 722nm, whose relative intensities are temperature dependent (Section 6.4). At 77K, the emission maximum is at 722nm with a shoulder at 690nm. It is possible that the 722nm and 690nm emission bands arise from two chemically distinct species, each with its own characteristic absorption spectrum. To test this I scanned the excitation spectra of the emission bands at 77K, Fig. 6.1. To minimize contributions due to overlap of the fluorescence peaks, I used 680nm and 730nm to represent the 690nm and 722nm emission bands, respectively.

The predominant excitation spectral features (590nm and 438nm) for both the 690nm and 722nm emission bands are characteristic of Chl a. The spectra in Fig. 6.1 have been normalized to their Soret maxima at 438nm. Differences in the excitation spectra below 450nm are not outside the signal-to-noise arising from the large Chl a absorbance. However, the spectral difference between 460nm and 500nm is significant and reproducible.

The differences in the 680nm and 730nm excitation spectra may reflect carotenoid absorption. Other workers have found CP1 to be devoid of Chl b (assayed by thin layer chromatography) while Chl a and carotenoids are present in ratios of 70 per P700 (determined by light-induced bleaching at 699nm, Chapter 4) and 5-6 per P700, respectively [5]. Carotenoids in spinach chloroplasts have absorption maxima at 485nm and 455nm and a shoulder at 428nm [6]. The broad increase in the excitation spectra of 680nm relative to 730nm, centered at 480-485nm may reflect the 485nm carotenoid absorption while the 455nm and 428nm features are lost in the Chl a Soret region. Thus, the excitation spectra at 77K indicate that (1) CP1 emission at both 690nm and 722nm arises from Chl a excitation and (2) the carotenoids in CP1 transfer their excitation preferentially to the 690nm emitting species.

6.4 Temperature Dependence of CP1 Emission

The CP1 emission spectrum has a dramatic temperature dependence. Fig. 6.2 is a temperature profile of a single sample. The temperature effect is completely reversible. As the temperature is lowered the 690nm peak at 295K becomes a 695nm shoulder at 77K. The apparent shift to the red is due, in part, to overlap with the increasing 722nm band.

Figure 6.2. Temperature Dependence of CP1 fluorescence emission. Fluorescence intensity vs. emission wavelength is displayed over the temperature range 119K to 293K.

CP1 is suspended in 30% glycerol, 5mM ascorbate, 15mM NaCl, 5mM $MgCl_2$ and 50mM Tris, pH 7.5. Measurements are done on the same sample. The temperature effect is reversible. Each spectrum is the sum of two scans and is corrected for any wavelength dependence of the emission monochromator and the PMT. Instrument settings: excitation wavelength, 436nm; scan rate, 1.0nm/s; response time, 500ms; front face detection; pathlength, 1.0cm; excitation and emission bandwidths, 4nm.

TEMPERATURE DEPENDENCE OF CP1 FLUORESCENCE EMISSION; EXCITATION AT 438NM

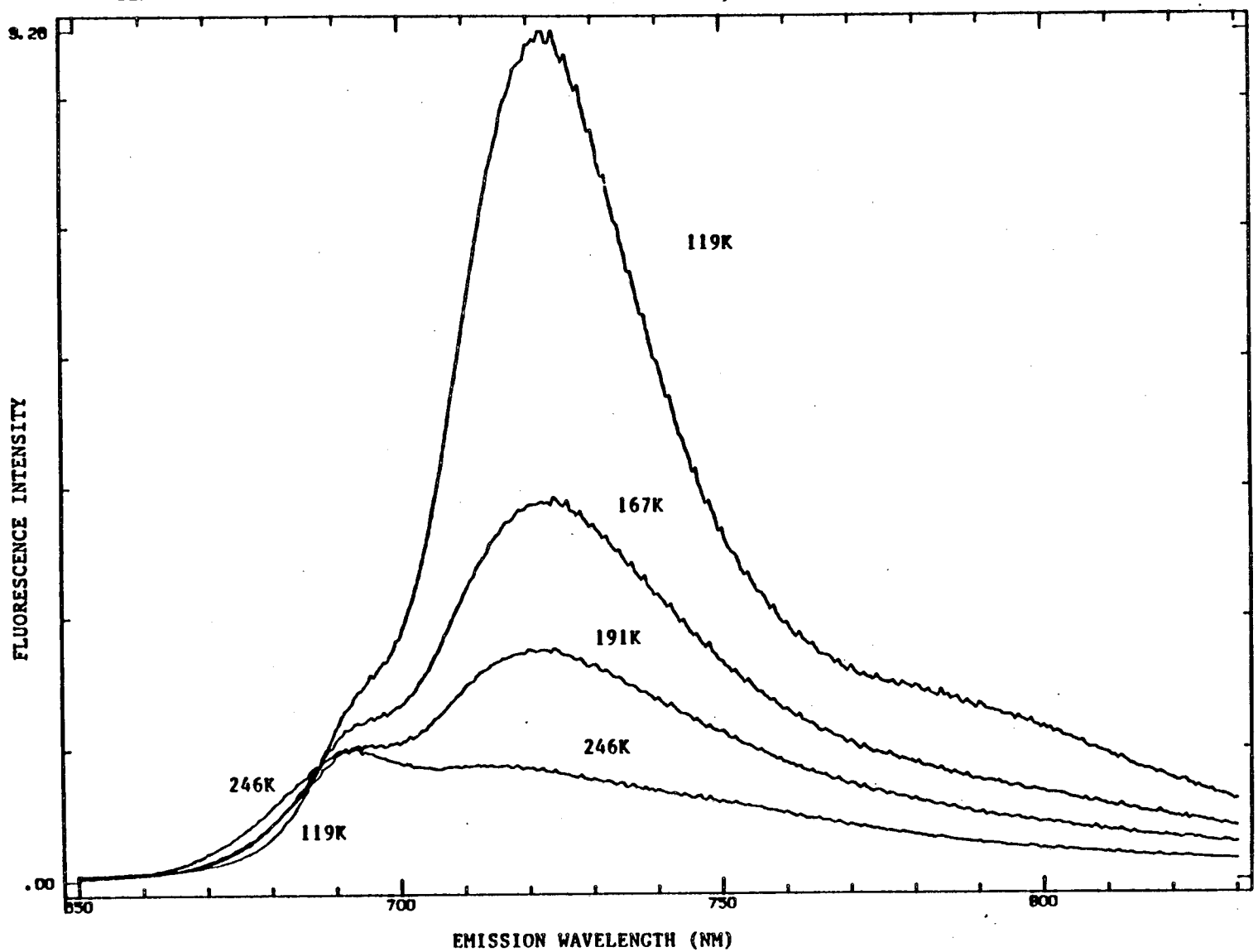

XBL 868-2897

Figure 6.3. Fluorescence intensity of the 722nm and 690nm emission bands as a function of temperature.

These points are obtained from steady state fluorescence spectra some of which are displayed in Fig. 6.2. No corrections are made to account for spectral overlap. The sample and experimental conditions are stated in Fig. 6.2.

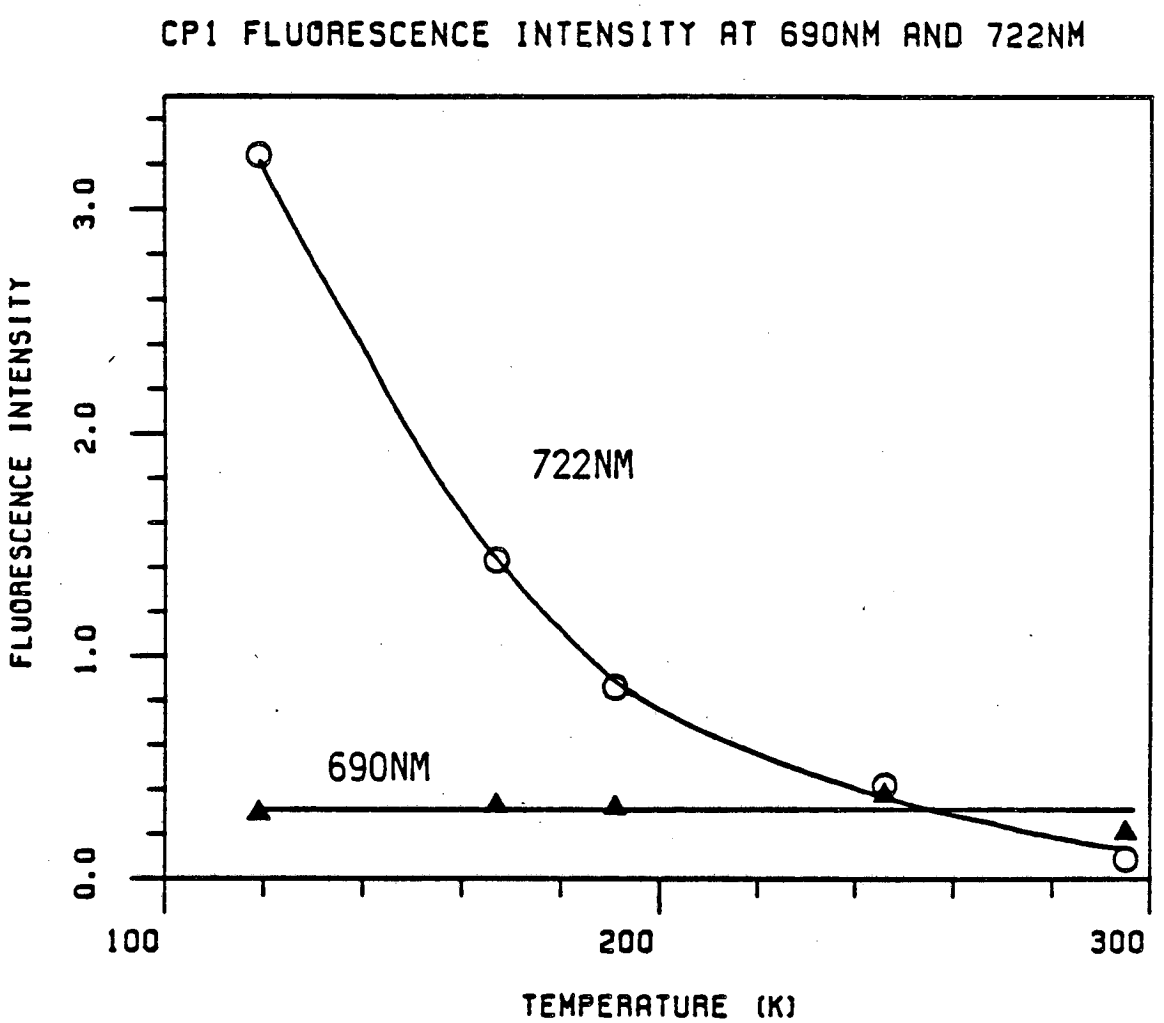
CP1 FLUORESCENCE INTENSITY AT 690NM AND 722NM
FLUORESCENCE INTENSITY
0.0
1.0
2.0
3.0
722NM
690NM
100
200
300
TEMPERATURE (K)

XBL 868-2893

A comparison of fluorescence intensity at 690nm and 722nm as a function of temperature is displayed in Fig. 6.3. The fluorescence intensity at 690nm increases only slightly with decreasing temperature, while the intensity at 722nm increases over 15-fold from 295K to 120K and 25- to 30-fold from 295K to 77K (data not shown). Since no corrections are made for spectral overlap, the observed increase at 690nm is most likely due entirely to contributions from the increasing 722nm emission. This is confirmed by the observation that the fluorescence yield at 680nm (less influenced by 722nm emission) decreases slightly upon lowering the temperature, Section 6.9.

The temperature behavior of CP1 fluorescence at 722nm is not an intrinsic property of isolated chl a *in vitro* [4] and must result from temperature changes in excitation quenching and energy transfer characteristic of the reaction center complex.

6.5 Picosecond Fluorescence Kinetics at 295K

The picosecond fluorescence decay kinetics at 295K over the emission range 680nm-800nm are best fit to three exponential components: fast, 65-90ps; middle, 200-350ps; and slow, 1.2-1.6ns, Fig. 6.4A. The CP1 particles are suspended in 5mM ascorbate. The low intensity (10^6-10^8 photons per cm^{-2} per pulse, 620nm) excitation pulses allow the reaction center to remain in the state P700A, as confirmed by the lack of variable fluorescence under these excitation conditions. All fluorescence rises are instrument limited at 50ps. The lifetimes vary little with emission wavelength. The absolute amplitudes, expressed as a product of the relative amplitude and the total fluorescence yield of an individual measurement, are corrected for any differences in data collection time and filter transmission, Fig. 6.4B. A global analysis fitting routine (Section 2.6) applied to the same data allows the component amplitudes and lifetimes to float to the best fit, but each lifetime is restricted to a constant value over the entire emission wavelength range. The results of the global analysis resolve the component lifetimes of 65ps, 320ps and 1.5ns, Fig. 6.5. and give similar absolute amplitude profiles as the individual kinetic analysis described above. Addition of a fourth component does not improve the fit. The fluorescence kinetics are indistinguishable for the excitation wavelengths 590nm, 600nm and 620nm.

The fast (65ps) component dominates the fluorescence decay amplitude and follows the steady state emission spectrum profile, Fig. 4.3, with a maximum amplitude at 690nm, Figs.

Figure 6.4. Prompt Fluorescence Decay Kinetics at 295K.

CP1 is suspended at 10μg Chl/ml in 15mM NaCl, 5mM $MgCl_2$, 5mM ascorbate and 50mM Tris, pH 7.5. The sample is stirred during measurements. For this set of data, the excitation wavelength is 620nm; similar results are obtained for excitation wavelengths 590nm and 600nm. Measurements are made with the PMT detector.

The fluorescence kinetics are fit allowing individual lifetimes and amplitudes at each wavelength. The rise is instrument limited at 50ps. The fluorescence decays, at emission wavelengths 680-800nm, are fit best to the sum of three exponential components: slow, 1.2-1.6ns; middle, 200-350ps; and fast, 65-90ps. χ^2 values ranged from 0.96 to 1.2.

A. Lifetimes of the three decay components vs. emission wavelength.

B. Absolute amplitudes of the three components vs. emission wavelength. The absolute amplitude is a product of the relative component amplitude and the total fluorescence yield of the kinetic measurement, corrected for differences in data collection time and filter transmission.

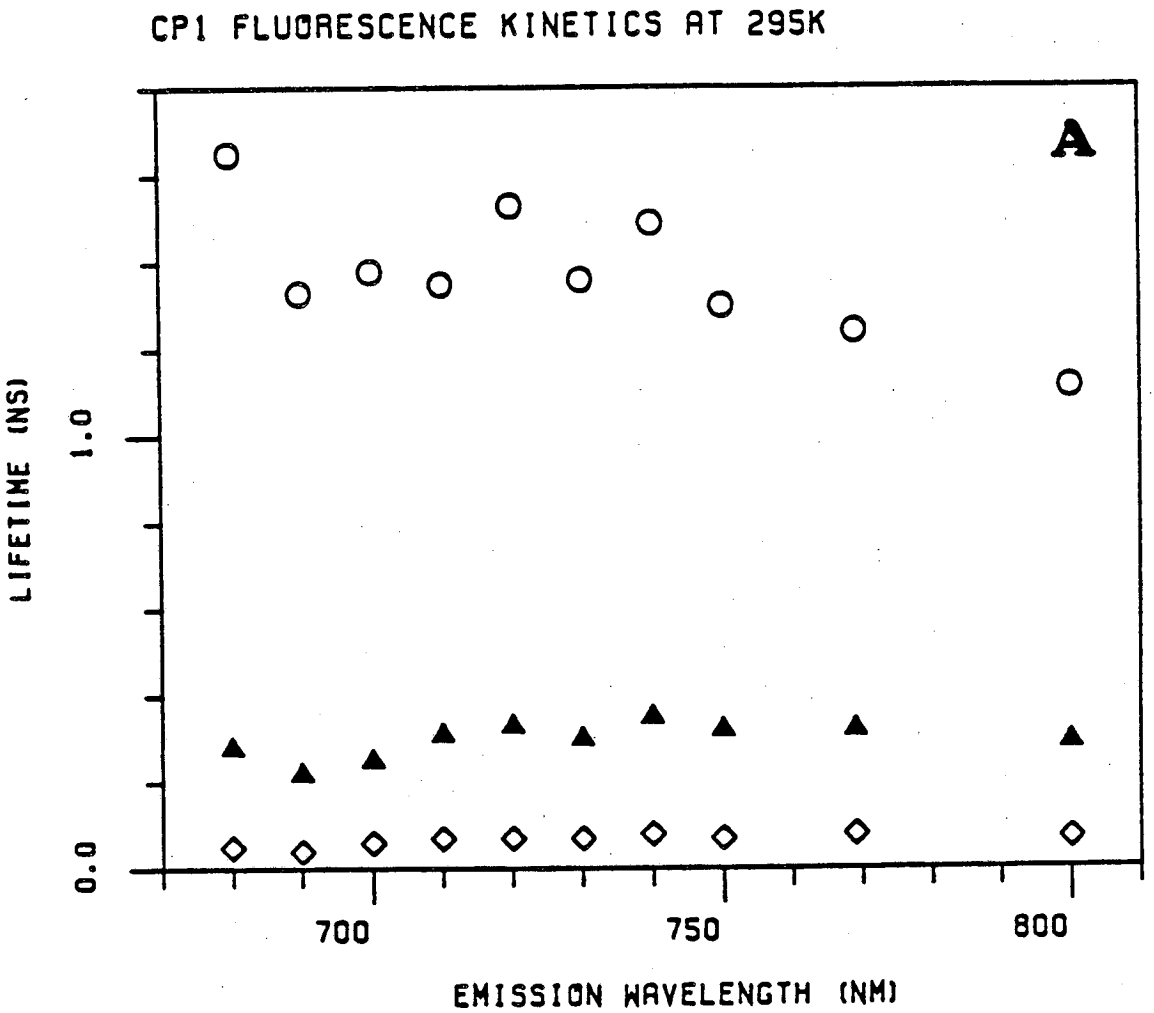
CP1 FLUORESCENCE KINETICS AT 295K
A
LIFETIME (NS)
1.0
0.0
700
750
800
EMISSION WAVELENGTH (NM)

XBL 868-2883

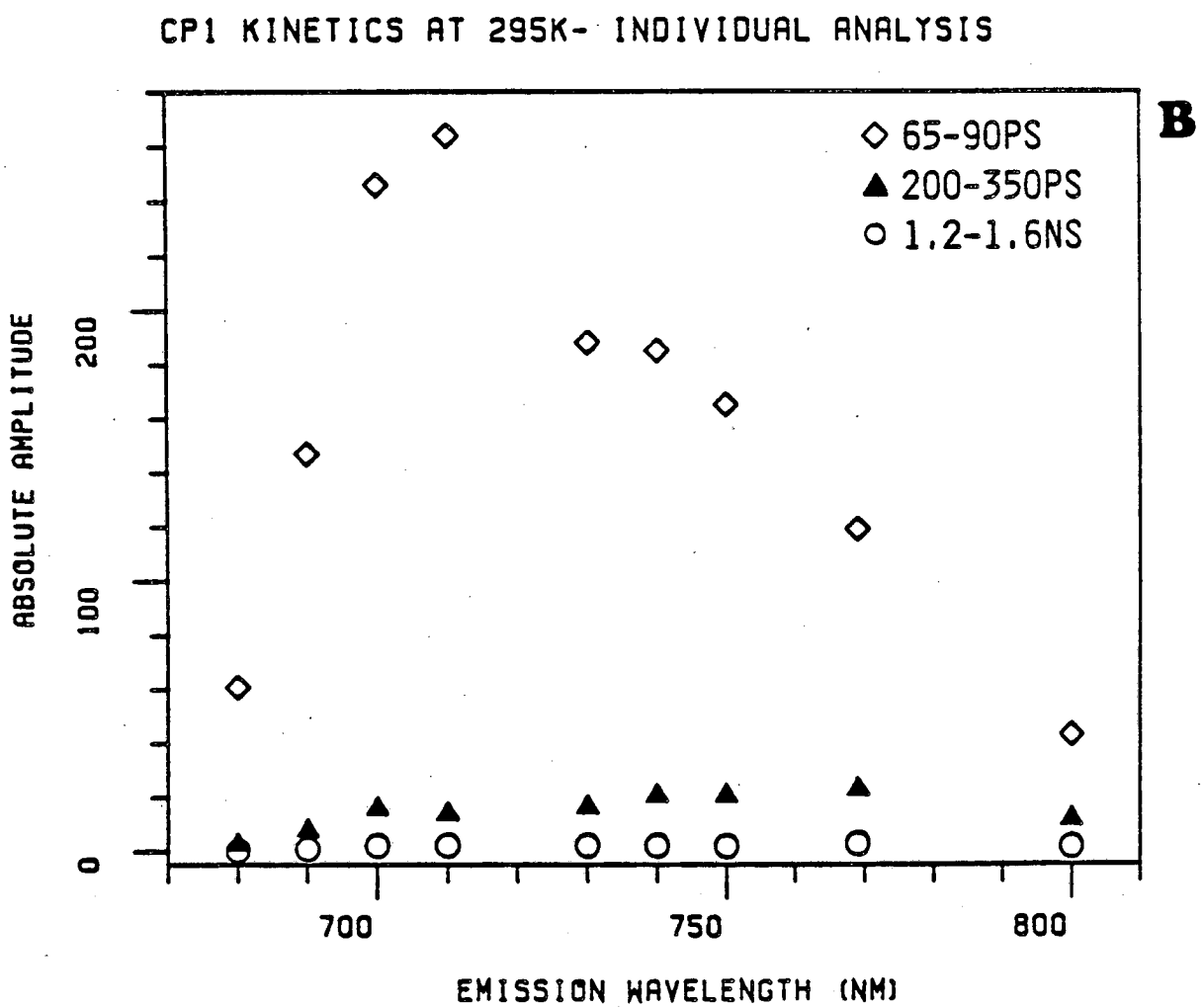
CP1 KINETICS AT 295K- INDIVIDUAL ANALYSIS
B
65-90PS
200-350PS
1.2-1.6NS
ABSOLUTE AMPLITUDE
0
100
200
700
750
800
EMISSION WAVELENGTH (NM)

XBL 868-2884

Fig. 6.5. Prompt Fluorescence Decay Kinetics at 295K, fit by Global Analysis.

The same experimental data as presented in Fig. 6.4 is analysed by global analysis (Section 2.6). The component lifetimes and amplitudes are allowed to float to the best fit, however the lifetimes are restricted to a constant value over the entire emission wavelength range.

The fluorescence rise is instrument limited at 50ps. The absolute amplitudes of the three fluorescence decay components (65ps, 320ps and 1.5ns) are displayed as a function of emission wavelength. χ^2 values range from 1.4 to 1.8.

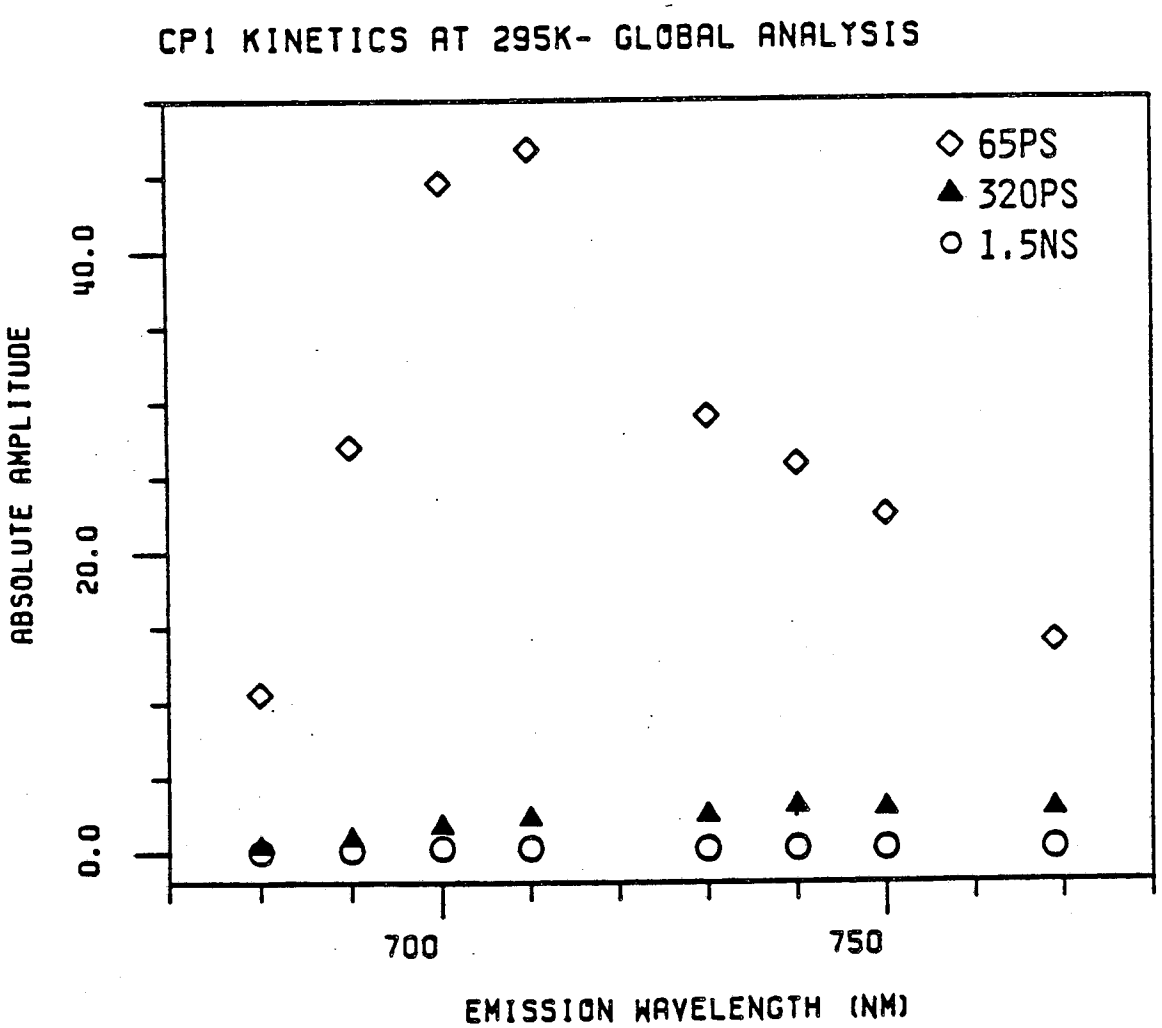
CP1 KINETICS AT 295K- GLOBAL ANALYSIS
65PS
320PS
1.5NS
ABSOLUTE AMPLITUDE
0.0
20.0
40.0
700
750
EMISSION WAVELENGTH (NM)

XBL 868-2885

6.4B and 6.5. The middle component (320ps) contributes to the emission amplitude at both 690nm and 722nm, its relative amplitude increases at longer wavelengths to as much as 25% (data not shown). The slow component (1.5ns) is also present in both emission bands however its amplitude is too small (relative amplitude <2%) for a preferential contribution to either emission band to be resolved.

6.6 Steady State Fluorescence Dependence on the Oxidation State of P700

The correlation between fluorescence quenching and the reaction center is important for understanding the excitation migration and trapping dynamics of PS I. The effects of P700 oxidation upon the 77K CP1 fluorescence emission is a direct measure of this behavior.

The state $P700^+A$ is achieved by two methods, addition of 1-5mM potassium ferricyanide to CP1 (10-20μg Chl/ml), or illumination of CP1 (10-20μg Chl/ml, 5-10mM ascorbate) for 60sec and cooling to 77K under illumination. The state P700 A is achieved by cooling CP1 (10-20μg Chl/ml, 5-10mM ascorbate) to 77K in the dark. Verification that these treatments prior to freezing produce $P700^+A$ and P700 A, respectively, is based upon optical photobleaching measurements at 700nm. Fig. 6.6 compares the 77K fluorescence emission of CP1 after treatment with 5mM ascorbate and freezing dark, 5mM ascorbate and freezing under illumination, and 1mM potassium ferricyanide. The treatments which produce $P700^+A$ have similar emission spectra and dramatically decrease the overall fluorescence yield, Fig. 6.6. Due to the shattered state of the frozen sample, the chlorophyll absorption can vary depending of the position of the sample relative to the excitation beam. The entire emission intensity can vary up to 20%. However, these experimental differences do not affect the relative peak intensities. The ratios of the fluorescence intensities of the two emission bands, F_{722}/F_{690}, is 15.5±1.0 for P700 A and 6.0±0.5 for $P700^+A$. The state $P700^+A$ preferentially quenches the 722nm emission relative to the 690nm emission. In addition, oxidation of P700 shifts the 722nm emission maximum slightly to 720nm.

The fluorescence changes arising from P700 oxidation can be partly reversed. When the $P700^+A$ sample obtained by illumination during freezing (5mM ascorbate) is warmed in the dark to 295K, dark adapted 10-30min and cooled to 77K in the dark, the ascorbate reduces $P700^+$ at room temperature and the state P700 A results. The F_{722}/F_{690} ratio increases to 9.5±0.5,

Figure 6.6. Fluorescence emission spectra at 77K of P700 A vs. $P700^+A$.

The CP1 is suspended at 20μg Chl/ml in 50% glycerol, 15mM NaCl, 5mM $MgCl_2$ and 50mM Tris, pH 7.5. The excitation wavelength is 640nm. Spectra are corrected for any wavelength dependence of the emission monochromator and PMT. The excitation and emission bandwidths are 4nm.

Three CP1 treatments are displayed: 1mM potassium ferricyanide, cooled in the dark to 77K; 5mM ascorbate, cooled in the dark to 77K; and 5mM ascorbate, illuminated 60sec and cooled under illumination to 77K.

The amplitudes of the spectra can be directly compared. However, there is an experimental variance in the overall fluorescence intensity of 20%, resulting primarily from non-uniform cracking of the sample suspension during freezing. The ratios of peak intensities are independent of these differences in overall intensity.

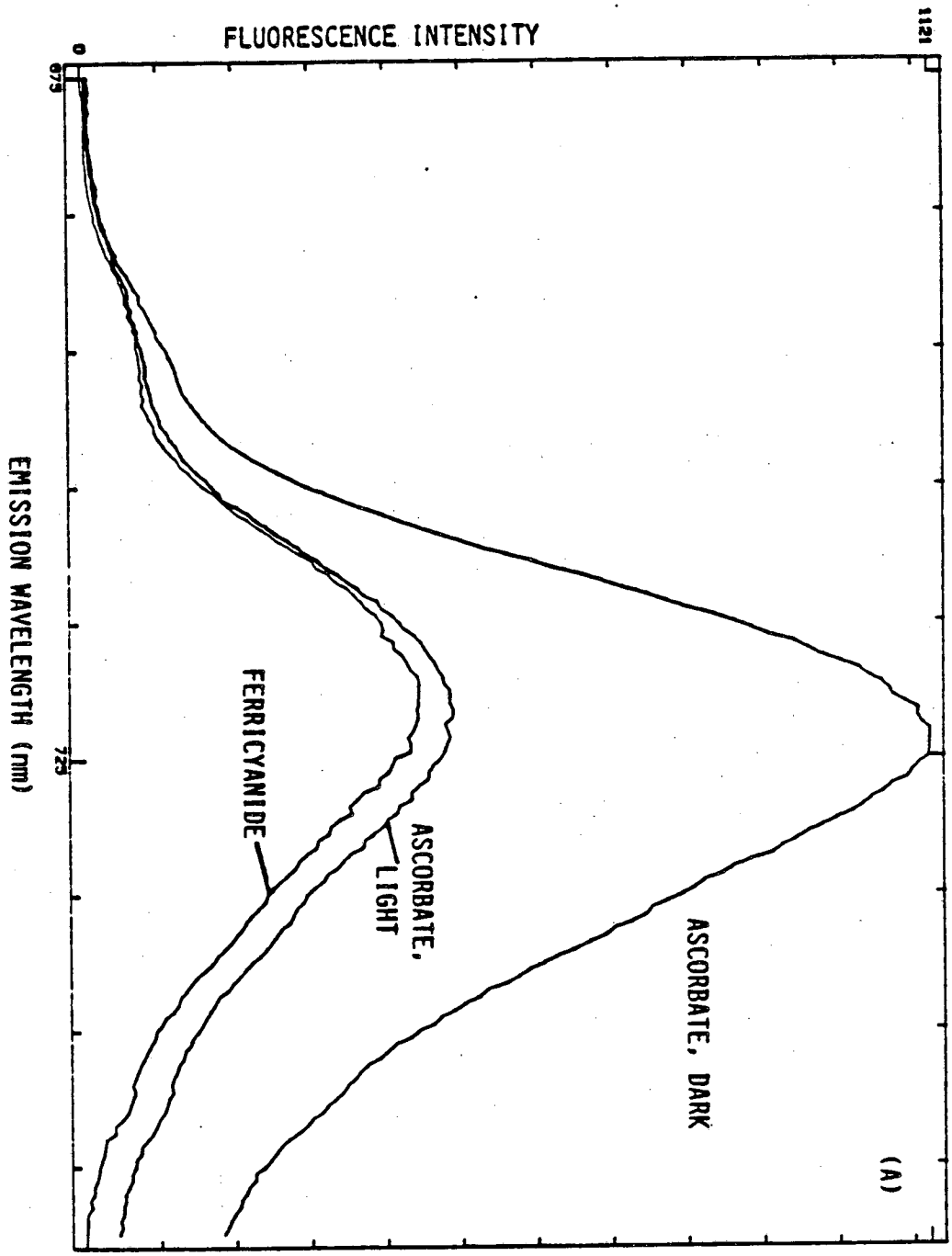
(A)
ASCORBATE, DARK
ASCORBATE, LIGHT
FERRICYANIDE
FLUORESCENCE INTENSITY
1121
0
675
725
EMISSION WAVELENGTH (nm)

Figure 6.7. Reversibility of Fluorescence Changes in CP1 at 77K due to P700 Oxidation. Experimental conditions are described in Fig. 6.6.

Three CP1 treatments are displayed: (DARK) 5mM ascorbate, cooled in the dark to 77K; (LIGHT) 5mM ascorbate, illuminated 60sec and cooled to 77K under illumination; (REVERSED) the (LIGHT) sample is warmed to 295K, dark adapted 30min and cooled in the dark to 77K.

The spectra are normalized to their emission maxima and are directly comparable.

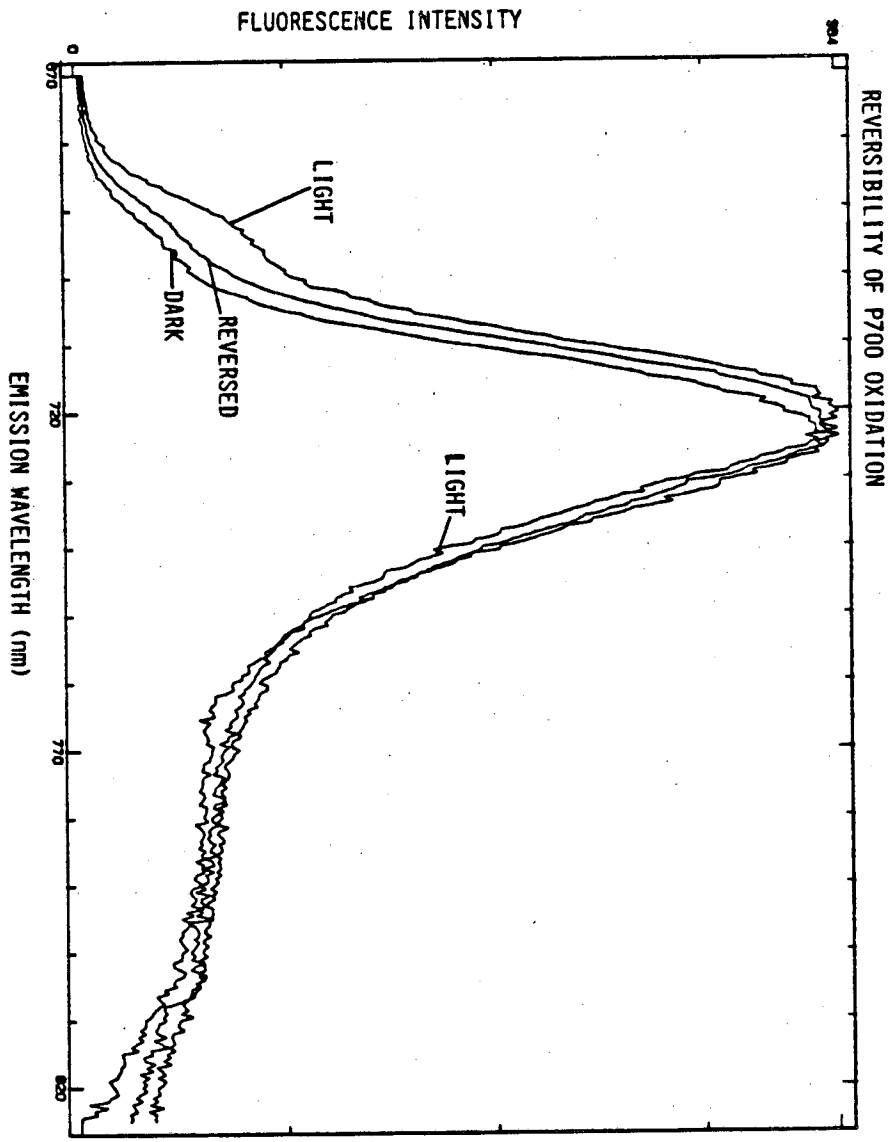
REVERSIBILITY OF P700 OXIDATION
FLUORESCENCE INTENSITY
EMISSION WAVELENGTH (nm)
LIGHT
DARK
REVERSED
LIGHT
0
670
720
770
820

XBL 868-2896

Fig. 6.7. In summary, oxidation of P700 by either pre-illumination or treatment with ferricyanide produces a 3-fold decrease in the fluorescence intensity at 722nm relative to 690nm at 77K.

6.7 Picosecond Fluorescence Kinetics at 77K

CP1 is suspended in 5mM ascorbate and frozen in the dark, trapping the state P700A. Steady state emission experiments confirm that CP1 remains in the equilibrium state P700A during kinetic measurements, Fig. 6.6. The prompt fluorescence kinetics of CP1 at 77K, over the emission wavelengths 670-740nm, are best described by four components, Fig. 6.8. A fifth component does not improve the fit. The lifetimes determined by global analysis are 70ps, 270ps, 1.3ns and 5.0ns. The small amplitude of the slowest decay component introduces a significant margin of error in the 5.0ns lifetime.

The absolute amplitudes of the fluorescence components are displayed as a function of emission wavelength in Fig. 6.8, where a negative amplitude represents a risetime (Section 2.6). The 70ps component dominates the 690nm emission decay at 77K and contributes as a rise to the 722nm emission. The slower decay components, 1.3ns and 5.0ns, comprise the 722nm emission. The 270ps decay appears to contribute to both emission bands. When the temperature is raised to 295K the fluorescence kinetics return to those observed prior to cooling, Fig. 6.4.

6.8 Dependence of the Prompt Fluorescence Kinetics at 77K on the Oxidation State of P700

In section 6.6 we saw that the oxidation of P700 decreased the relative fluorescence intensity at 722nm in CP1 particles at 77K. It is informative to observe how this behavior is related in changes in the prompt fluorescence kinetics. In this section, the picosecond fluorescence kinetics of CP1 particles in the open state, PA, are compared to the closed state, P^+A, Fig. 6.10. Open centers are prepared by treating the CP1 particles with 5mM ascorbate, in the dark, prior to freezing (reduced samples). Closed centers are prepared by treating CP1 particles with 5mM ferricyanide prior to freezing (oxidized samples).

The total relative fluorescence yields obtained from the kinetic measurements are displayed as a function of emission wavelength, Fig. 6.9. These yields are determined by numerical integration of the deconvoluted fluorescence decay curves (see Materials and Methods). The

Figure 6.8. Prompt Fluorescence Kinetics of CP1 at 77K.

CP1 is suspended at A_{675} = 0.2 in 10% glycerol, 5mM ascorbate, 15mM NaCl, 5mM $MgCl_2$ and 50mM Tris, pH 7.5.

The absolute amplitudes of resolved fluorescence rise and decay components as a function of emission wavelength. The excitation wavelength is 620nm. A negative amplitude indicates a rise. The data are fit by global analysis to four exponential components: 5.0ns; 1.3ns; 270ps; and 70ps. Measurements are made with the MCP detector. The χ^2 values range from 1.1 to 1.6.

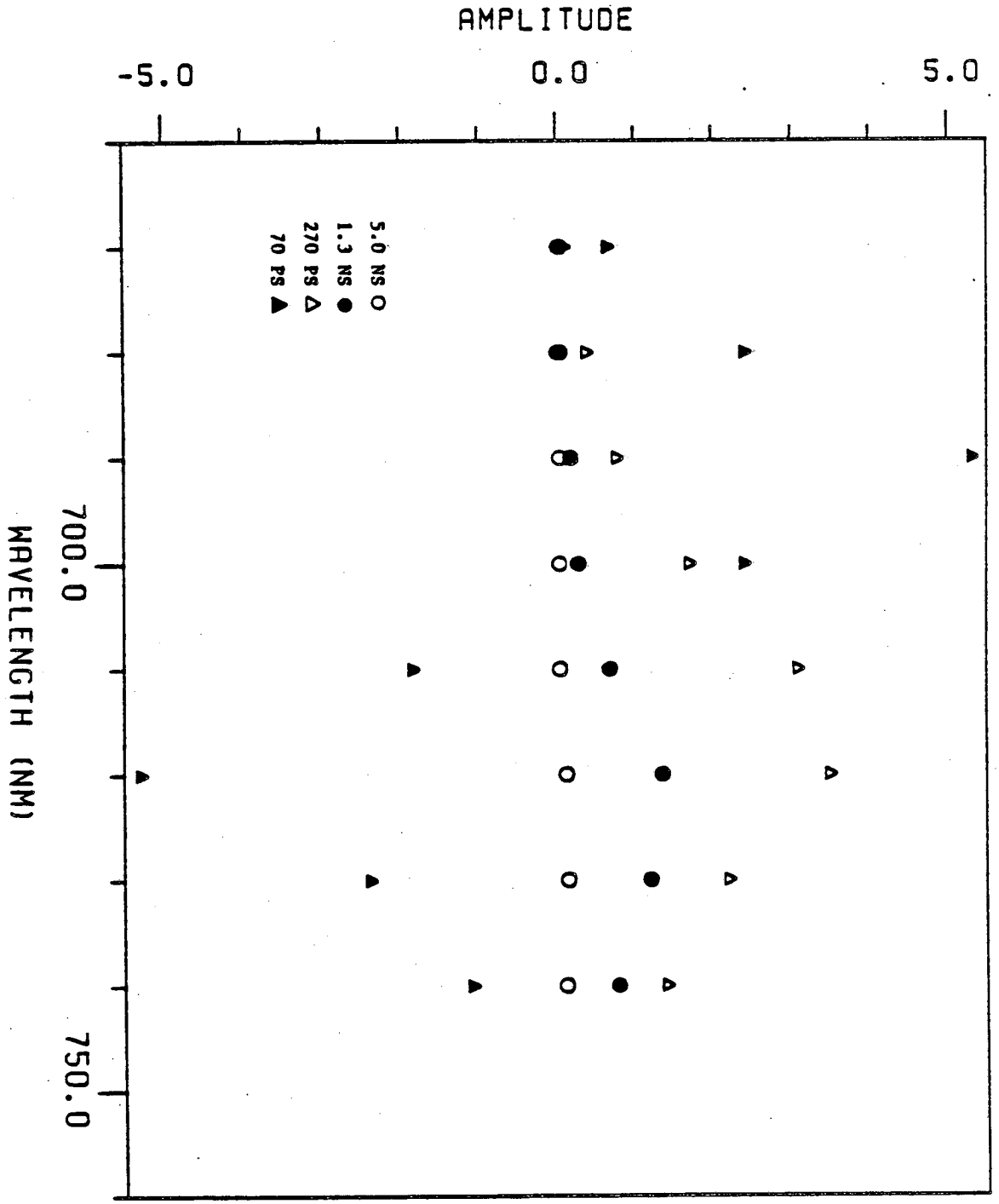
AMPLITUDE
-5.0
0.0
5.0
5.0 NS ○
1.3 NS ●
270 PS △
70 PS ▲
700.0
750.0
WAVELENGTH (NM)

Figure 6.9 Dependence of the Fluorescence Yields Obtained from Kinetic Measurements on the Oxidation State of P700.

The fluorescence yields of CP1 in the oxidized state (P^+A) and reduced state (P A) as a function of emission wavelength are obtained from picosecond kinetic measurements. Corrections are made for differences in data collection time and filter transmission.

CP1 is suspended at A_{675} = 0.2, in 15mM NaCl, 5mM $MgCl_2$, 10% glycerol and 50mM Tris, pH 7.5. The reduced sample is treated with 5mM ascorbate. The oxidized sample is treated with 5mM ferricyanide. The chlorophyll concentrations are identical. However, due to the shattered state of the sample, the chlorophyll absorption can vary, resulting in differences in the emission spectrum intensity of up to 20%.

The excitation wavelength is 620nm. The data were recorded with the MCP detector.

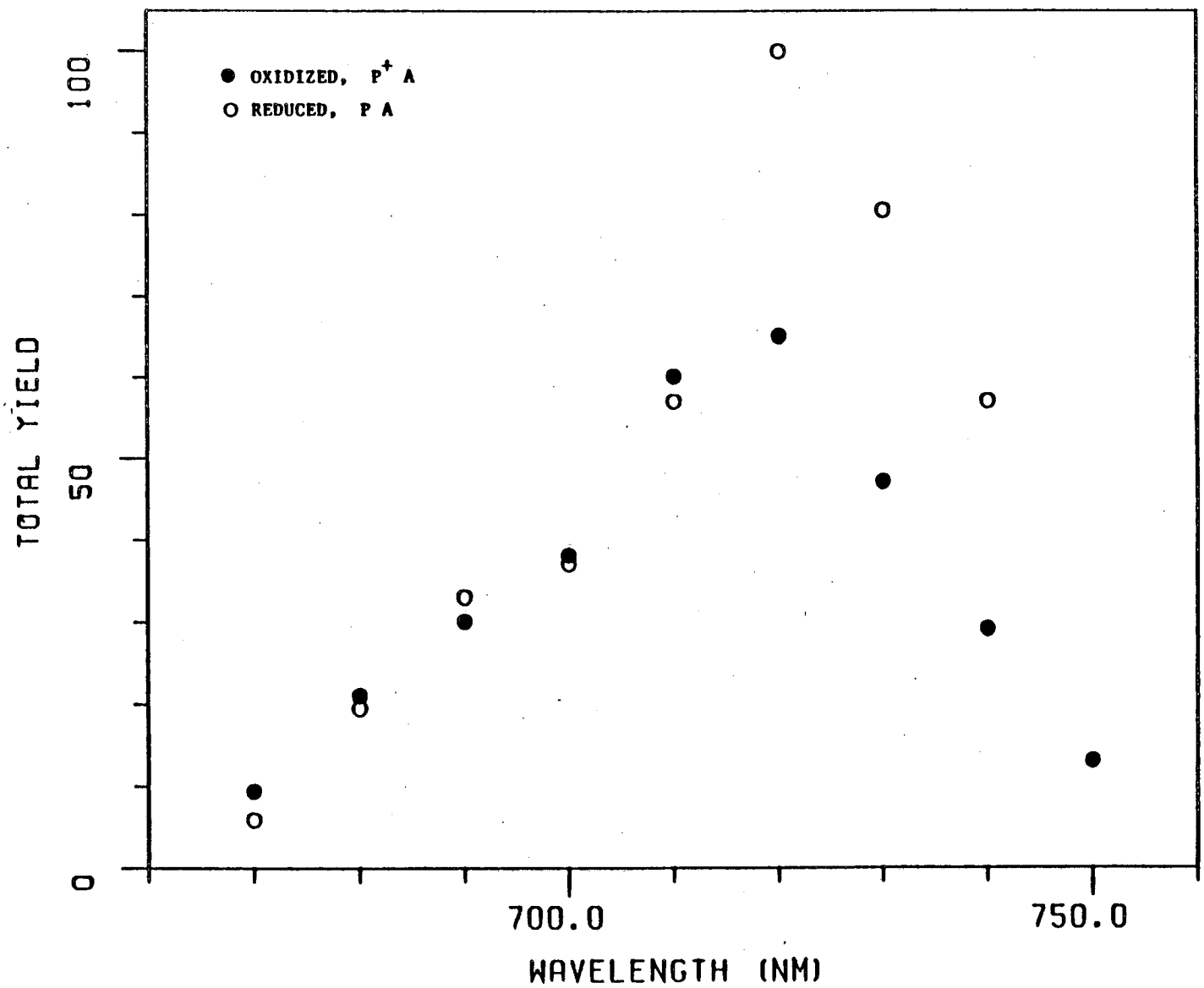
● OXIDIZED, P+ A
O REDUCED, P A
TOTAL YIELD
0
50
100
700.0
750.0
WAVELENGTH (NM)

Figure 6.10 Dependence of the Prompt Fluorescence Kinetics on P700 Oxidation.

The experimental and sample conditions are described in Figure 6.10.

The component yields ($\phi_i = \alpha_i \tau_i$) of the resolved fluorescence rise and decay components are displayed as a function of emission wavelength. A negative yield indicates a rise. The data are fit by global analysis to four exponential components.

The chlorophyll concentrations are the same; the component yields of the oxidized and reduced samples are directly comparable. However, due to the shattered state of the frozen sample, the chlorophyll absorbance varies, which can be reflected in differences in the yields of up to 20%. The component lifetimes are independent of the oxidation state of P700 within our resolution (10%).

A. Reduced P700. CP1 is treated with 5mM ascorbate and has the dark adapted state, P700 A. The component lifetimes are: 5.0ns, 1.3ns, 270ps and 70ps.

B. Oxidized P700. CP1 is treated with 5mM ferricyanide and has the dark adapted state, $P700^+$ A. The component lifetimes are: 4.5ns, 1.2ns, 250ps and 70ps.

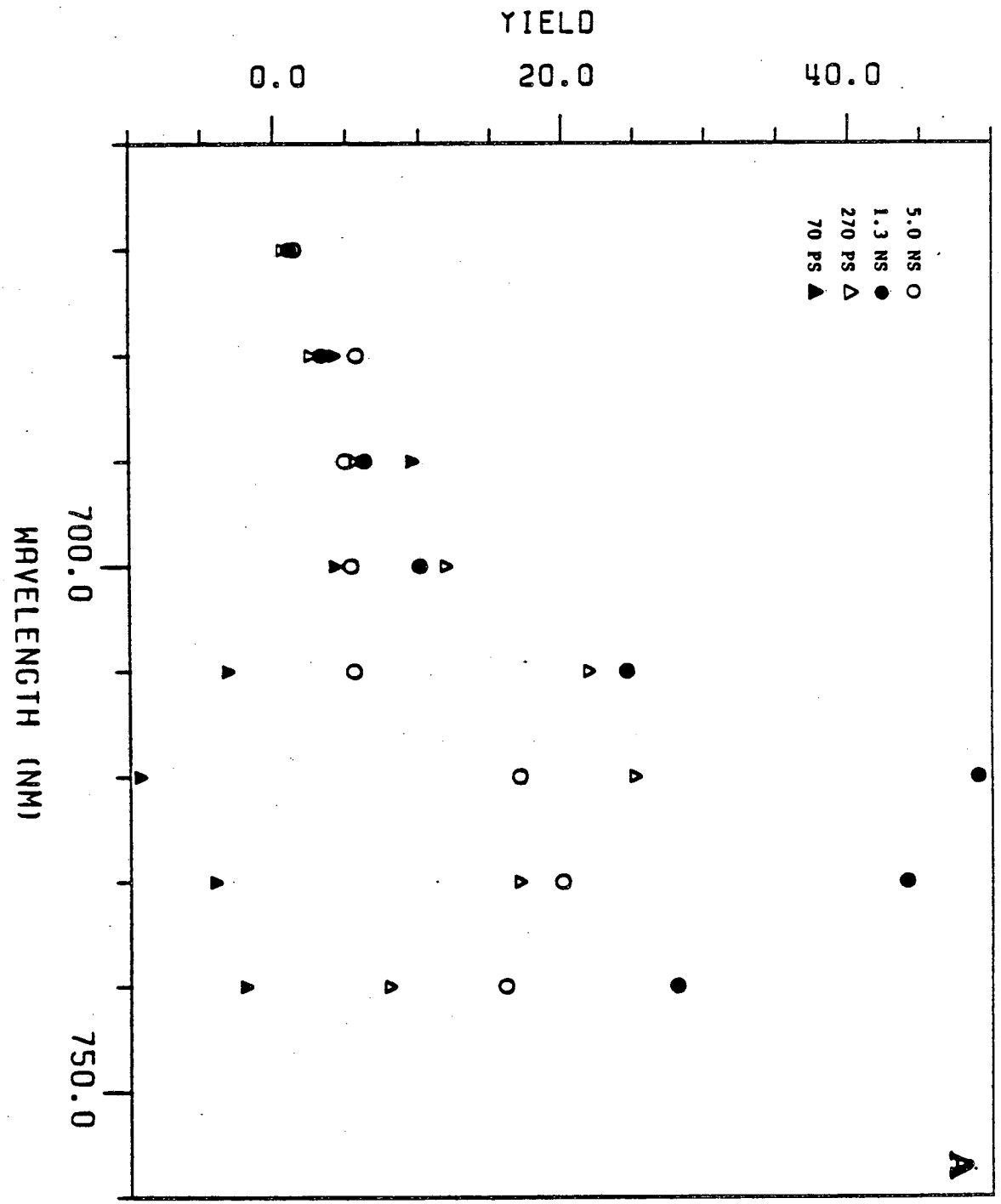
YIELD
0.0
20.0
40.0
5.0 NS ○
1.3 NS ●
270 PS △
70 PS ▲
700.0
750.0
WAVELENGTH (NM)
A

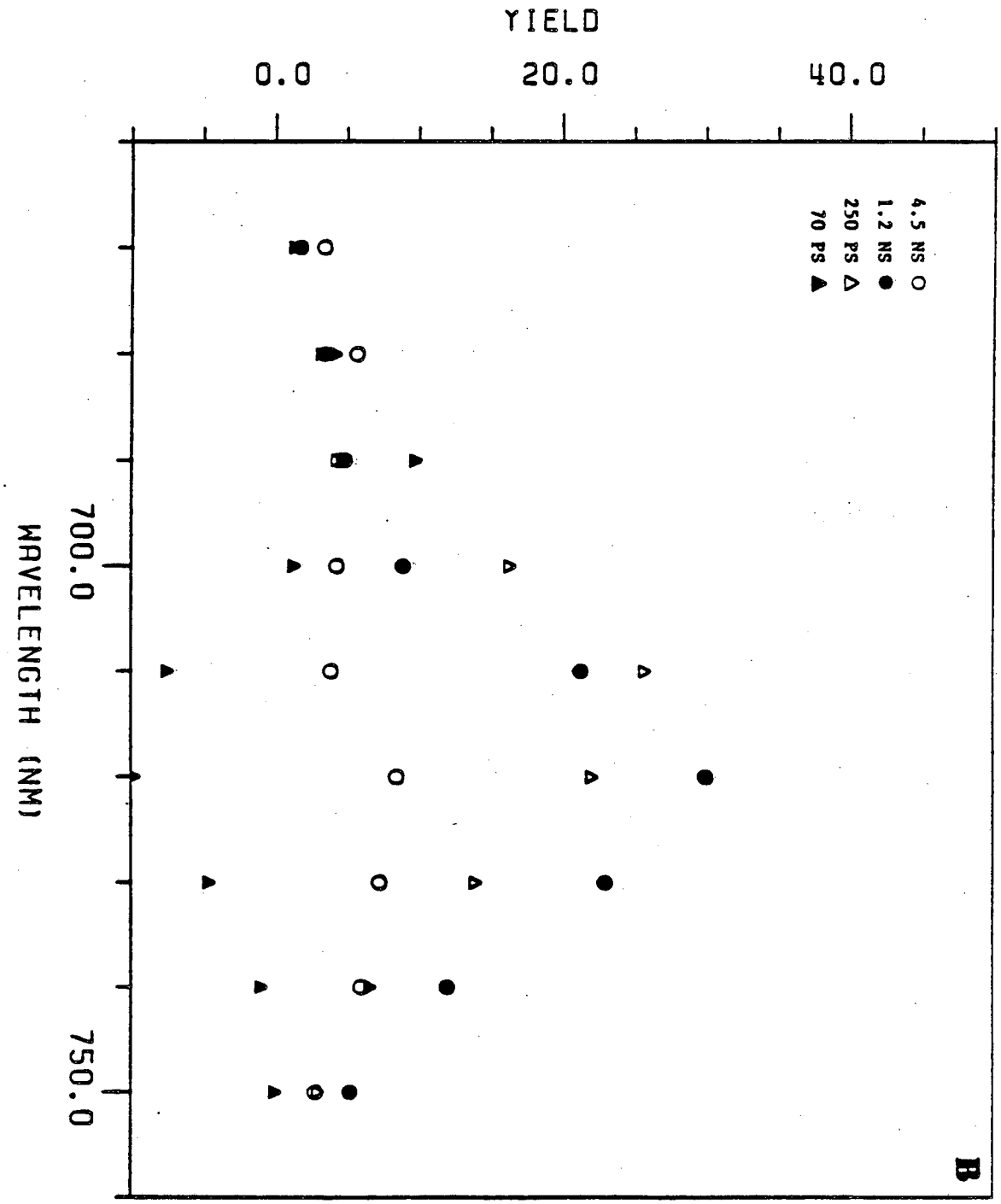
YIELD
0.0
20.0
40.0
4.5 NS ○
1.2 NS ●
250 PS △
70 PS ▲
B
700.0
750.0
WAVELENGTH (NM)

values of the total relative fluorescence yield for the two preparations are scaled to a total yield of 100 at 720nm in ascorbate-treated samples. The chlorophyll concentrations are identical, so the yields between the oxidized and reduced samples are directly comparable. However, due to differences in chlorophyll absorption arising from cracks in the frozen sample, there is a 20% variability in the fluorescence yields. Nevertheless, the fluorescence yields from the prompt kinetic measurements have a wavelength dependence similar to that of the steady state emission spectrum, Fig. 6.6. Treatment of CP1 particles with ferricyanide, P^+A, produces a decrease in the 720nm emission relative to ascorbate treated samples, PA. The similarity between the yields from the fluorescence kinetic measurements and the steady state emission spectra is important for two reasons. (1) It confirms that the prompt fluorescence kinetic measurements made on ascorbate treated CP1 particles (Sections 6.5 and 6.7) were monitoring excitation transfer with the centers in the open state, PA. (2) We can assume that changes in the picosecond fluorescence kinetics of ferricyanide treated samples, arise from closing the reaction centers, P^+A. (The possibility of ferricyanide oxidation of bulk antenna Chl is addressed below). Thus, the prompt fluorescence kinetics provide important information on the source of the relative fluorescence decrease at 722nm upon oxidation of P700.

The characteristics of the 77K prompt fluorescence kinetics of ascorbate treated CP1 particles (reduced) were described in Section 6.7. The same lifetimes (within our instrument resolution) are observed in ferricyanide treated CP1 particles (oxidized): 70±10ps, 260±25ps, 1.25±0.13ns and 4.5±0.5ns. The component yields are displayed as a function of emission wavelength in Figure 6.10, where a negative yield represents a rise component. The experimental conditions and chlorophyll concentrations are identical for both oxidized and reduced samples so that the yields can be directly compared. The oxidation state of P700 has no measurable influence on the 70ps and 260ps components. However, the yields of the slower decay components, 1.25ns and 4.5ns, decrease about 2-fold in the 720nm emission band when P700 is oxidized, P^+ A. It is unlikely that ferricyanide treatment produces a significant amount of free or dissociated bulk antenna chlorophyll, which should give rise to an increase in the yield of a 5-6ns decay component [7].

Chemical oxidation of P700 decreases the relative fluorescence intensity of the 720nm emission of CP1 at 77K. The effect of P700 oxidation on the CP1 emission spectrum does

not reflect a change in the lifetimes of the prompt fluorescence kinetics, but rather a 2-fold decrease in the yield at 720nm of the 1.25ns and 4.5ns decay components.

6.9 Temperature Dependence of Fluorescence Yields from Kinetic Measurements

The temperature dependence of the fluorescence yields from CP1 at 680nm and 730nm obtained from the prompt fluorescence kinetics measurements is displayed in Fig. 6.11. The total relative fluorescence yield is obtained by numerical deconvolution of the fluorescence decay and corrected for differences in the data collection time and filter transmission (see Materials and Methods). The yields are scaled to 100 at the lowest temperature (103K) and can be directly compared between the two emission wavelengths. Thus, we obtain a temperature profile of the fluorescence yields at 680nm and 730nm.

It is informative to compare this profile to the temperature dependence of the fluorescence intensities at 690nm and 722nm, Fig. 6.3, to estimate the contribution of the 722nm emission to the 690nm fluorescence intensity. The temperature dependence of the CP1 fluorescence intensity at 722nm and 730nm is the same. The fluorescence intensity at 680nm decreases slightly with temperature while at 690nm it increases slightly. The 690nm values are somewhat elevated due to overlap with 722nm emission. Therefore, the slight decrease in fluorescence intensity with decreasing temperature, as observed at 680nm, is a better representation of the temperature dependence of the 690nm emission band. The most accurate analysis comes from the integration of the steady state emission bands to obtain the yields of 690nm and 722nm fluorescence as a function of temperature. For each emission peak, this involves assuming a bandshape (eg. Gaussian) to correct for spectral overlap.

6.10 Picosecond Fluorescence Kinetics at 680nm as a Function of Temperature

CP1 steady state fluorescence has a dramatic temperature dependence, Fig. 6.2. It is important to understand how this temperature dependence is reflected in the fluorescence kinetic components. The fluorescence yield at 680nm decreases only slightly over the temperature range 295K to 100K, Fig. 6.11. Likewise, the lifetimes of the prompt fluorescence decay components at 680nm are not particularly temperature dependent, Fig. 6.12A.

The fluorescence kinetics of the 690nm emission band are measured at 680nm to minimize the effects due to spectral overlap with the 722nm emission band. The kinetics are

Figure 6.11 Temperature Dependence of the Fluorescence Yields Obtained from Kinetic Measurements.

The fluorescence yields of CP1 at 680nm and 730nm as a function of temperature are obtained during the picosecond kinetic measurements. Corrections are made for differences in data collection time and filter transmission. The lines through the data are not fits, only a visual aid.

The effects of changing temperature are completely reversible. The excitation wavelength is 600nm. The sample conditions are described in Fig. 6.12. At 680nm the PMT detector was employed. At 730nm both the PMT and the MCP detectors produced the same results (data not shown).

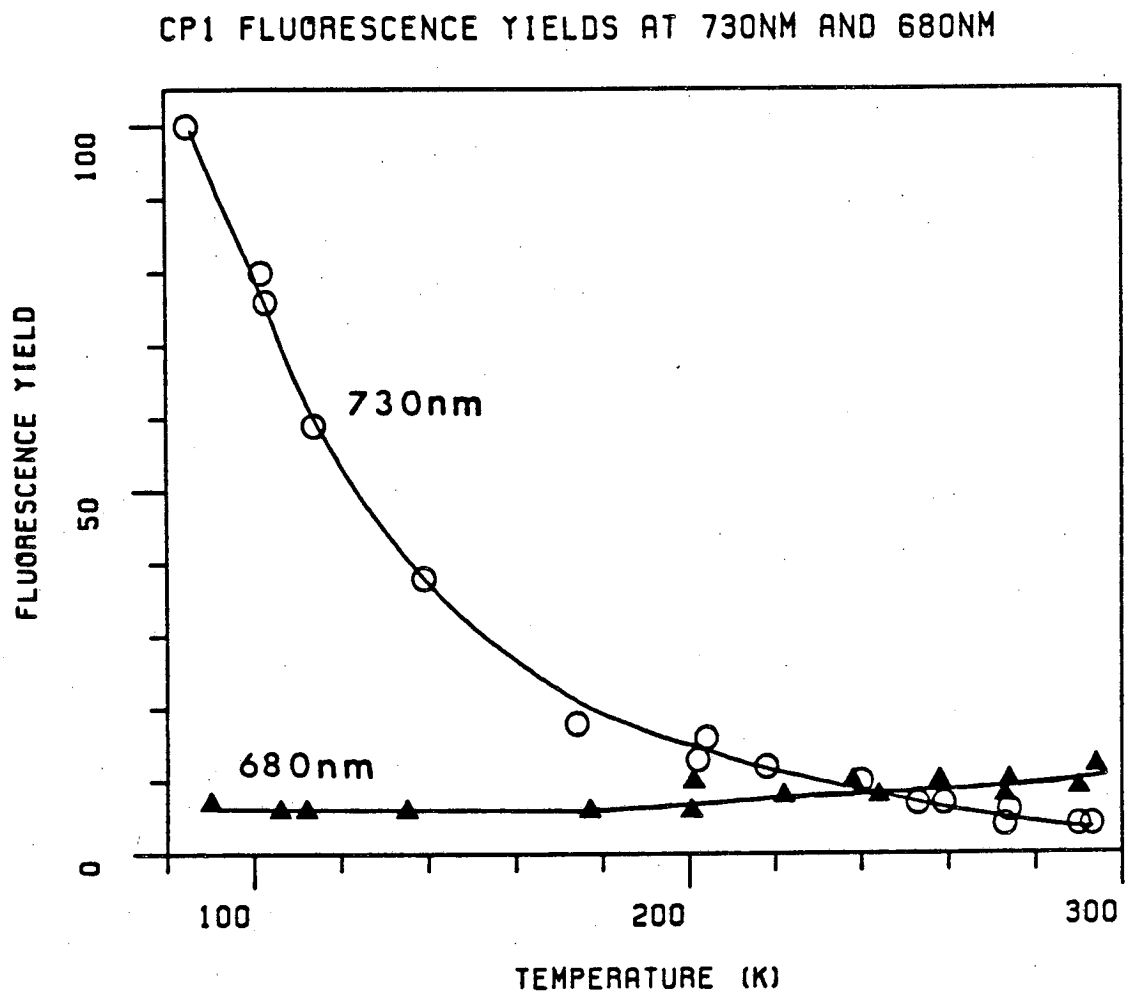
CP1 FLUORESCENCE YIELDS AT 730NM AND 680NM
FLUORESCENCE YIELD
100
50
0
730nm
680nm
100
200
300
TEMPERATURE (K)

XBL 868-2887

Figure 6.12 Temperature Dependence of CP1 Fluorescence Kinetics at 680nm.

The CP1 sample has an absorbance at 675nm of 0.19. It is suspended in 10% glycerol, 5mM ascorbate, 15mM NaCl, 5mM $MgCl_2$ and 50mM Tris, pH 7.5. The excitation wavelength is 600nm. The PMT detector (50ps response) is employed.

The decay fit best to the sum of three exponential components: slow, 2.0-2.5ns; middle, 290-370ps; and fast, 50-70ps. The rise is instrument limited at 50ps. χ^2 values range from 0.99 to 1.16. The lines through the data are not fits, only a visual aid.

A. Lifetimes (1/e) of the three decay components vs. temperature (K).

B. Relative amplitudes of the components vs. temperature (K).

C. Absolute amplitudes of components vs. temperature (K). Absolute amplitude is a product of the relative component amplitude and the fluorescence yield of each kinetic measurement corrected for differences in data collection time and filter transmissions.

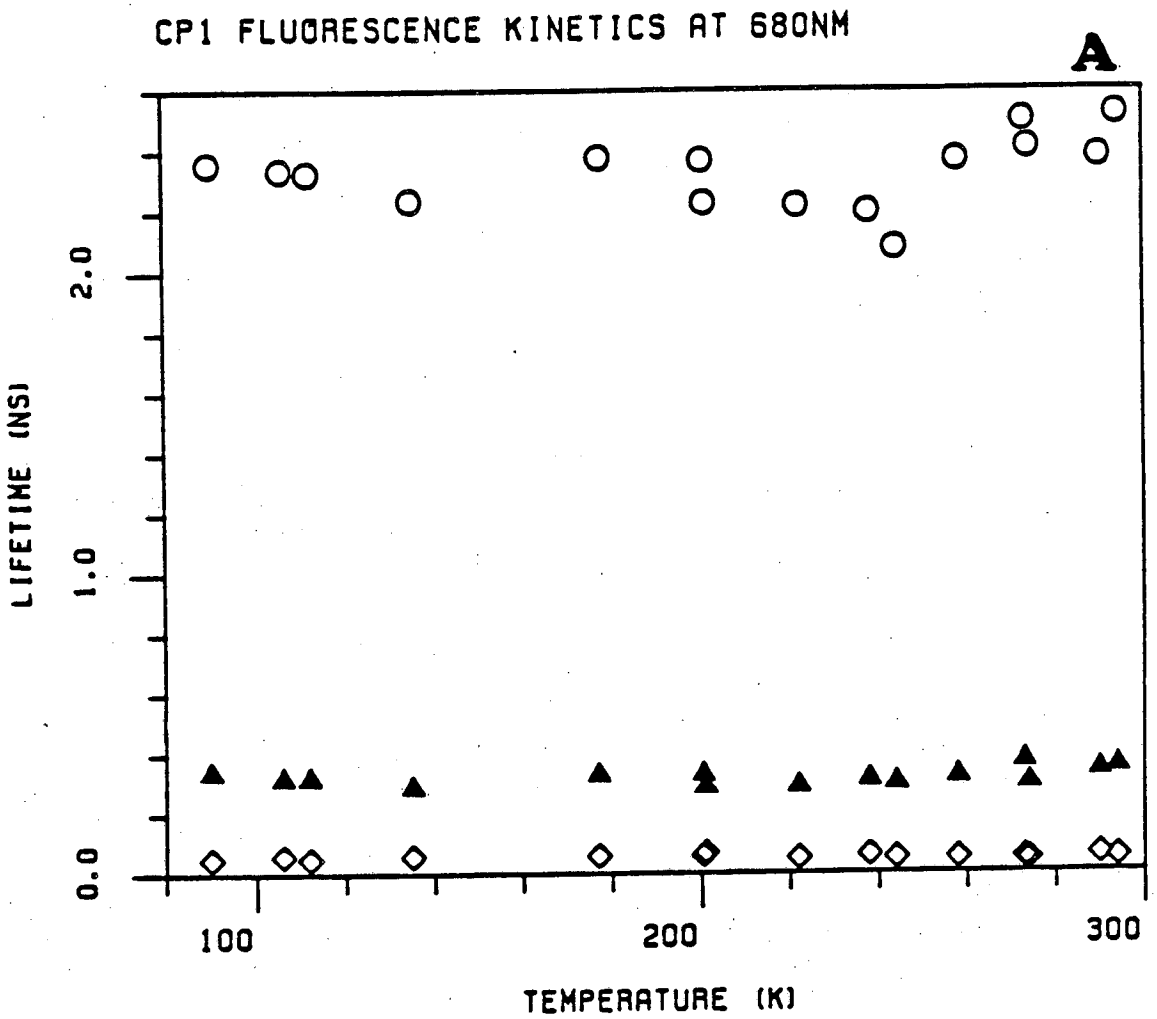
CP1 FLUORESCENCE KINETICS AT 680NM
A
LIFETIME (NS)
0.0
1.0
2.0
100
200
300
TEMPERATURE (K)

XBL 868-2888

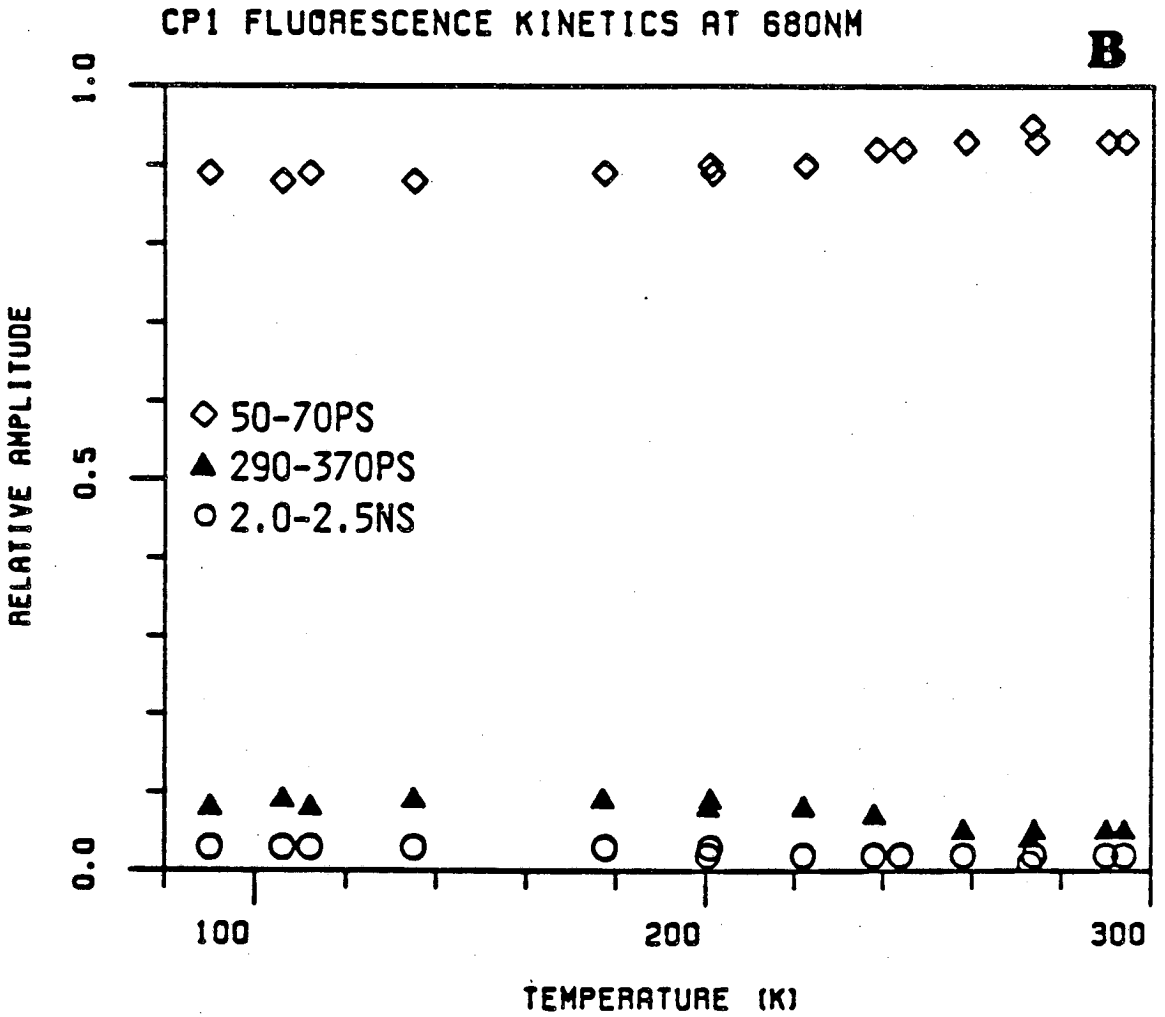
CP1 FLUORESCENCE KINETICS AT 680NM
B
1.0
0.5
0.0
RELATIVE AMPLITUDE
◇ 50-70PS
▲ 290-370PS
○ 2.0-2.5NS
100
200
300
TEMPERATURE (K)

XBL 868-2889

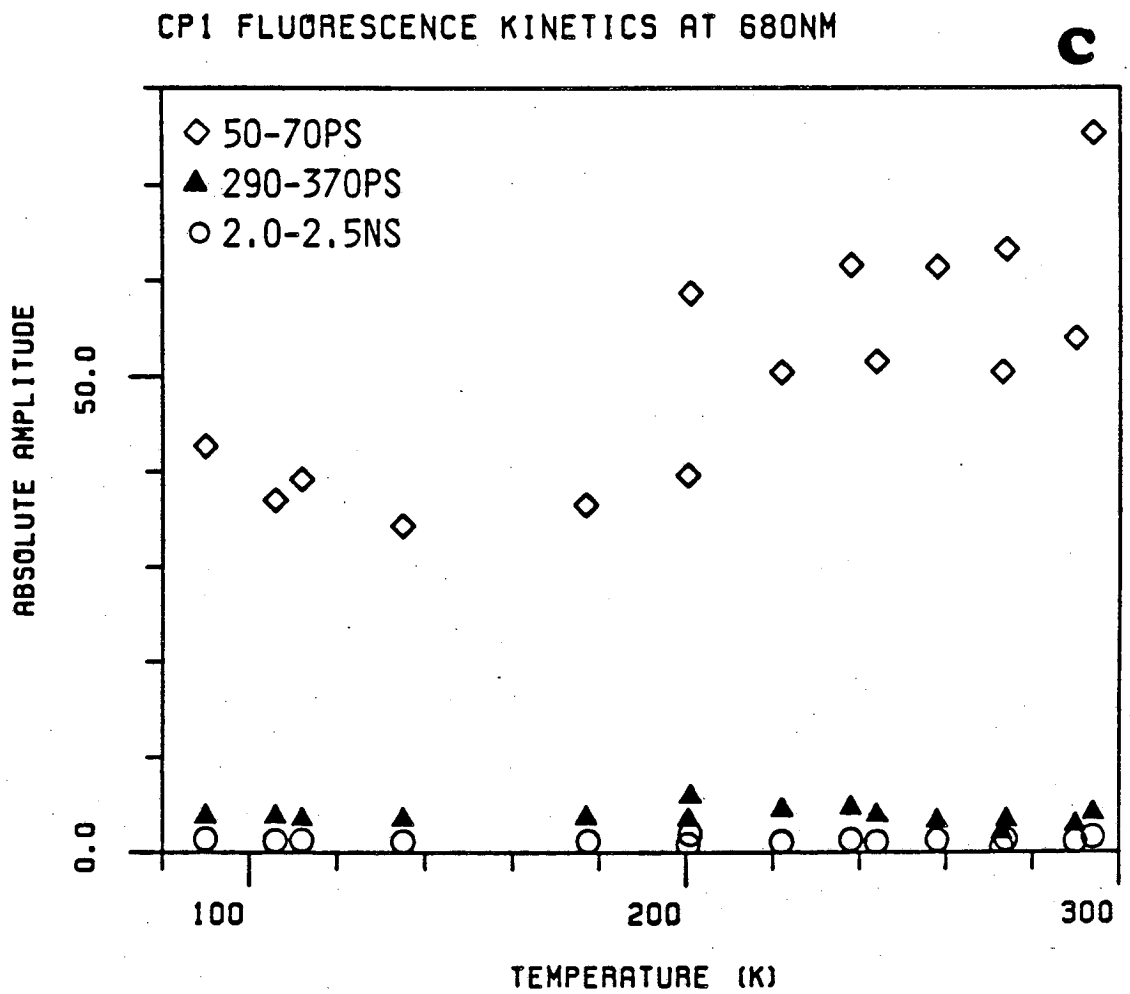
CP1 FLUORESCENCE KINETICS AT 680NM
C
◇ 50-70PS
▲ 290-370PS
○ 2.0-2.5NS
ABSOLUTE AMPLITUDE
50.0
0.0
100
200
300
TEMPERATURE (K)

XBL 868-2890

measured with the PMT detector (50ps resolution), and the MCP detector (25ps resolution). The fluorescence risetime of CP1 at 680nm is instrument limited at less than 50ps from 77K to 295K. The fluorescence decay kinetics are best fit to a sum of three exponential components: slow, 2.1-2.5ns; middle, 290-370ps; and fast, 50-70ps, Fig. 6.12A. The relative amplitudes of the individual components are unchanged from 90K to 295K, Fig. 6.12B. The fast component dominates with a relative amplitude of 88-95%. The middle and slow components comprise 5-9% and 1-3%, respectively.

The absolute amplitudes, expressed as the product of the relative component amplitude and the total fluorescence yield of the kinetic measurement at an individual temperature (Fig. 6.11), are displayed in Fig. 6.12C. The absolute amplitude of the fast component appears to decrease slightly with decreasing temperature, while those of the middle and slow components remain constant.

In summary, there is no significant change in the CP1 fluorescence kinetics at 680nm over the temperature range 90-295K. The risetime is faster than 25ps. The decay is best described by three exponential components, (fast, 50-70ps; middle, 290-370ps; slow, 2.1-2.5ns), with the fast component comprising 88-95% of the relative amplitude.

6.11 Picosecond Fluorescence Kinetics at 730nm as a Function of Temperature

The temperature dependence of the picosecond fluorescence kinetics at 730nm is of particular interest due to the dramatic increase (25- to 30- fold from 295K to 77K) in the fluorescence intensity of the 722nm emission band with decreasing temperature. The CP1 picosecond fluorescence kinetics at 730nm measured with the MCP detector (25ps response) are displayed in Fig. 6.13. All temperature effects are reversible.

In the temperature range measured, 103K to 295K, the fluorescence decay is best fit to a sum of three exponential components: slow, ranging from 1.3 to 2.1ns; middle, increasing from 270ps at 295K to 710ps at 103K; and fast, increasing from 30ps at 295K to 200ps at 103K, Fig. 6.13A,B. At temperatures below 260K a risetime is measured with a 1/e lifetime which increases from 25ps at 262K to 42ps at 103K, Fig. 6.13A,B. Addition of another rise or decay component does not improve the fit. However, the lifetime of the slow component does not show a single trend as a function of temperature which indicates that it may represent the sum

Figure 6.13. Temperature Dependence of CP1 Fluorescence Kinetics at 730nm.

CP1 is suspended in 10% glycerol, 5mM ascorbate, 15mM NaCl, 5mM $MgCl_2$ and 50mM Tris, pH 7.5. The sample is maintained in the dark. The absorbance at 675nm is 0.2.

Measurements are made with the MCP detector (25ps response), and the temperature effects are completely reversible.

At all temperatures measured (103K - 298K) the fluorescence decay is best fit to three exponential components: slow, 1.3-2.1ns; middle, 260-710ps; and fast, 30-200ps. At temperatures above 260K the rise is instrument limited at 25ps. Below 260K, the measured rise is fit to a single exponential of 25-42ps. χ^2 values range from 1.01 to 1.24.

A. Lifetimes (1/e) of the fluorescence rise and decay components vs. temperature (K).

B. An expanded scale of Fig. 6.13A showing the lifetimes (ns) of the fast decay component and rise component vs. temperature (K).

C. The absolute amplitudes of the fluorescence kinetic components vs. temperature (K). The absolute amplitude is expressed as the product of the relative amplitude and the fluorescence yield of each kinetics measurement corrected for differences in the data collection time and filter transmittance, Fig. 6.11. A rise is represented by a negative amplitude.

D. An expanded scale of 6.13C, displaying the absolute amplitude of the slow and middle decay components vs. temperature (K).

E. The yields of the fast decay and rise components vs. temperature (K). The yield is a product of the absolute amplitude and the lifetime. The rise component is expressed as minus the yield.

F. The yields of the middle and slow decay components vs. temperature (K).

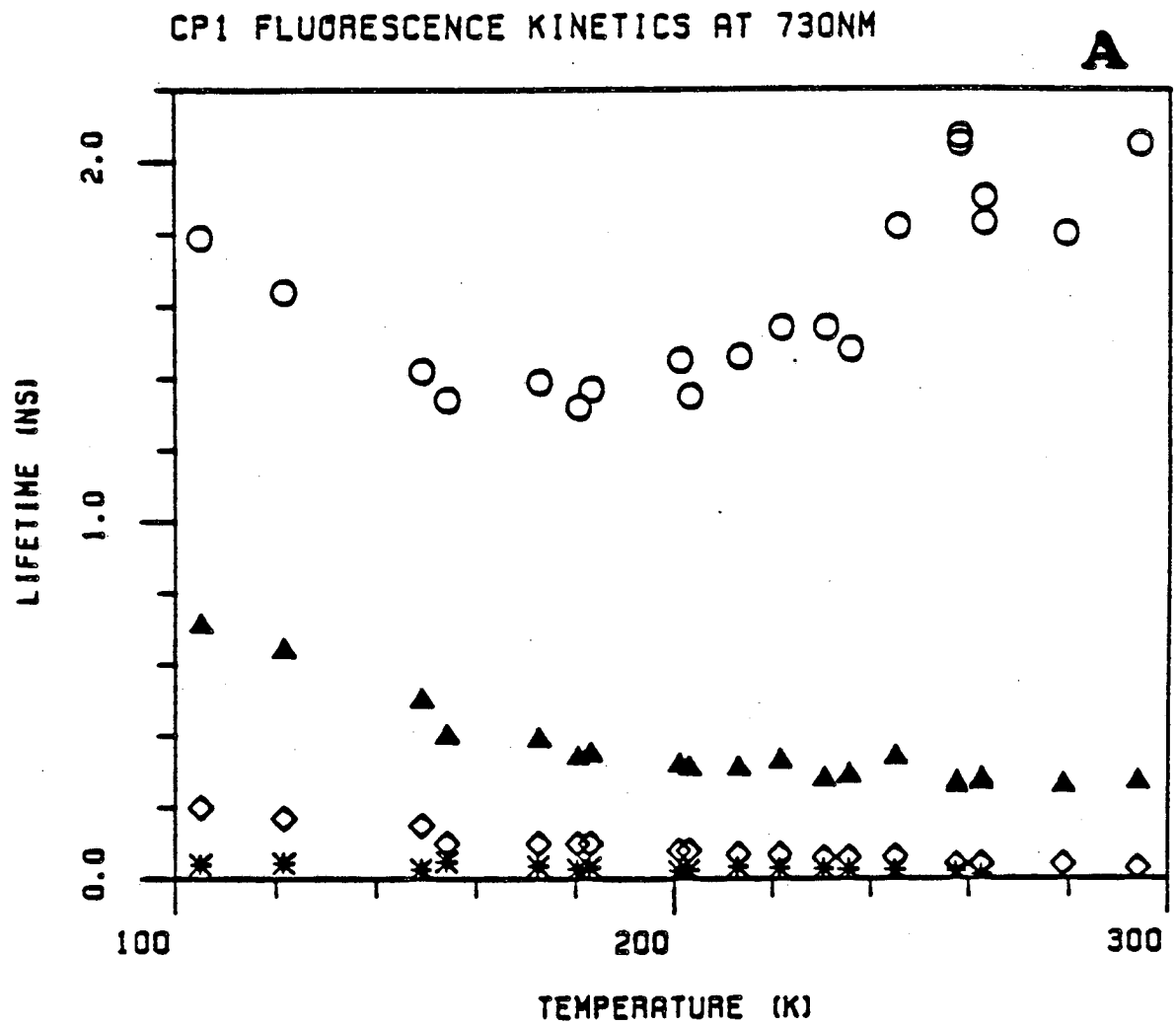
CP1 FLUORESCENCE KINETICS AT 730NM
A
LIFETIME (NS)
2.0
1.0
0.0
100
200
300
TEMPERATURE (K)

XBL 868-2891

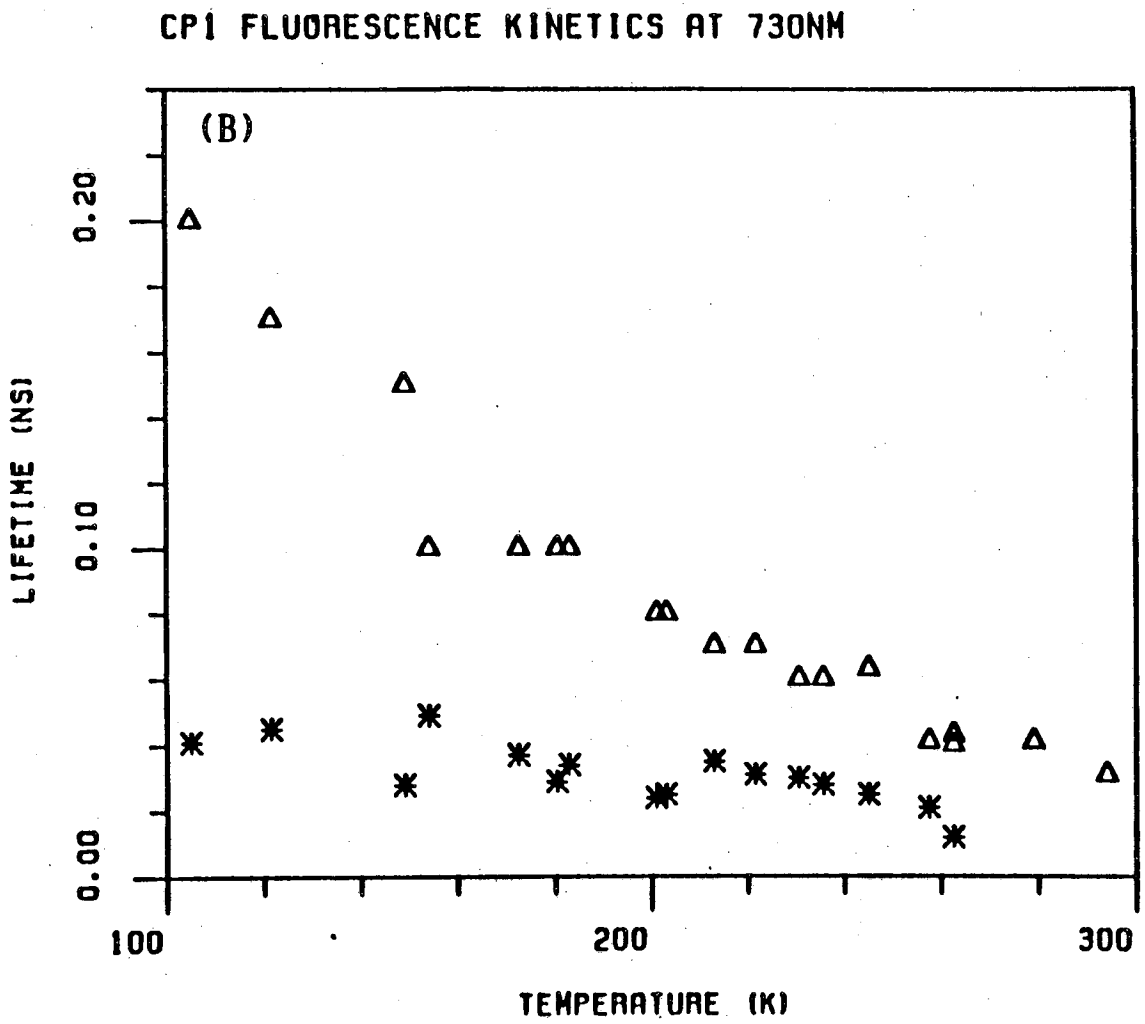
CP1 FLUORESCENCE KINETICS AT 730NM
(B)
LIFETIME (NS)
0.00
0.10
0.20
100
200
300
TEMPERATURE (K)

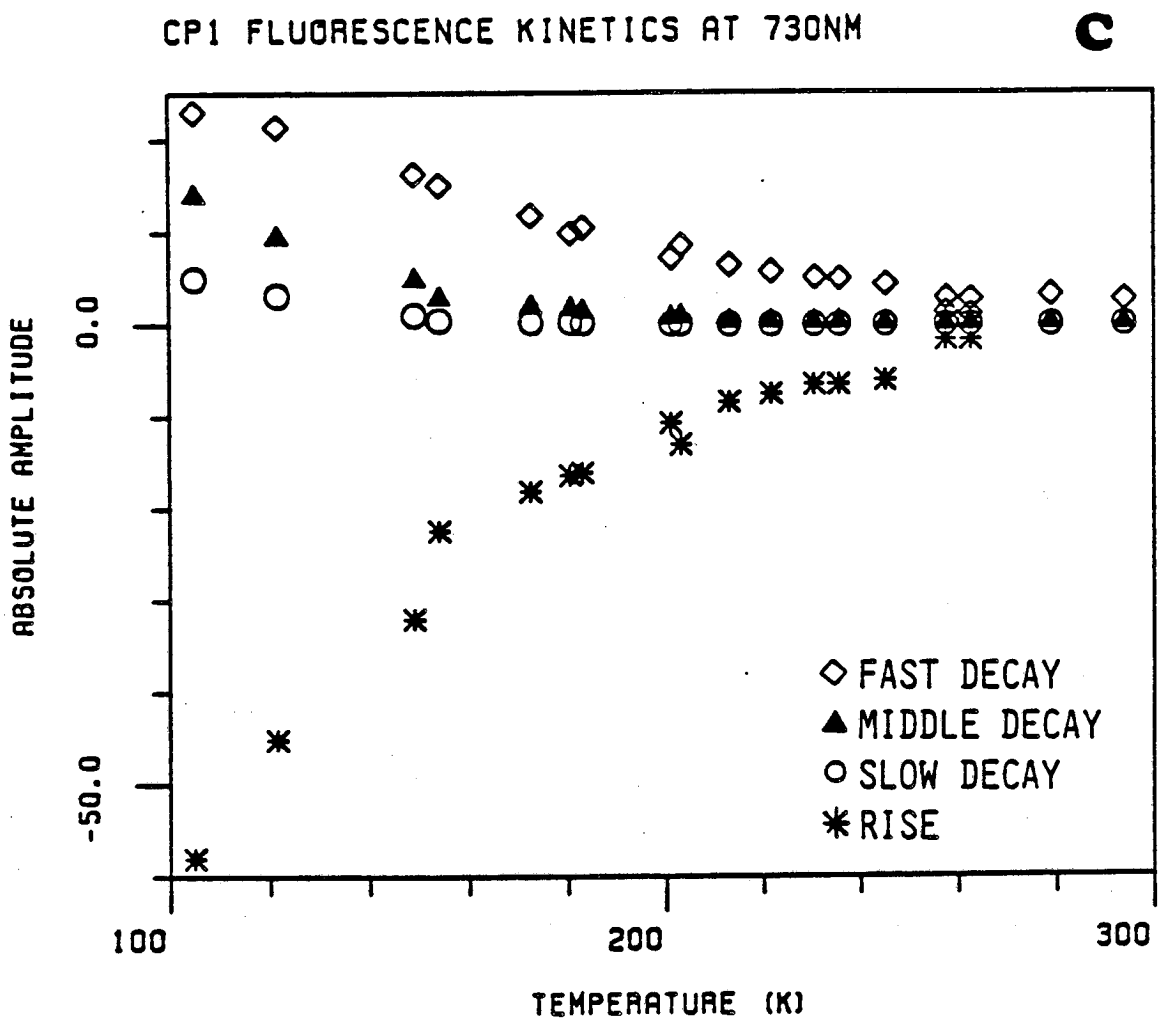
CP1 FLUORESCENCE KINETICS AT 730NM
C
ABSOLUTE AMPLITUDE
0.0
-50.0
100
200
300
TEMPERATURE (K)
FAST DECAY
MIDDLE DECAY
SLOW DECAY
RISE

XBL 868-2892

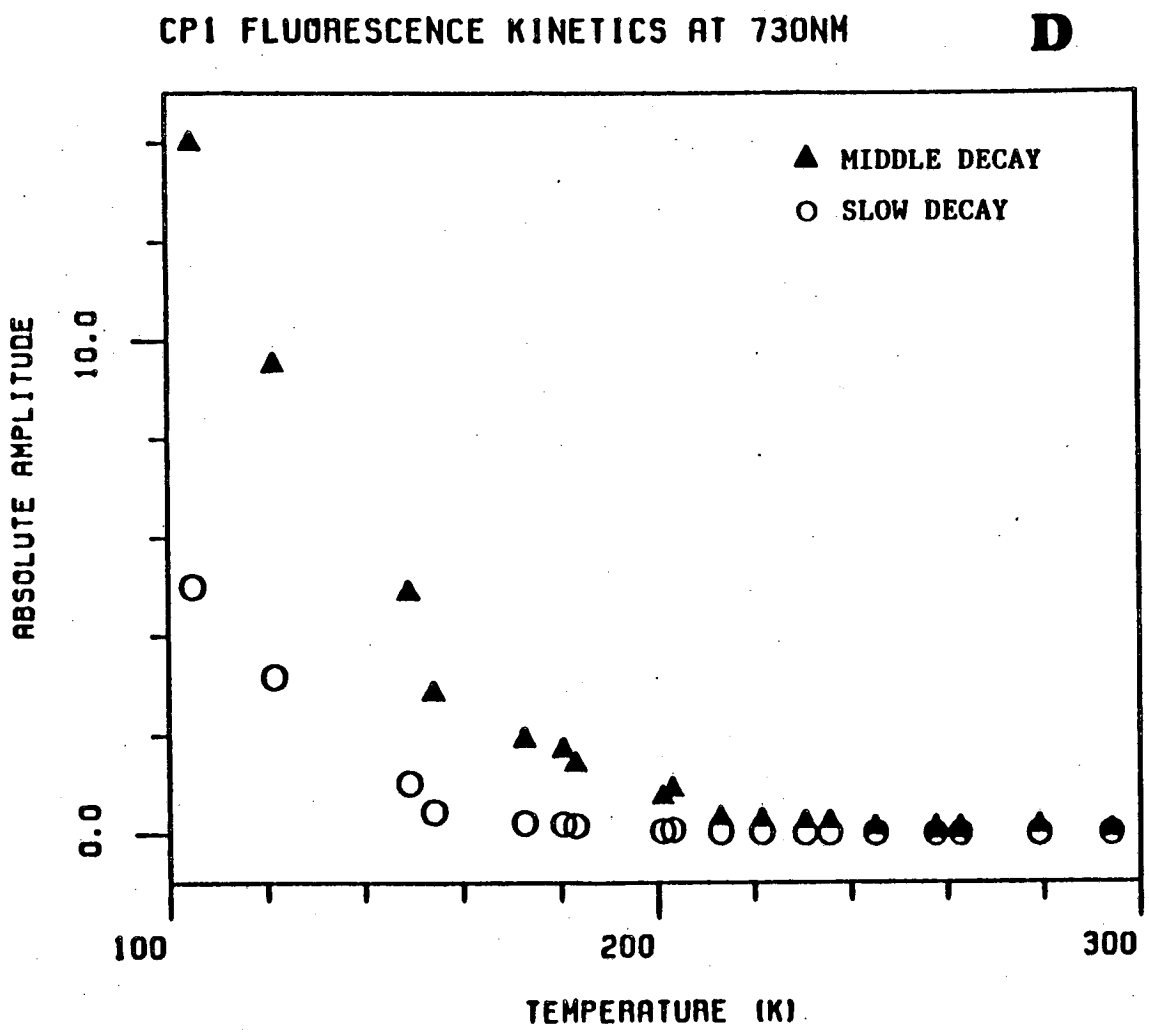
CP1 FLUORESCENCE KINETICS AT 730NM
D
MIDDLE DECAY
SLOW DECAY
ABSOLUTE AMPLITUDE
10.0
0.0
100
200
300
TEMPERATURE (K)

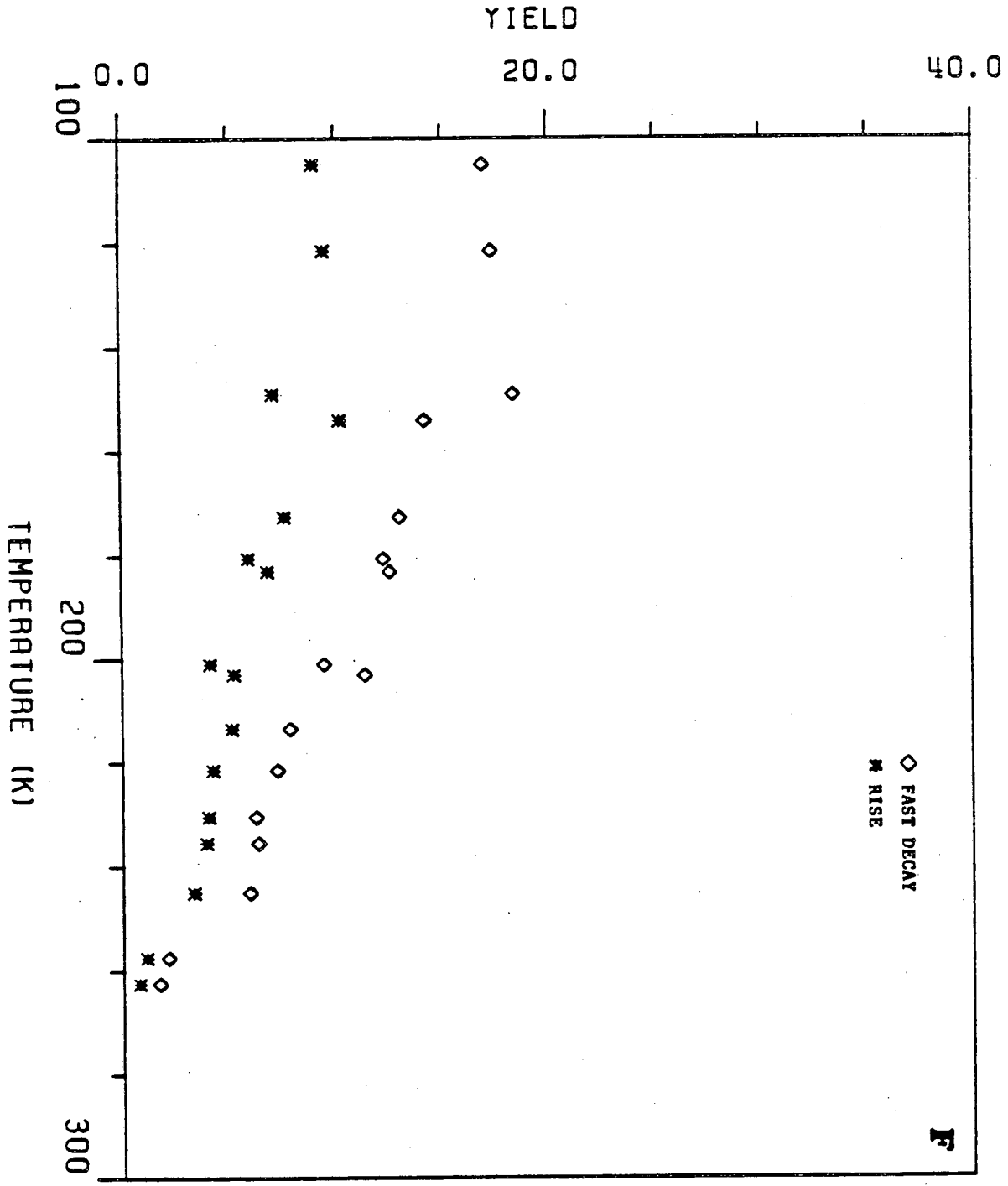

F

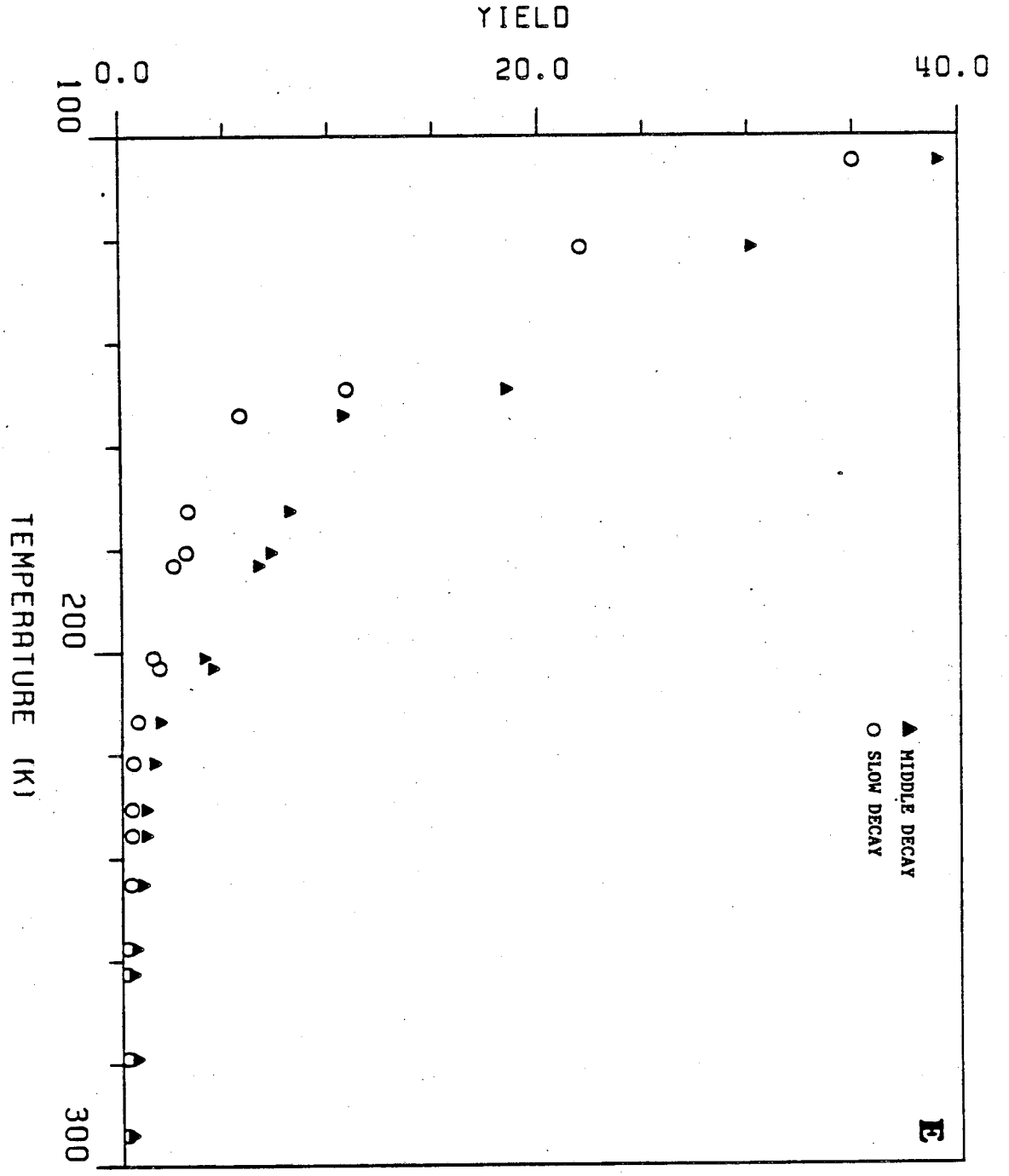
YIELD
0.0
20.0
40.0
100
200
300
TEMPERATURE (K)
▲ MIDDLE DECAY
O SLOW DECAY
E

of two decay components. Unfortunately, the amplitude of the slow component is too small to resolve further.

The absolute amplitudes, Fig. 6.13C, are expressed as the product of the relative component amplitude and the total fluorescence yield of each kinetics measurement corrected for differences in data collection time and filter transmittance, Fig. 6.9. The relative amplitudes are determined such that $\sum_{i=1}^{n} |\alpha_i| = 1.0$, and a negative amplitude represents a rise component. All components increase in absolute amplitude as the temperature is lowered: slow decay increases from .003 at 295K to 5.0 at 103K; middle decay increases from .05 at 295K to 14. at 103K; fast decay increases from 2.6 at 295K to 23. at 103K; and the rise increases in amplitude from 0.0 at 260K to -58 at 103K, Fig. 6.13C,D. The amplitude of the rise remains approximately equal to the sum of the decay components (data not shown). Thus, the rise can provide all of the amplitude necessary for the three decay components.

The component yields are expressed as the product of the absolute amplitude and the lifetime, Fig. 6.13E,F. The yield of all kinetic components increases with decreasing temperature. However, two distinct temperature dependences are observed. The yields of the middle and slow decay components rise sharply from 200K to 100K, while the yields of the fast decay and rise components show a saturating behavior.

6.12 Activation Energies at 730nm

The activation energies of temperature dependent quenching mechanisms can be determined if the yields of the fluorescence kinetic components exhibit Arrhenius behavior. The quantum yield of fluorescence, ϕ_f, is given by the ratio of the fluorescence rate to the sum of the rates of all deexcitation processes. $\phi_f = \frac{k_f}{(k_f+k_i+k_t)}$

Competing deactivation mechanisms include intersystem crossing to a triplet state, thermal relaxation through internal conversion, and photochemistry. For the purpose of this analysis, these processes can be described by k_i and k_t which are the rates of temperature independent and temperature dependent quenching mechanisms, respectively. Assuming that the excited state reaches a Boltzmann population prior to deexcitation and that k_t represents an Arrhenius quenching mechanism, the fluorescence yield can be expressed as:

$$\phi_f = \frac{k_f}{k_f+k_i+Ae^{-E_a/RT}}$$

A is a pre-exponential factor, R is the gas constant and E_a is the activation energy of the

Figure 6.14 Analysis of the temperature dependence of the prompt fluorescence kinetic components at 730nm. The sample and experimental conditions are described in Figure 6.13. The total absolute fluorescence yields, ϕ_T, are obtained by numerical integration of the deconvoluted fluorescence decay (see Materials and Methods). ϕ_T is the sum of the component yields.

Figures A and B present $\frac{1}{\phi_i}$ vs. $\frac{1}{T}$ for the rise and fast decay components of the fluorescence kinetics at 730nm. The curves are the best single exponential fits by an iterative least squares analysis, where $\frac{1}{\phi_i} = A + B\,e^{-E_a/RT}$. The fits and sum of squares deviations (SS) are listed below.

A. Rise Component: $\frac{1}{\phi_r} = 97.6 + 11560e^{-1032/T}$; SS = 5.0.

B. Fast Decay Component: $\frac{1}{\phi_f} = 49.6 + 7864e^{-1040/T}$; SS = 7.4.

Figures C and D are graphical representations of the expression,

$$\ln\left[\frac{1}{\phi_f} - \frac{k_f+k_i}{k_f}\right] = \ln\frac{A}{k_f} - \frac{E_a}{RT}.$$

The linear regression analyses and correlation coefficients for both the middle and slow decay components are listed below.

C. Middle Decay Component: $\ln\left[\frac{1}{\phi_f} - \frac{k_f+k_i}{k_f}\right]$ vs. $\frac{1}{T}$, where a value of 25, obtained from the low temperature (100K) limit of $\frac{1}{\phi_m}$ vs. $\frac{1}{T}$, is assumed for $\frac{(k_f+k_i)}{k_f}$. The y-intercept is 11.9, the slope is -1247 and the correlation coefficient is -0.990.

D. Slow Decay Component: $\ln\left[\frac{1}{\phi_s} - \frac{k_f+k_i}{k_f}\right]$ vs. $\frac{1}{T}$, where a value of 23, obtained from the low temperature (100K) limit of $\frac{1}{\phi_s}$ vs. $\frac{1}{T}$, is assumed for $\frac{(k_f+k_i)}{k_f}$. The y-intercept is 13.0, the slope is -1296 and the correlation coefficient is -0.992.

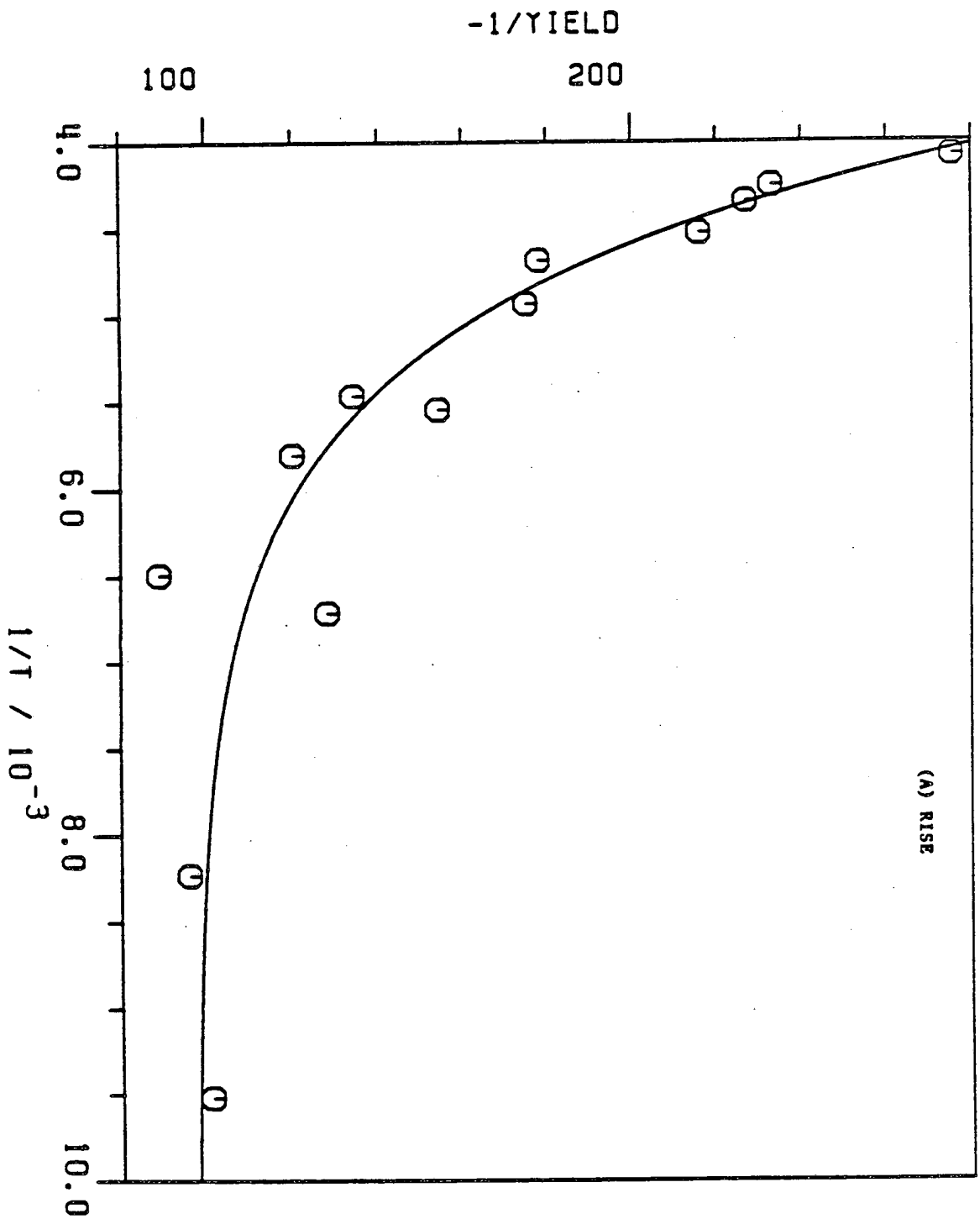
(A) RISE
-1/YIELD
100
200
1/T / 10^-3
4.0
6.0
8.0
10.0

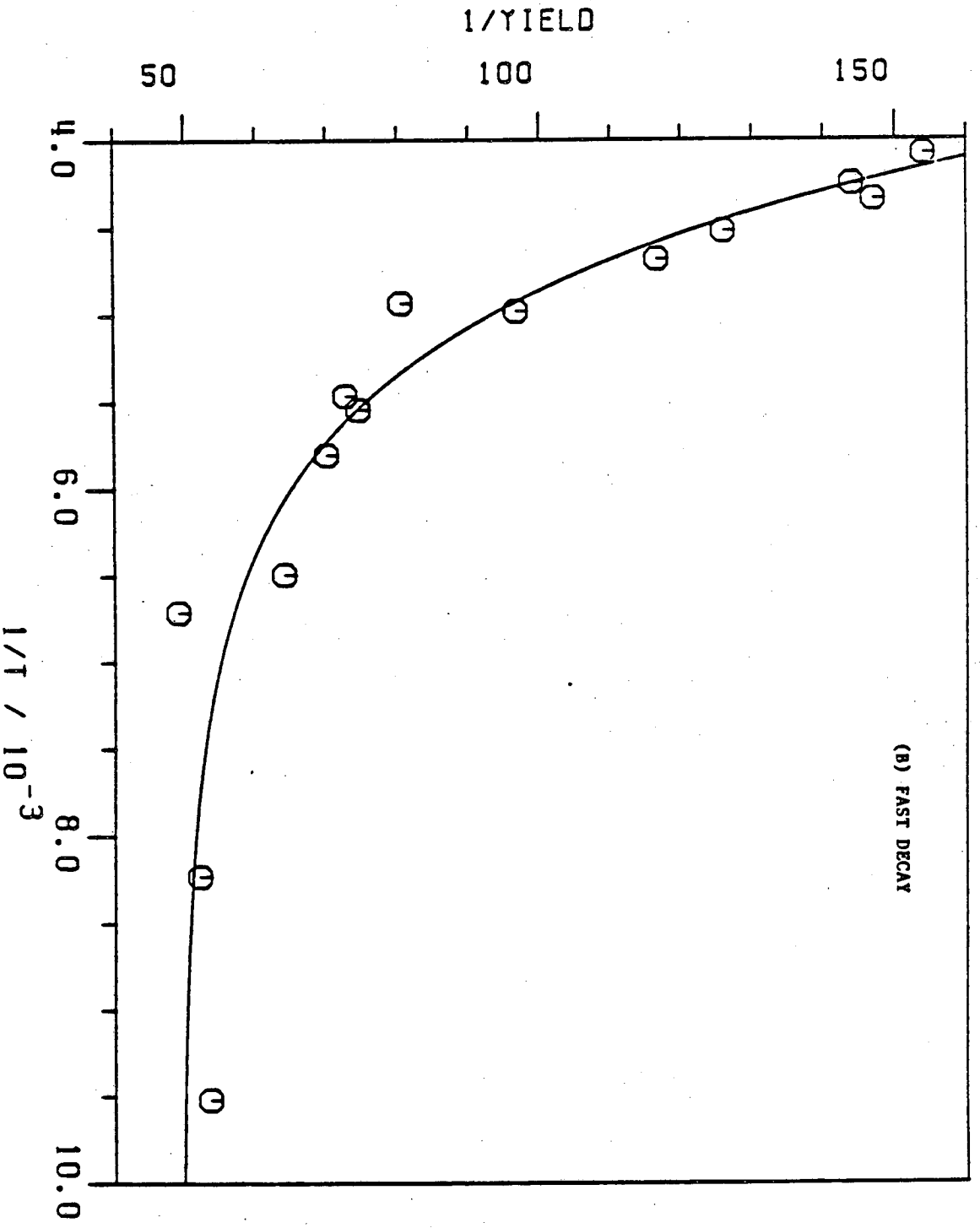

(B) FAST DECAY

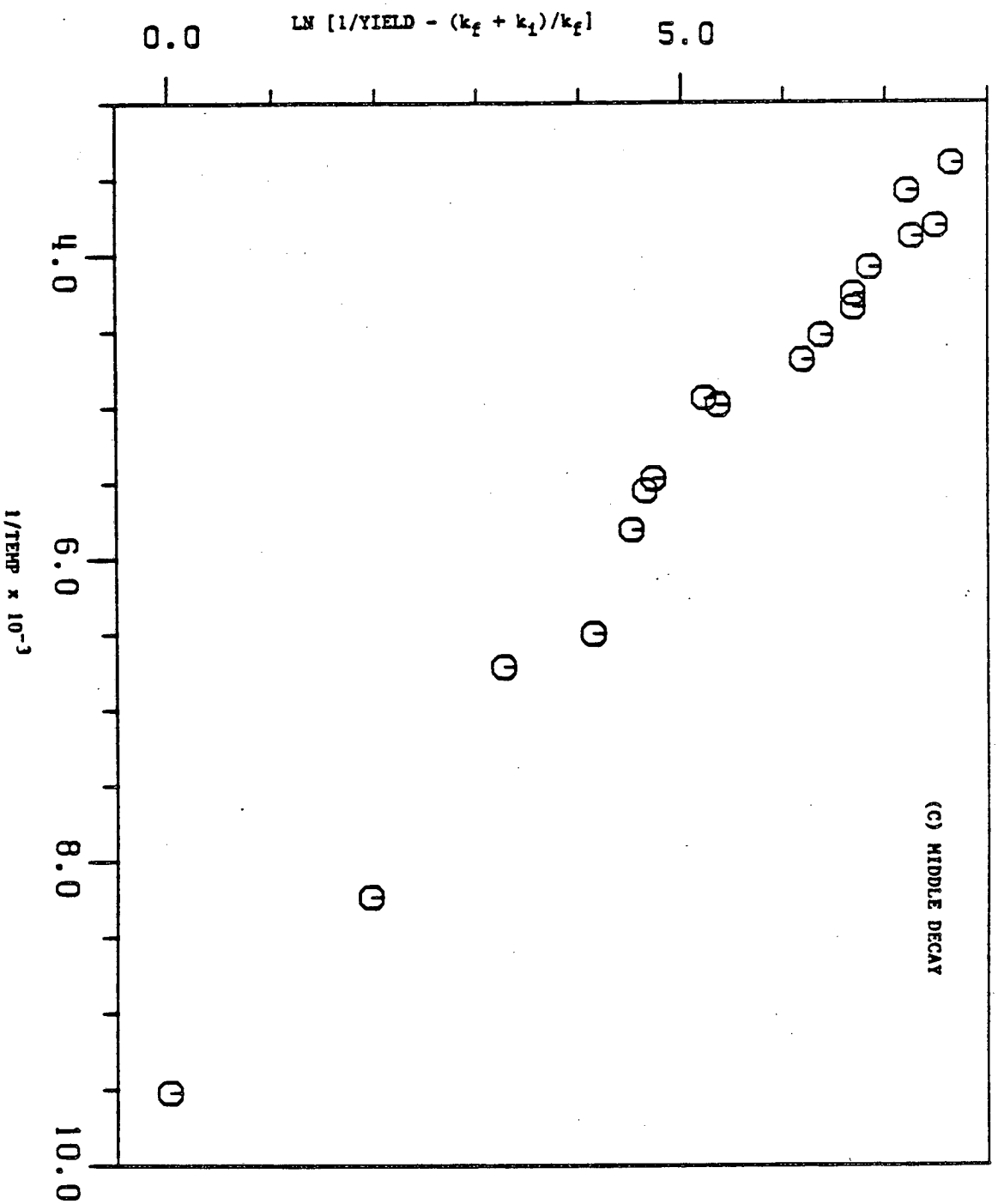
5.0
LN [1/YIELD - (k_f + k_i)/k_f]
0.0
10.0
8.0
6.0
4.0
1/TEMP x 10^-3
(C) MIDDLE DECAY

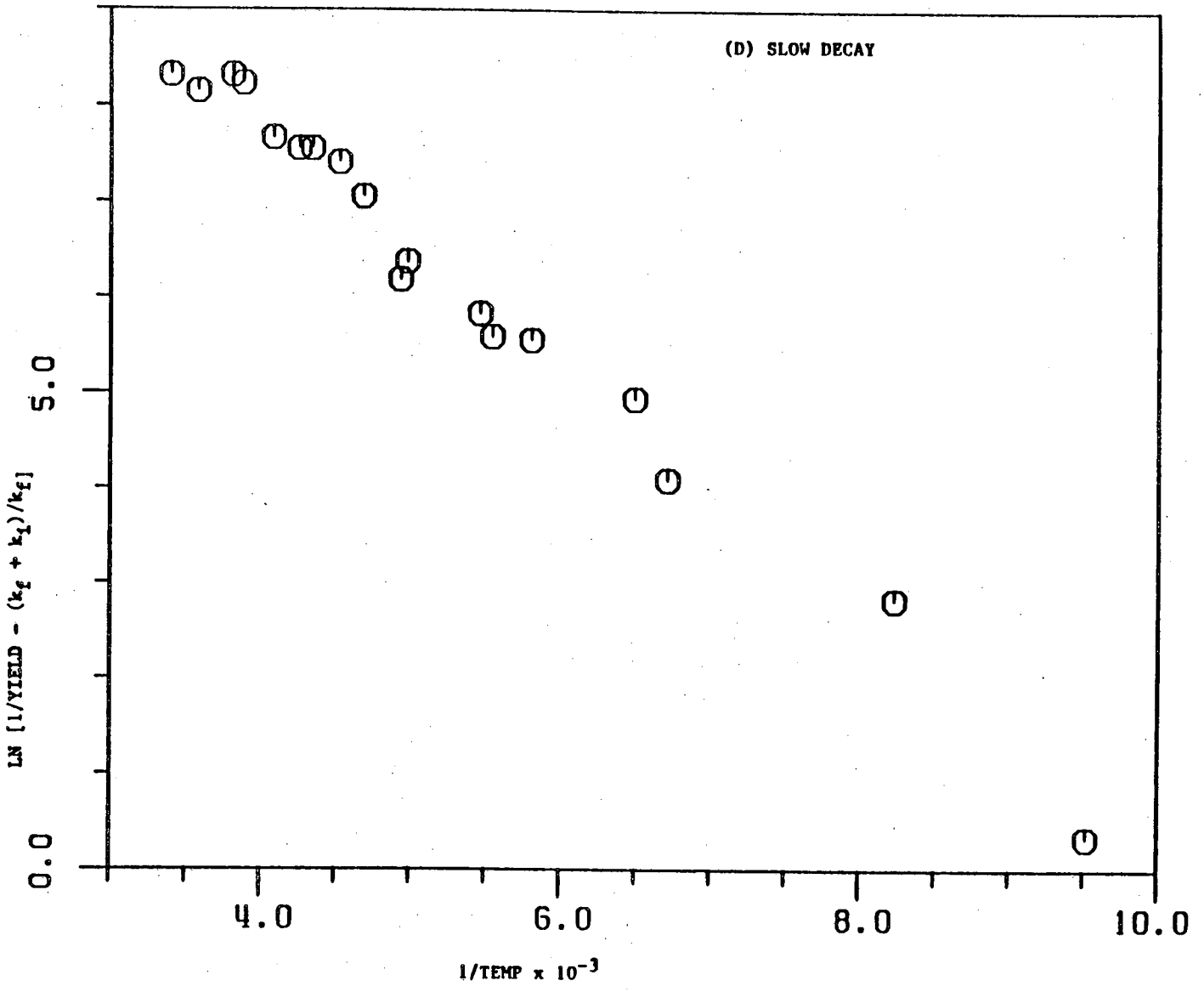
(D) SLOW DECAY
LN [1/YIELD - (k_f + k_I)/k_f]
0.0
5.0
4.0
6.0
8.0
10.0
1/TEMP x 10^-3

quenching mechanism. This can be rewritten as:

$$\frac{1}{\phi_f} = \frac{k_f+k_i}{k_f} + \frac{A}{k_f}\, e^{-E_a/RT}.$$

If $\frac{1}{\phi_f}$ vs $\frac{1}{T}$ for an individual fluorescence component can be fit to a single exponential curve,

$$y = A + Be^{-C/T}$$

We can obtain the activation energy ($\frac{E_a}{R} = C$) for the temperature dependent quenching mechanism.

Figures 6.14A and 6.14B present $\frac{1}{\phi_i}$ vs. $\frac{1}{T}$ for the rise and fast decay components of the prompt fluorescence kinetics at 730nm. These are the absolute component yields obtained by numerical integration of the deconvoluted fluorescence decay, see Materials and Methods. The curves through the data in Figures 6.14A,B are the best single exponential fit by an iterative least squares analysis. The parameters and sum of squares deviations are in the figure caption. The temperature independent deexcitation rate constant, k_i, can be obtained from $\frac{(k_f+k_i)}{k_f}$, using a natural lifetime for chlorophyll a of 15ns. The activation energies, E_a, and the temperature independent deexcitation rate constants, k_i, are listed below.

$\frac{1}{\phi_f}$ vs. $\frac{1}{T}$ for the middle and slow decay components do not fit well to a single exponential, particularly at temperatures below 150K. Therefore, we employed a slightly different approach to evaluate the temperature dependent quenching mechanisms. The expression,

$$\frac{1}{\phi_f} = \frac{k_f+k_i}{k_f} + \frac{A}{k_f}\, e^{-E_a/RT}$$

can be written as,

$$\ln\left[\frac{1}{\phi_f} - \frac{k_f+k_i}{k_f}\right] = \ln\frac{A}{k_f} - \frac{E_a}{RT}.$$

From the plots of $\frac{1}{\phi_f}$ vs. $\frac{1}{T}$ we obtained the low temperature (100K) values of $\frac{(k_f+k_i)}{k_f}$ for the middle and slow decay components of 23 and 25, respectively. Figures 6.14C and 6.14D present $\ln\left[\frac{1}{\phi_f} - \frac{k_f+k_i}{k_f}\right]$ vs. $\frac{1}{T}$, where ϕ_f is the absolute component yield. Both the middle and slow decay components produced linear plots. The parameters and correlation coefficients are in the figure caption. The activation energies, E_a, and temperature independent deexcitation rate constants, k_i, are listed below.

Component	E_a (kcal/mol)	k_i (sec^{-1})
Rise	2.1±0.1	$6.4 \times 10^9 \pm 0.3 \times 10^9$
Fast Decay	2.1±0.3	$3.3 \times 10^9 \pm 0.5 \times 10^9$
Middle Decay	2.5±0.5	$1.5 \times 10^9 \pm 0.3 \times 10^9$
Slow Decay	2.6±0.5	$1.6 \times 10^9 \pm 0.3 \times 10^9$

6.13 Discussion

Fluorescence spectra and decay kinetics provide important information on the mechanisms of energy transfer and storage in chloroplasts. The fluorescence in higher plants is dominated by emission from PSII. The isolation of CP1, enriched in photochemically active P700, produces a valuable complex for characterizing PSI fluorescence.

Many of the PS1 kinetic rates outlined in Figure 6.15 have been determined. Room temperature absorption difference measurements of Triton isolated PS1 particles (60-70 Chl/P700) provide the rates of antenna Chl a (Ant) excited state decay and $P700^+$ formation [1]. The excited state lifetime of antenna Chl a has been measured by the decay of ΔA_{678} and is best described by three exponential components, 20-45ps, 100-300ps and greater than 500ps [1]. Charge separation (R_1), measured by the formation of ΔA_{700}, occurs in 15-40ps [1,3] and decays by several pathways. (1) R_{-1} represents repopulation of the excited antenna Chl a state and subsequent deexcitation by fluorescence or non-radiative mechanisms. Although the kinetics have not been measured in CP1, recombination of the PS1 state $P700^+A^-X^-F\Phi_{A,B}^{\mp}$ occurs biphasically in 10ns and 3μs [8]. (2) R_{RPT} represents $P700^+A^-$ relaxation to form a radical pair triplet on P700. This P700 RPT is observable at 10K by EPR (Chapter Four). It is formed in microseconds, which may reflect the 3μs recombination time listed above, and decays in milliseconds (data not shown). The CP1 photochemical model presented is a foundation upon which the results of the temperature dependence of the prompt fluorescence kinetics and steady state emission experiments can be evaluated. The goal is to understand the fluorescence kinetic components of the two CP1 emission bands (690nm and 722nm) in terms of photochemical excitation quenchers specific to PS1.

There are a few specific characteristics of CP1 that should be mentioned. All photochemically active components are thought to be Chl a species (assuming A represents only A_0). Chl a populations are present in a ratio of 70 antenna Chl a molecules (Ant) to one primary donor

Chl a dimer (P700) to one primary acceptor Chl a dimer (A_0) [2]. An important distinction must be made when considering the CP1 photochemistry monitored in the experiments presented in this chapter. Unlike the variable fluorescence and photobleaching measurements in Chapter Five where high intensity continuous illumination was used, the prompt kinetic measurements employ a series of low intensity excitation pulses and the steady state fluorimeter uses a low intensity measuring beam. As a result, while the photobleaching and variable fluorescence monitor the formation of the state $P700^+A$ in CP1, the prompt kinetic and steady state fluorescence measurements reflect the distribution between P700A and $P700^+A^-$. The absence of measurable $P700^+A$ produced formation during the prompt kinetic and steady state fluorescence measurements described in this chapter is confirmed by three observations. (1) At 295K, the formation of the state $P700^+A$ decreases the 690nm fluorescence in 10-20s (Chapter Five). This does not occur during the time resolved measurements since no change is observed in the fluorescence yield as monitored by the fluorescence photon count ratemeter. (2) There is a significant difference between the 77K steady state emission spectra of CP1 samples in the poised states $P700^+A$ and P700A, Section 6.6. Repetitive steady state fluorescence scans of CP1 particles in the state P700A produce no change in the emission spectrum, confirming that $P700^+A$ is not produced by the measuring beam. (3) CP1 samples poised in the states P700 A and $P700^+A$ have different prompt fluorescence decay kinetics, Section 6.8. Thus, we conclude that the experimental results presented in this chapter reflect photochemistry in CP1 particles undergoing primary charge separation and recombination.

A dramatic increase in the long wavelength fluorescence intensity, F_{735}, of chloroplasts upon decreasing the temperature has been previously reported [9-12]. Based upon excitation spectra, F_{735} has been attributed to a chlorophyll species associated with PS1, C_{705} [12]. The fluorescence yield and average lifetime of F_{735} were found to increase proportionally with decreasing temperature, indicating that the increased yield reflects C_{705} becoming more fluorescent rather than receiving more excitation [10]. It was later proposed that excitation transfer from C_{705} to P700 is a thermally activated process [13]. More recently, it has been demonstrated that F_{735} arises from a PS1 associated light harvesting complex [14-16]. The PS1 light harvesting complexes are absent from CP1; however, I also observe a similar temperature dependence at 722nm. Perhaps the temperature dependent behavior of F_{735} and F_{722}

reflect similar thermally activated quenching mechanisms characteristic of the PS1 reaction center complex. By measuring the steady state emission and prompt fluorescence kinetics of CP1 particles as a function of temperature and oxidation state of P700, I have been able to characterize the components and mechanisms of excitation transfer and quenching in PS1.

The CP1 emission spectra is most simply described by two fluorescing populations, F_{690} and F_{722}. Both populations have a Chl a fluorescence excitation spectra and F_{690} also receives excitation from carotenoids (Section 6.3). F_{690} and F_{722} have different temperature dependent behavior. The fluorescence kinetics at 680nm are temperature independent from 77K to 295K (Section 6.10). The fluorescence at 680nm (excited at 590, 600 or 620nm) rises in less than 50ps and decays by three exponential components 60±15ps, 330±40ps and 2.0±0.5ns. The fast component comprises 90-95% of the relative amplitude. At 295K the emission maximum is at 690nm and the fluorescence kinetics are essentially unchanged over the emission wavelength range 680-800nm. The fluorescence kinetics at 730nm are dramatically temperature dependent (Section 6.11). The kinetics are described by four components whose lifetimes increase with decreasing temperature: fast decay, 45ps at 295K and 270ps at 77K; middle decay, 260ps at 295K and 1.3ns at 77K; slow decay, 1.3ns at 295K and 5.0ns at 77K; rise, less than 25ps at 295K and 70ps at 77K. As the temperature is lowered the amplitudes of the middle and slow decay components increase relative to the fast decay component. This is observed as an increase in the fluorescence yield at 722nm with decreasing temperature. The rise component can provide all of the amplitude necessary for the three decay components.

It appears that F_{722} is not resolved in the prompt fluorescence kinetic measurements at temperatures above 265K. This is supported by two experimental observations. (1) The fluorescence decay kinetics describing F_{690} over the temperature range 77K to 295K are also observed over the emission wavelengths 680-800nm at temperatures above 265K. (2) The lifetime behavior of the slow decay component at 730nm, Fig. 6.13A, could be a composite of the 2.0ns F_{690} component and a F_{722} component which increases from about 1.0ns at 265K to 1.8ns at 103K. A simple explanation is that the 722nm emission is fluorescence from a Chl a species whose excitation is efficiently quenched at room temperature by a non-radiative mechanism which is less efficient at lower temperatures. A similar temperature dependent quenching mechanism has been proposed for F_{735} in chloroplasts [10]. F_{735} decay was not

resolved at temperatures above 200K using an earlier version of our prompt fluorescence kinetic system [11]. A comparison of the yield of F_{735} with the photooxidation of P700 over the temperature range of 195K to 77K showed that these two processes compete for excitation [17]. F_{735} arises from the PS1 associated chlorophyll species, C_{705} [12]. Thus, in chloroplasts, C_{705} is responsible for F_{735} which is less fluorescent at higher temperatures because of greater energy transfer to P700. Since F_{722} has similar temperature behavior to that of F_{735}, the competing non-radiative quenching mechanism which predominates at higher temperatures in CP1 is probably P700 photochemistry.

I addressed the role of P700 as an excitation trap competing with fluorescence at 722nm and 690nm by comparing the prompt fluorescence kinetics at 77K of CP1 particles poised with P700 oxidized, P^+A, to P700 reduced P A (Section 6.8). The yields of the middle (1.25ns) and slow (4.5ns) decay components of F_{722} decrease about 2-fold when P700 is oxidized. However, the oxidation state of P700 has no measurable effect upon the yields of the fluorescence decay components of F_{690} or the rise (70ps) and fast decay (260ps) components of F_{722}. Thus, $P700^+$ quenches only excitation which gives rise to the middle (1.25ns) and slow (4.5ns) decay components of F_{722}. This behavior is consistent with the temperature dependence of the F_{722} kinetic components (Section 6.11). The yields of all F_{722} components increase gradually with decreasing temperature. However, below 160K the yields of the slow and middle components increase significantly, while the yields of the rise and fast decays level off. It appears that only the middle and slow decay components at 730nm are dependent on PS1 reaction center photochemistry; the fast decay component is quenched by alternative mechanisms (perhaps radiationless decay, intersystem crossing or energy transfer). As the temperature decreases, photochemistry becomes less efficient, producing a lower steady state level of $P700^+$ which we observe as increases in the yields of the middle and slow fluorescence decay components.

All fluorescence decay components at 730nm compete with temperature dependent deex-citation mechanisms which exhibit Arrhenius behavior (100K to 265K) with activation energies of 2.0-2.5kcal/mol. Most likely, the apparent Arrhenius behavior of the rise component is due to band narrowing with decreasing temperature which enables a more accurate separation of the rise from the fluorescence decay components. However, it is possible that the activation energy for the rise component represents a thermally activated excitation transfer from another

Boltzmann populated excited state, perhaps the Chl a species which gives rise to F_{690}.

The prompt fluorescence kinetics of CP1 are summarized in Figure 6.16. We can draw the following conclusions about excitation transfer and quenching mechanisms in CP1.

(1) CP1 emission can be described by two fluorescing species, F_{722} and F_{690}. Both are populated by Chl a excitation.

(2) The lifetimes and yields of the fluorescence kinetic components at 690nm are essentially independent of temperature (77K to 295K).

(3) F_{722} is observed only at temperatures below 265K.

(4) All fluorescence decay components at 730nm arise from temperature dependent quenching mechanisms which exhibit Arrhenius behavior (for 100K to 265K) with activation energies of 2.0-2.5kcal/mol.

(5) At 77K, $P700^+$ is an effective quencher of the middle and slow decay components of F_{722}. The yields of these components increase dramatically at temperatures below 150K, which may reflect a decrease in the steady state concentration of $P700^+$ at lower temperatures.

(6) The amplitude of the rise component is equal in magnitude to the sum of the amplitudes of the decay components of F_{722}. Therefore, F_{722} could receive its excitation primarily through energy transfer rather than direct photon absorption. This would indicate that the population of the chlorophyll molecules giving rise to F_{722} is a small fraction of the total antenna pool.

(7) The emission maxima indicate that F_{690} has a higher excited state energy level than F_{722}. This facilitates excitation transfer from F_{690} to F_{722} which I propose to be the primary deexcitation pathway for F_{690}. This excitation transfer is temperature independent and represents the 60ps quenching of F_{690} fluorescence.

(8) I measure the rise in F_{722} to be 25-70ps and the fast decay in F_{690} to be 50-70ps. These rise and decay rates are consistent with energy transfer, the differences arise from differing experimental conditions. The PMT detector with 50ps resolution was used for the 680nm measurements while the MCP detector with 25ps resolution was used for 730nm measurements. Thus, excitation transfer occurs from F_{690} to to F_{722} in 25ps at 265K and increases to 70ps at 77K.

(9) The excitation transfer from F_{690} to F_{722} may be a temperature dependent Arrhenius process with an activation energy of 2.1kcal/mol.

(10) Energy transfer to F_{722} is the primary deexcitation pathway of F_{690} (77K to 295K) since the fast decay represents 92% of the relative amplitude.

These observations can be combined into a coherent picture of energy transfer in PS1.

I propose the following mechanisms and components of excitation transfer in CP1. A simple model of CP1 photochemistry is diagrammed in Figure 6.15. The antenna Chl a is divided into two populations. $(Ant)_2$ is able to transfer excitation to P700, whereas $(Ant)_1$ can transfer excitation only to $(Ant)_2$. F_{690} is associated with $(Ant)_1$, which emits at 690nm and absorbs photons directly, in addition to receiving excitation transferred from carotenoids. The primary deexcitation pathway for the excited state of $(Ant)_1$ is a rapid 50-60ps excitation transfer to $(Ant)_2$, R_{et}, which may exhibit Arrhenius behavior with an activation energy of 2.1kcal/mol. F_{722} is associated with antenna chlorophyll molecules, $(Ant)_2$, and emits at 722nm. $(Ant)_2$ could receive its excitation from $(Ant)_1$ or absorb photons directly. At higher temperatures a rapid, non-radiative decay mechanism quenches F_{722} excitation. As the temperature is lowered, this quencher becomes less efficient. This is observed as a dramatic increase in the yields of the slow and middle fluorescence decay components of F_{722}. At 77K, $P700^+$ is an effective quencher of the middle and slow decay components of $(Ant)_2$. The increased yields of the middle and slow fluorescence decay components at lower temperature may reflect a reduction in the amount of $P700^+$ present. This can be explained by an increase in the formation of the P700 radical pair triplet at lower temperatures. The microsecond lifetime of P700 RPT would significantly decrease the steady state concentration of $P700^+$. An additional excitation trap, which is not dependent on the oxidation state of P700, is necessary to provide the fast temperature dependent quenching of $(Ant)_2$, which gives rise to the fast fluorescence decay component, perhaps by intersystem crossing, internal conversion or energy transfer. Finally, there are many similarities between the behavior of the emission arising from $(Ant)_2$ in CP1 particles and C_{705} in chloroplasts. Perhaps in the presence of PS1 light harvesting complexes C_{705} transfers its excitation to LHCP1b [14] and emission is observed at 730-735nm. However, when the light harvesting complexes are absent, as in CP1, C_{705} fluoresces directly at 722nm. Thus, $(Ant)_2$ and C_{705} may be synonymous.

Figure 6.15 A kinetic model of CP1 photochemistry induced by low intensity excitation. $(Ant)_1$ is a Chl a antenna population which fluoresces at 690nm. $(Ant)_2$ is a Chl a antenna population which fluoresces at 722nm. P is the primary donor and thought to be a Chl a dimer. A is either A_0 or A_0A_1, where A_0 is thought to be Chl a and A_1 is thought to be a quinone.

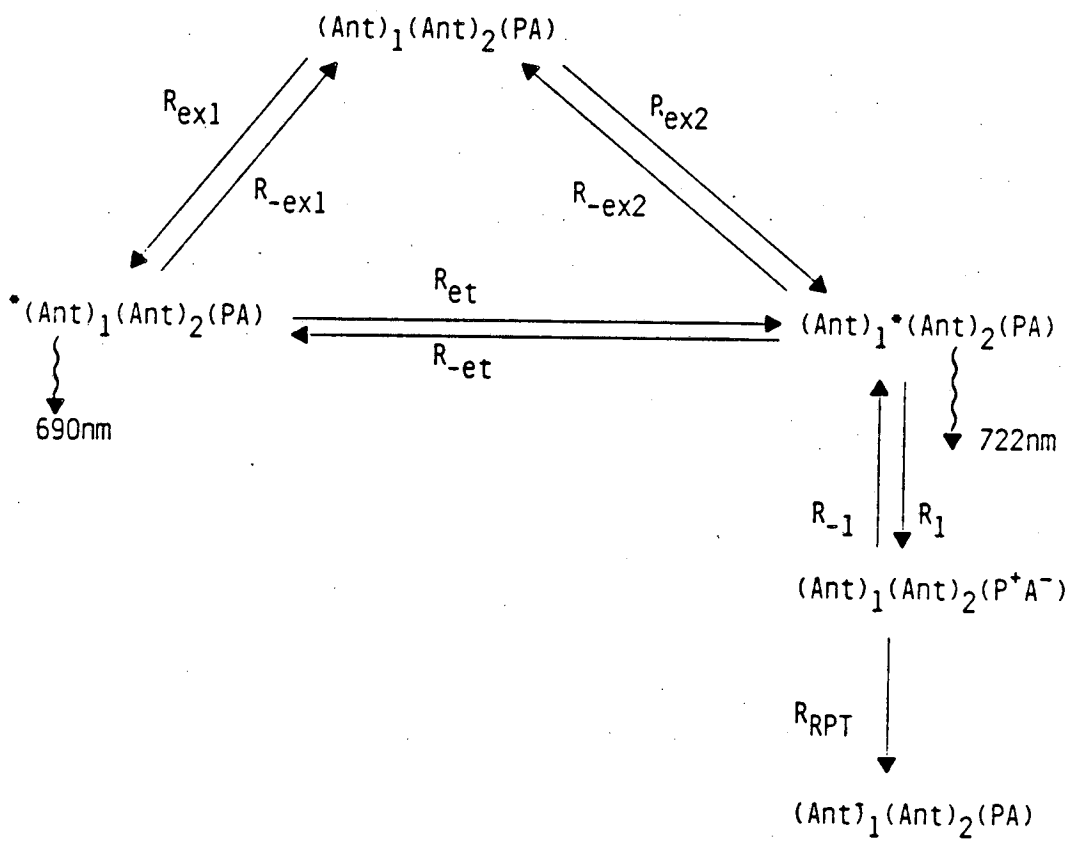

Figure 6.16. A summary of the prompt fluorescence kinetics in CP1.

	690nm		720nm	
Reduced (P A)				
295K	fast decay:	60ps 92% relative amplitude		
	middle decay:	330ps →	same	
	slow decay:	2.0ns		
	rise:	<50ps not resolvable		
77K	↓		fast decay:	260ps yield = 25.
	same		middle decay:	1.25ns yield = 49.
			slow decay:	4.5ns yield = 17.
			rise:	70ps yield = -9.4
Oxidized (P^+A)				
77K	↓		fast decay:	260ps yield = 22.
	same		middle decay:	1.25ns yield = 30.
			slow decay:	4.5ns yield = 8.5
			rise:	70ps yield = -10.

6.14 References

[1] Il'ina, M.D., Krasanskas, V.V., Rotomskis, R.J. and Borisov, A.Y. (1984) *Biochim. Biophys. Acta* 767, 501-506.

[2] Shuvalov, V.A., Klevanik, A.V., Sharkov, A.V., Kryukov, P.G. and Ke, B. (1979) *FEBS Lett.* 107, 313-316.

[3] Kamogawa, K., Morris, J.M., Takagi, Y., Nakashima, N., Yoshihara, K. and Ikegami, I. (1983) *Photochem. Photobiol.* 37, 207-213.

[4] Goedheer, J.C. (1964) *Biochim. Biophys. Acta* 88, 304-317.

[5] Setif, P., Acker, S., Lagoutte, B. and Duranton, J. (1980) *Photosynthesis Research* 1, 17-27.

[6] Sauer, K. and Calvin, M. (1962) *Biochim. Biophys. Acta* 64, 324-339.

[7] Baugher, J., Hindman, J.C. and Katz, J.J. (1979) *Chem. Phys. Lett.* 63, 159-163.

[8] Shuvalov, V.A., Ke, B. and Dolan, E. (1979) *FEBS. Lett.* 100, 5-8.

[9] Rijgersberg, C.P., Amesz, J., Thielen, A.P.G.M. and Swager, J.A. (1979) *Biochim. Biophys. Acta* 545, 473-482.

[10] Butler, W.L., Tredwell, C.J., Malkin, R. and Barber, J. (1979) *Biochim. Biophys. Acta* 545, 309-315.

[11] Reisberg, P., Nairn, J.A. and Sauer, K. (1982) *Photochem. Photobiol.* 36, 657-661.

[12] Butler, W.L. (1961) *Arch. Biochem. Biophys.* 93, 413-422.

[13] Tusov, V.B., Korvatovskii, B.N., Paschenko, V.Z. and Rubin, L.B. (1980) *Dokl. Akad. Nauk. SSSR* 252, 1500-1504.

[14] Lam, E., Oritz, W. and Malkin, R. (1984) *FEBS Lett.* 168, 10-14.

[15] Mullet, J.E., Burke, J.J. and Arntzen, C.J. (1980) *Plant Physiol.* 65, 823-827.

[16] Kuang, T.Y., Argyroudi-Akoyunoglou, J.H., Nakatani, H.Y., Watson, J. and Arntzen, C.J. (1984) *Arch. Biochem. Biophys.* 235, 618-627.

[17] Satoh, K. and Butler, W.L. (1978) *Biochim. Biophys. Acta* 502, 103-110.

[18] Mathis, P., Sauer, K. and Remy, R. (1978) *FEBS Lett.* 88, 275-278.

Chapter Seven: Future Directions

Fluorescence is an important tool for studying energy transfer in photosynthetic systems. Fluorescence experiments in conjunction with measurements that monitor the photochemical state of the reaction center (ie. EPR or absorption difference spectra) are particularly useful in determining the efficiency of excitation trapping. This report describes the implementation of these techniques to study the primary photochemistry of PSI and PSII from spinach. The results and conclusions have been discussed, however many of these experiments have opened doors for future work.

Fluorescence (both steady state induction and time resolved) supported by EPR measurements indicate that linolenic acid blocks electron transfer in PSII at the site of P680Ph//$Q_A Q_B$ without inhibiting primary charge separation and recombination. These conclusions were drawn from the following effects of linolenic acid upon PSII: (1) an instantaneous rise to the F_{max} fluorescence level, (2) an increase in the yield and lifetime of the slow (1-2ns) fluorescence decay component and (3) the presence of a RPT on P680 in dithionite-treated PSII particles. However, changes in the absorption and emission spectra due to linolenic acid treatment of PS11 particles and chloroplasts indicate that linolenic acid significantly alters the chloroplast membrane structure. These structural changes must be characterized before the role of linolenic acid as an inhibitor of PS11 electron transfer can be precisely defined. In addition, the absence of a RPT on P680 in PSII particles treated with linolenic acid alone remains to be explained. Characterizing the reduced acceptors by EPR in linolenic acid-treated samples illuminated prior to freezing would verify the site of linolenic acid inhibition of electron transfer. Repeating the steady state induction and picosecond fluorescence measurements at low temperature would provide a more accurate correlation with the RPT measurements by EPR.

Upon illumination of CP1 at room temperature, the fluorescence intensity at 690nm decreases as much as 25% to a steady state level. The behavior of the variable fluorescence and $P700^+$ induced optical bleaching of CP1 are similar under a variety of experimental conditions. (1) The kinetics of both variable fluorescence and photobleaching are best described by two exponential components, $K_F = 0.4sec^{-1}$ and $K_S = 0.07sec^{-1}$ (5mM ascorbate,

$1000\mu Em^{-2}s^{-1}$). (2) Treatment of CP1 with ascorbate or PMS increases the rates of both photobleaching and variable fluorescence. (3) The magnitudes of photobleaching and variable fluorescence show the same dependence upon titration with ferricyanide/ferrocyanide, with a mid-point near 450mV, consistent with that of $P700^+/P700$. Thus, by comparing the behavior of variable fluorescence to $P700^+$ induced optical photobleaching under a variety of experimental conditions we conclude that 690nm emission from CP1 is quenched by the state $P700^+A$. However, further experiments are necessary to obtain better resolution of the kinetics of photobleaching and variable fluorescence and to confirm the quenching states giving rise to variable fluorescence in CP1 treated with ascorbate or PMS. It is necessary to measure the light induced absorption difference spectrum in the presence of sufficient concentrations of these donors and acceptors (ie. 10mM ascorbate or 5μM PMS) to determine if the photobleaching at 699nm arises from $P700^+$ and/or A^-. It is important to determine if A represents the state A_0 or A_0A_1. This can be learned by monitoring the accumulation of reduced acceptors by EPR at cryogenic temperatures of dithionite-treated CP1 particles frozen under illumination. In addition, isolation of a PS1 reaction center complex with fewer antenna Chl a per P700 would give rise to variable fluorescence with better signal-to-noise so that more accurate measurements could be obtained. The spectrum of ΔF as a function of emission wavelength is necessary to know if variable fluorescence is also present in the 722nm fluorescence emission band in CP1. This is of particular interest at 77K where the state $P700^+A$ dramatically decreases the fluorescence intensity at 722nm relative to 690nm.

CP1 fluorescence can be described by two emitting populations, F_{690} and F_{722}. The effects of temperature and P700 oxidation state on the steady state emission and prompt fluorescence decay kinetics of CP1 led to the following conclusions. F_{690} represents emission from antenna Chl a. Deexcitation of F_{690} is independent of temperature (77K to 295K) and is predominantly a rapid (50-70ps) transfer of energy to the Chl a antenna emitting at 722nm. F_{722} is not observed at temperatures above 265K. The kinetics of F_{722} are best described by four components: a rise, which represents energy transfer from F_{690}, and three decay components. At 77K, the middle (1.25ns) and slow (4.5ns) decay components are quenched by $P700^+$ and their yields increase dramatically with decreasing temperature (295K to 77K). Thus, the temperature dependence of the middle and slow decay components at 722nm

appears to reflect the efficiency of PS1 photochemistry. All fluorescence decay components at 730nm compete with temperature dependent deexcitation mechanisms exhibiting Arrhenius behavior (100K to 265K) with activation energies of 2.0-2.5kcal/mol. The yields of the middle and slow decay components are increasing significantly at 100K, therefore additional prompt fluorescence measurements over a wider temperature range (less than 77K) are necessary to obtain a more accurate picture of the quenching mechanisms giving rise to the middle and slow fluorescence components. In addition, measuring the prompt fluorescence kinetics of CP1 poised in the state $P700^{+}A$ as a function of temperature would clarify the effect of the oxidation state of the reaction center upon energy transfer and excitation quenching in PS1.

LAWRENCE BERKELEY LABORATORY
TECHNICAL INFORMATION DEPARTMENT
UNIVERSITY OF CALIFORNIA
BERKELEY, CALIFORNIA 94720